

# **Chapter Two**

## **Experimental Part**

## 2. Experimental Part

### 2.1 Chemicals

The following chemicals were used throughout this research work without further purification.

#### 2.1.1 Solid Chemicals

<b>Chemicals</b>	<b>Purity</b>	<b>Company</b>
FeSO <sub>4</sub> .7H <sub>2</sub> O	99%	RIEDEL-DEHAEN AG SEELZE HANNOVER
Sodium acetate	98%	RIEDEL-DEHAEN AG SEELZE HANNOVER
1-10 phenanthroline	97%	BDH
TiO <sub>2</sub> Hombikat uv100	99%	Sachtleben
Commercial TiO <sub>2</sub>	99%	Fluka AG Buchs SG (Anatase)
Phenol red	98%	THOMAS BAKER
NanoTiO <sub>2</sub>	99.5%	Sky spring nanomaterials (anatase 10-25 nm)
Na <sub>2</sub> S <sub>2</sub> O <sub>8</sub>	95%	BDH limited poole England
Nano TiO <sub>2</sub>	99.5%	ALDRICH

## 2.1.2 Liquid Chemicals

Chemicals	Purity	Company
H <sub>2</sub> SO <sub>4</sub>	98%	HIMEDIH
Iso propanol	99.8%	RIEDEL-DEHAEN AG SEELZE HANNOVER
Titanium iso propoxide	97%	ALDRICH
HNO <sub>3</sub>	69.5%	Medex
Ethanol	97%	Merck
H <sub>2</sub> O <sub>2</sub>	50% wt/wt	Scharlau

## 2.2 procedures

### 2.2.1 Measurement of light intensity using actinometric method

The intensity measurement of the incident light was carried out with a potassium ferrioxalate actinometer as described by Hatchard and Parker [57]. This method is usually used to determine the number of quanta entering the reaction vessel and consequently, the apparent quantum yields for the photocatalytic reaction will be estimated. The actinometer solution ( $6 \times 10^{-3}$  mol/L) was prepared by dissolving (2.947 g) of K<sub>3</sub>Fe(C<sub>2</sub>O<sub>4</sub>)<sub>3</sub>.3H<sub>2</sub>O in 800 milliliter of nano filtered deionized water (NFDW).

One hundred milliliter of 1N H<sub>2</sub>SO<sub>4</sub> was added and the whole solution was diluted to one liter with NFDW.

The method used for the determination of light intensity involves irradiation of actinometer solution for known period time (1 hour).

A calibration curve for Fe<sup>+2</sup> was drawn using the following solutions :

- 1-  $4 \times 10^{-4}$  mol.L<sup>-1</sup> of FeSO<sub>4</sub> in 0.1 N H<sub>2</sub>SO<sub>4</sub>.
- 2- 0.1% w/v phenanthroline monohydrate in water.

3- Buffer solution was prepared by mixing 600 milliliter of 1N sodium acetate and 360 milliliter of 1N H<sub>2</sub>SO<sub>4</sub> then diluted to one liter.

Different concentrations of Fe<sup>+2</sup> were prepared by further dilution of solution (1) in 25 milliliter volumetric flask. Then add to each flask;

- a- Two milliliter phenanthroline solution.
- b- Five milliliter of buffer solution.
- c- Different volumes of 0.1N H<sub>2</sub>SO<sub>4</sub> solution to make the acid equivalent to 10 milliliter 0.1 N H<sub>2</sub>SO<sub>4</sub> and finally dilute the whole solution to 25 milliliter with NFDW.

The volumetric flask was covered with aluminum foil and kept in the dark for 30 minutes. Then the optical densities at wavelength = 510 nm were measured.

A blank solution was used as reference which contained all the solutions except the ferrous ion solution.

Draw plot for optical density versus ferrous ion concentration, Figure (2-1)

The slope of the straight line obtained which gives the extinction coefficient (absorptivity) of FeSO<sub>4</sub> solution.

In order to determine the light intensity, 50 milliliter of actinometer solution was irradiated in the irradiation cell. Post illumination, one milliliter of the irradiated solution was transferred into 25 milliliter volumetric flask, two milliliter of phenanthroline solution and 0.5 milliliter of buffer solution were added to the flask, then it was diluted to 25 milliliter using NFDW.

Blank solution was prepared by mixing one milliliter of unirradiated potassium ferrioxalate solution with other components.

The mixture was kept in the dark for 30 minutes and then the optical density was measured.

The incident light intensity was calculated as follows [58]:

$$I_0 = A \times V_1 \times 10^{-3} \times V_3 / Q_y \times \epsilon \times V_2 \times t$$

Where:

$I_0$  = photo flow (incident light intensity)

$A$  = optical density (absorbance) at 510 nm

$V_1$  = initial volume (50 milliliter)                       $V_3$  = final volume (25 milliliter)

$Q_y$  = quantum yield at 365 nm = 1.21 [58]

$\epsilon$  = extinction coefficient = slope of calibration curve ( $1.112 \times 10^4 \text{ L mol}^{-1} \text{ cm}^{-1}$ )

$V_2$  = volume taken from irradiated solution (1 milliliter).

$t$  = irradiation time in seconds (sec)

then the apparent quantum yield is calculated using the following expression :

$$\Phi_{\text{app}} = \text{rate of reaction} / \text{rate of absorbed photons } (I_0)$$

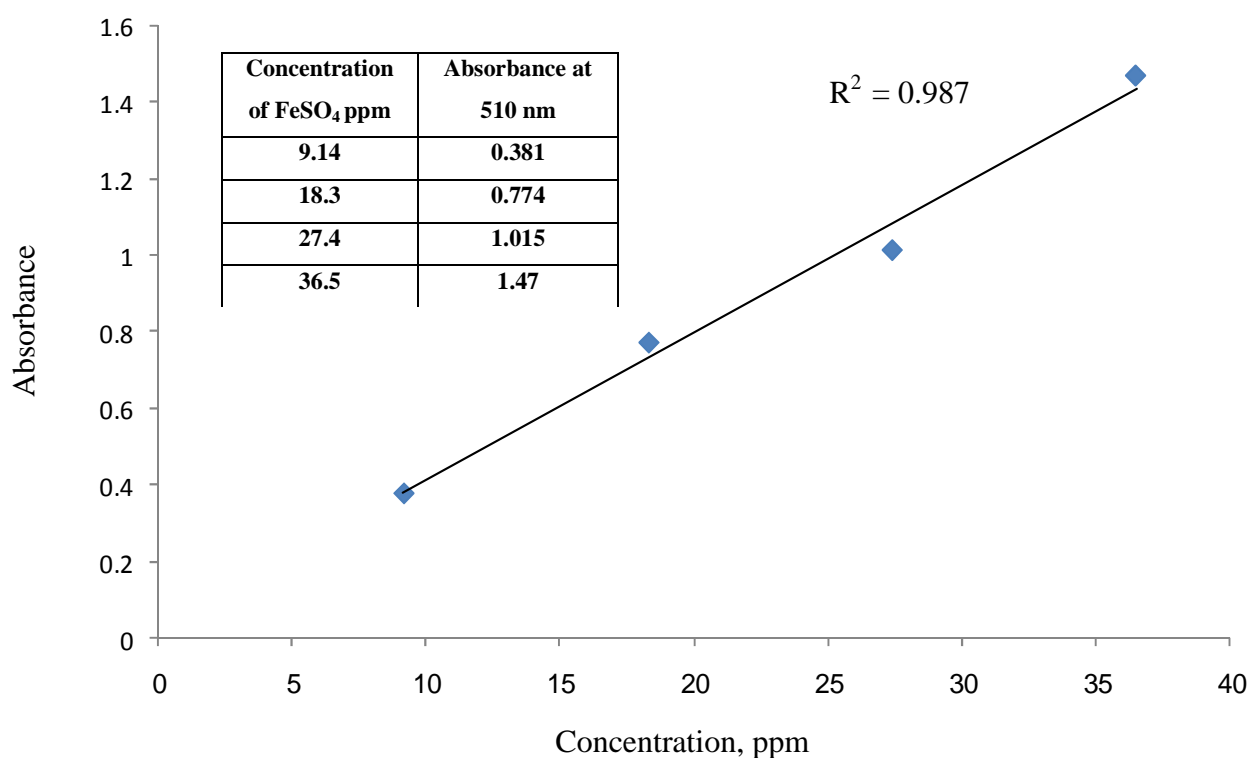


Figure (2-1): Calibration curve of Fe<sup>2+</sup>

$$Y_2 - Y_1 = 1 - 0.6 = 0.4$$

$$X_2 - X_1 = 25 - 15 = 10 \text{ ppm} / 278000 = 0.00003597 \text{ mol/L}$$

$$\text{Slope} = 0.4 / 0.00003597 = 11120.3781 = 1.112 \times 10^4 \text{ L mol}^{-1} \text{ cm}^{-1}$$

### **2.2.2 TiO<sub>2</sub> nanoparticles catalyst synthesis**

Titanium dioxide nanosized catalyst was synthesized by the sol-gel method by means of a gradual addition of a solution of titanium isopropoxide (5 milliliter isopropanol + 5 milliliter titanium isopropoxide) on to 200 milliliter of DNFW at pH=5 with a rate of addition of 2 milliliter /minutes. The mixture was kept, after completion of addition, under continuous vigorous mixing at room temperature until the completion of hydrolysis for 2 hours. The resulting transparent colloidal solution was left aging for 24 hours then filtered, dried at 90 C° for two hours, and finally was calcined at 400 C° for 4 hours. Grinding into fine powder, if needed, overcomes the agglomeration [41].

### **2.2.3 Preparation of phenol red and calibration curve**

- 1- A stock solution of phenol red of 100 ppm was prepared by dissolution of 0.1 g of phenol red into 1000 milliliter NFDW.
- 2- The stock solution was diluted to prepare different concentrations of phenol red (3 , 6 , 9 , 12 and 15 ppm) for the preparation of the calibration curve.
- 3- The absorbance of each diluted solution was measured spectrophotometrically at 432 nm and subsequently the calibration curve Figure (2-2) was drawn.

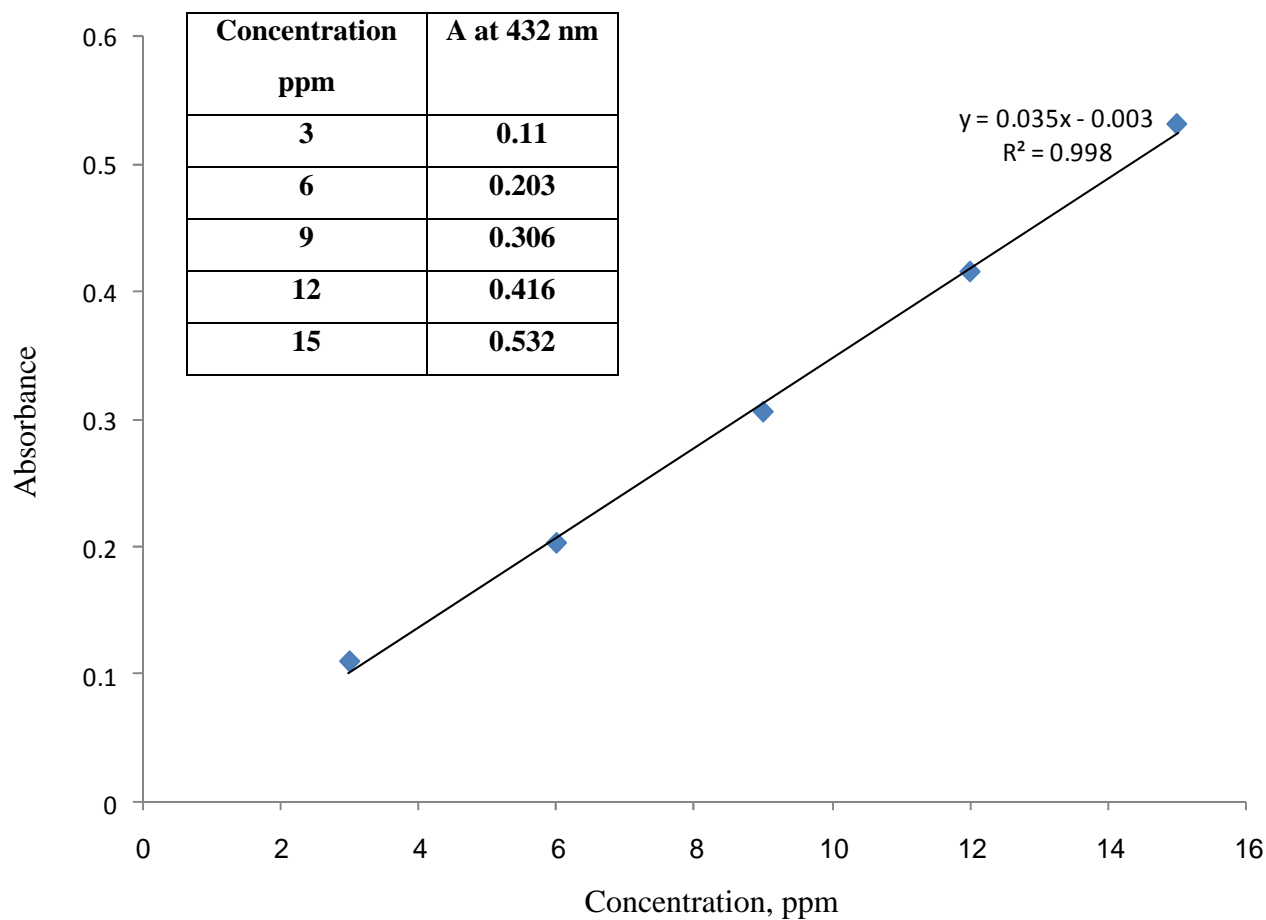


Figure (2-2):Calibration curve for phenol red

#### 2.2.4 Determination of the light intensities for UV source at different distances using the actinometer solution

- 1- Fifty milliliter of actinometer solution was added in to the photolysis cell.
- 2- Irradiate the solution for 60 minutes employing various cell- light source distance (14 cm, 24 cm, 37 cm).

N.B. The presence and absence of lens were tested at all the distances.

- 3- pipette one milliliter of irradiated solution, transfer it into a volumetric flask of 25 milliliter volume then add 2 milliliter 1,10 phenanthroline , 0.5 milliliter buffer solution, and fill to the mark with NFDW.
- 4- Keep the volumetric flask in the dark after it is wrapped with aluminum foil for 30 minutes, then measure the absorbance at 510 nm.

Note : the blank is (1 milliliter actinometer solution + 2 milliliter 1,10 phenanthroline + 0.5 milliliter buffer solution and filled to the mark with NFDW.

### **2.2.5 Testing of degradation of phenol red in the dark**

- 1- Thirty milliliters of phenol red (10 ppm) was added into a beaker, then afterwards add 50 mg  $\text{TiO}_2$ (Hombickat UV 100).
- 2- Keep the beaker in the dark for 3 hours with continuous stirring.
- 3- Measure the absorbance at 432 nm before addition the  $\text{TiO}_2$ .
- 4- After every 30 minutes, pipette a portion of phenol red, centrifuge it for 15 minutes then measure the absorbance for phenol red at 432 nm to compute the changes in concentration.

### **2.2.6 Testing of Degradation of phenol red in the absence of $\text{TiO}_2$**

- 1- Fifty milliliters of phenol red (10 ppm) was added into the cell.
- 2- Irradiate the cell containing the phenol red using 24 cm cell- light source distance in the presence of lens for 3 hours.
- 3- Measure the absorbance of phenol red before irradiation at 432 nm.
- 4- Measure the absorbance of phenol red every 30 minutes at 432 nm in order to calculate the changes in concentration.

### **2.2.7 Multi results experiments by air equilibration**

- 1- Take 75 milliliter of phenol red (10 ppm) and adjust the pH to 4.0 using diluted HNO<sub>3</sub>.
- 2- Add 40 mg of TiO<sub>2</sub> to the cell.
- 3- Start air equilibration through stirring for 20 minutes in the dark.
- 4- Irradiate the solution for 3 hours using 24 cm cell-light source distance in the presence of lens.
- 5- Pipette five milliliter every 30 minutes, centrifuge for 10 minutes using 3000 RPM, separate the supernatant and measure the pH and absorbance at 432 nm.

### **2.2.8 Effect of light intensity on the degradation of phenol red**

- 1- Add 50 milliliter of phenol red (10 ppm) into photocatalysis cell and adjust the pH to 4.0 using dilute HNO<sub>3</sub>.
- 2- Measure the absorbance, pH and conductivity before the irradiation.
- 3- Add 30 mg of TiO<sub>2</sub> to the cell.
- 4- Stir the solution for 20 minutes in dark for equilibration.
- 5- Irradiate the solution for 3 hours at different cell-light source distances (37 cm , 24 cm and 14 cm) in the existence of lens.
- 6- Take 5 milliliter from the irradiated phenol red, centrifuge for 10 minutes at 3000 RPM, then measure pH and absorbance at 432 nm.

### **2.2.9 Multi parameters measurement for O<sub>2</sub> equilibration**

- 1- Add 75 milliliter of phenol red (10 ppm) into the cell and adjust the pH to 4.0 using dilute HNO<sub>3</sub>.
- 2- Add 40 mg of TiO<sub>2</sub> to the cell.
- 3- Stir the solution with O<sub>2</sub> bubbling in the dark for 20 minutes.

- 4- Irradiate the solution for 3 hours at 24 cm of cell-light source distance in the presence of lens and O<sub>2</sub> bubbling.
- 5- Pipette 5 milliliter every 30 minutes interval from illuminated solution, centrifuge at 3000 RPM for 10 minutes, then measure the pH and absorbance at 432nm.

#### **2.2.10 Effect of pH on the degradation of phenol red**

- 1- Take 75 milliliter of phenol red (10 ppm) and adjust the solution to different pHs (2.0 , 3.0 , 4.0 , 4.5 , 5.0 , 6.0 , 8.0) using diluted HNO<sub>3</sub> or NH<sub>4</sub>OH.
- 2- Add 40 mg of TiO<sub>2</sub> onto the cell, containing the above solutions.
- 3- Equilibrate with O<sub>2</sub> for 20 minutes in the dark.
- 4- Irradiate the solution for 3 hours at 14 cm cell-light source distance in the presence of lens and O<sub>2</sub>.

Note : O<sub>2</sub> used is standard with purity (97.5%) and the flow rate of O<sub>2</sub> is 30 ml\min.

- 5- Pipette 5 milliliter every 30 minutes interval from illuminated solution, centrifuge at 3000 RPM for 10 minutes, then measure the pH and absorbance at 432nm.

#### **2.2.11 Effect of irradiation time on the degradation of phenol red**

- 1- Take 75 milliliter of phenol red (10 ppm) and adjust the solution to pH = 4.0 using buffer solution PH=4.0.
- 2- Add 40 mg of TiO<sub>2</sub> onto the cell, containing the above solution.
- 3- Equilibrate with O<sub>2</sub> for 20 minutes in the dark.
- 4- Irradiate the solution for 5 hours at 14 cm cell-light source distance in the presence of lens and O<sub>2</sub>.

Note : the flow rate of O<sub>2</sub> is 30 ml\min.

- 5- At the end of illumination time (5 hours), take 5 milliliter of irradiated phenol red solution, centrifuge for 10 minutes at 3000 RPM, then measure the pH and absorbance at 432 nm.

### **2.2.12 Effect of H<sub>2</sub>O<sub>2</sub> on the degradation of phenol red**

- 1- Take 75 milliliter of phenol red (10 ppm) and adjust to pH=4.5 using dilute HNO<sub>3</sub>, then add different amounts of H<sub>2</sub>O<sub>2</sub> (0.5, 1.0, 1.5, 2.0, 2.5 and 3.0 milliliters).
- 2- Add 40 mg of TiO<sub>2</sub> to the cell containing the above solutions.
- 3- Equilibrate with O<sub>2</sub> for 20 minutes in the dark.
- 4- Irradiate the solution for 5 hours at 14 cm cell-light source distance in the presence of lens and O<sub>2</sub>.

Note : the flow rate of O<sub>2</sub> is 30 ml\min.

- 5- At the end of irradiation time (5 hours), take 5 milliliter of irradiated phenol red, centrifuge for 10 min at 3000 RPM, then measure the pH and absorbance at 432 nm.

### **2.2.13 Effect of initial phenol red concentration on the rate of reaction**

- 1- Take 75 milliliter of phenol red solution (5ppm, 10ppm, 15ppm, 20ppm and 25ppm ) and adjust the solution to pH = 4.5 using dilute HNO<sub>3</sub>, then add 3 milliliter H<sub>2</sub>O<sub>2</sub>.
- 2- Add 40 mg of TiO<sub>2</sub> onto the cell containing the above solutions.
- 3- Equilibrate with O<sub>2</sub> for 20 minutes in the dark.
- 4- Irradiate the solution for 5 hours at 14 cm cell-light source distance in the presence of lens and O<sub>2</sub>.

Note : the flow rate of O<sub>2</sub> is 30 ml\min.

- 5- At every one hour interval, take 5 milliliter of irradiated phenol red, centrifuge for 10 minutes at 3000 RPM, then measure the pH and absorbance at 432 nm.

#### **2.2.14 Effect of TiO<sub>2</sub> loading on the degradation of phenol red**

- 1- Take 75 milliliter of phenol red (10ppm) and adjust to pH =4.5 using dilute HNO<sub>3</sub>, then add 3 milliliter H<sub>2</sub>O<sub>2</sub>.
- 2- Add different amounts of TiO<sub>2</sub> to the cell.(10mg, 20mg, 30mg, 40mg, 50mg and 100mg).
- 3- Equilibrate with O<sub>2</sub> for 20 minutes in the dark.
- 4- Irradiate the solution for 5 hours at 14 cm cell-light source distance in the presence of lens and O<sub>2</sub>.

Note : the flow rate of O<sub>2</sub> is 30 ml\min.

- 5- At every one hour interval, take 5 milliliter from phenol red, centrifuge for 10 minutes at 3000 RPM, then measure the pH and absorbance at 432 nm.

#### **2.2.15 Effect of particle size of TiO<sub>2</sub> on the degradation of phenol red**

- 1- Take 75 milliliter of phenol red (10ppm) and adjust to PH=4.5 using dilute HNO<sub>3</sub>, then add 3 milliliter H<sub>2</sub>O<sub>2</sub>.
- 2- Add 40 mg of TiO<sub>2</sub> to the cell.
  - a- TiO<sub>2</sub> (Fulka AG Buchs SG)(pure anatase)=150 micron
  - b- TiO<sub>2</sub> (Fulka AG Buchs SG)(pure anatase)=75 micron
  - c- TiO<sub>2</sub> (ALDRICH)(anatase 80%+rutile 20%) = < 100nm
  - d- TiO<sub>2</sub> (sky spring nano material)(anatase) = < 25nm
  - e- TiO<sub>2</sub> (prepared) = < 10nm
- 3- Equilibrate with O<sub>2</sub> for 20 minutes in the dark.

- 4- Irradiate the solution for 5 hours at 14 cm cell-light source distance in the presence of lens and O<sub>2</sub>.

Note : the flow rate of O<sub>2</sub> is 30 ml\min.

- 5- At every one hour interval, take 5 milliliter of irradiated phenol red, centrifuge for 10 minutes at 3000 RPM, then measure the pH and absorbance at 432 nm.

### **2.2.16 Effect of H<sub>2</sub>O<sub>2</sub> in the dark on the degradation of phenol red**

- 1- Take 75 milliliter of phenol red (10ppm) and adjust to PH=4.5 using dilute HNO<sub>3</sub>, then added 3 ml of H<sub>2</sub>O<sub>2</sub>.
- 2- Add 40 mg of TiO<sub>2</sub> to the beaker.
- 3- Stir the solution in the dark for 5 hours.
- 4- After 5 hours take a certain volume of phenol red and measure the absorbance at 432nm.

### **2.2.17 Effect of H<sub>2</sub>O<sub>2</sub> in the absence of TiO<sub>2</sub> on the degradation of phenol red**

- 1- Take 75 milliliter of phenol red (10ppm) in the cell and adjust to PH=4.5 using dilute HNO<sub>3</sub>, then add 3 milliliter of H<sub>2</sub>O<sub>2</sub>.
- 2- Irradiate the solution for 5 hours at 14 cm of cell-light source distance and in the presence of lens and O<sub>2</sub>.
- 3- After 5 hours take a certain volume of phenol red and measure the absorbance at 432nm.

### **2.2.18 Effect of temperature on the degradation of phenol red**

- 1- Take 75 milliliter of phenol red solution (10ppm) and adjust the solution to pH = 4.5 using dilute HNO<sub>3</sub>, then add 3 milliliter H<sub>2</sub>O<sub>2</sub>.
- 2- Add 40 mg of TiO<sub>2</sub> onto the cell containing the above solutions.

- 3- Equilibrate with O<sub>2</sub> for 20 minutes in the dark, and use water bath circulator to keep the temperature of solution at (20, 25, 30, 35, 40 and 45° C).
- 4- Irradiate the solution for 5 hours at 14 cm cell-light source distance in the presence of lens and O<sub>2</sub>.

Note : the flow rate of O<sub>2</sub> is 30 ml\min.

- 5- At every one hour interval, take 5 milliliter of irradiated phenol red, centrifuge for 10 minutes at 3000 RPM, then measure the absorbance at 432 nm.

### **2.2.19 Effect of Na<sub>2</sub>S<sub>2</sub>O<sub>8</sub> as oxidant**

- 1- Take 75 milliliter of phenol red solution (10ppm) and adjust the solution to pH = 4.5 using dilute HNO<sub>3</sub>, then add (1 and 3 milliliter Na<sub>2</sub>S<sub>2</sub>O<sub>8</sub>).
- 2- Add 40 mg of TiO<sub>2</sub> onto the cell containing the above solutions.
- 3- Equilibrate with O<sub>2</sub> for 20 minutes in the dark.
- 4- Irradiate the solution for 5 hours at 14 cm cell-light source distance in the presence of lens and O<sub>2</sub>.

Note : the flow rate of O<sub>2</sub> is 30 ml\min.

- 5- After 5 hours take a certain volume of phenol red and measure the absorbance at 432nm.

### **2.2.20 Effect of isopropanol as hydroxyl radical scavenger**

- 1- Take 75 milliliter of phenol red solution (10ppm) and adjust the solution to pH = 4.5 using dilute HNO<sub>3</sub>, then add 3 milliliter H<sub>2</sub>O<sub>2</sub> and different amount of isopropanol (1, 2, 3 and 5 milliliter).
- 2- Add 40 mg of TiO<sub>2</sub> onto the cell containing the above solutions.
- 3- Equilibrate with O<sub>2</sub> for 20 minutes in the dark.

- 4- Irradiate the solution for 5 hours at 14 cm cell-light source distance in the presence of lens and O<sub>2</sub>.

Note : the flow rate of O<sub>2</sub> is 30 ml\min.

- 5- At every one hour interval, take 5 milliliter of irradiated phenol red, centrifuge for 10 minutes at 3000 RPM, then measure the absorbance at 432 nm.

### **2.2.21 General photolysis procedure**

Photocatalytic degradation experiments for the synthesized nano anatase TiO<sub>2</sub> photocatalyst were carried out in the photolysis cell with 125 milliliter capacity under ultraviolet irradiation. The stock solution of phenol red (100 ppm) was prepared with NFDW water and diluted to different concentrations for photocatalytic reaction. For one integral experiment, 75 milliliter of phenol red solutions with certain concentrations, an appropriate amount of hydrogen peroxide and 40 mg photocatalyst were poured into the cell. The pH of the phenol red solution was already adjusted to pH= 4.5 by addition of dilute aqueous solution of HNO<sub>3</sub>. Oxygen gas was bubbled in the solution to keep all the TiO<sub>2</sub> in the suspension. Prior to irradiation, the suspension was magnetically stirred for 20 minutes in the dark to ensure adsorption equilibrium, followed by irradiation for 5 hours with 125W medium pressure UV bulb at 14 centimeter cell-light source distance in the presence of O<sub>2</sub> gas. The samples (5 milliliter) were collected every 60 minutes and centrifuged at 3000rpm for 10 minutes and subsequently to separate the photocatalyst particles from liquid samples. The degradation of phenol red, was followed by measuring the change in absorption intensity using a single beam visible spectrophotometer, which was set at a wavelength of 432 nm for analysis of phenol red.

## **2.3 Instruments**

### **2.3.1 Photolysis unit**

The photolysis unit which is shown in Image (2-1), is laboratory-built (local market) system consisting of ultraviolet light source (125 W) medium pressure mercury lamp (MPML) fitted with a focusing lens to assure parallel beam of light. The foregoing source emits UV light in the wave length range 260-450 nm with maximum intensity at 365 nm as its spectra is explicitly shown in Figure (2-3)[58]. The intensity level of light is controlled by fixing the distance between the source of light and the quartz window of the photolysis cell. The photoreaction experiments were conducted in a cylindrical Pyrex cell (volume 100 cm<sup>3</sup>) coupled with a water jacket for temperature control. The photolysis cell is supplied with two openings of 5 mm in diameter and these were used for gas purging and sampling processes. A magnetic stirrer was used to keep the catalyst aqueous suspension in homogeneous form during the photolysis experiments. The reaction temperature was controlling by circulating thermostat water bath type WiseCircu.



Image (2-1): Photolysis unit

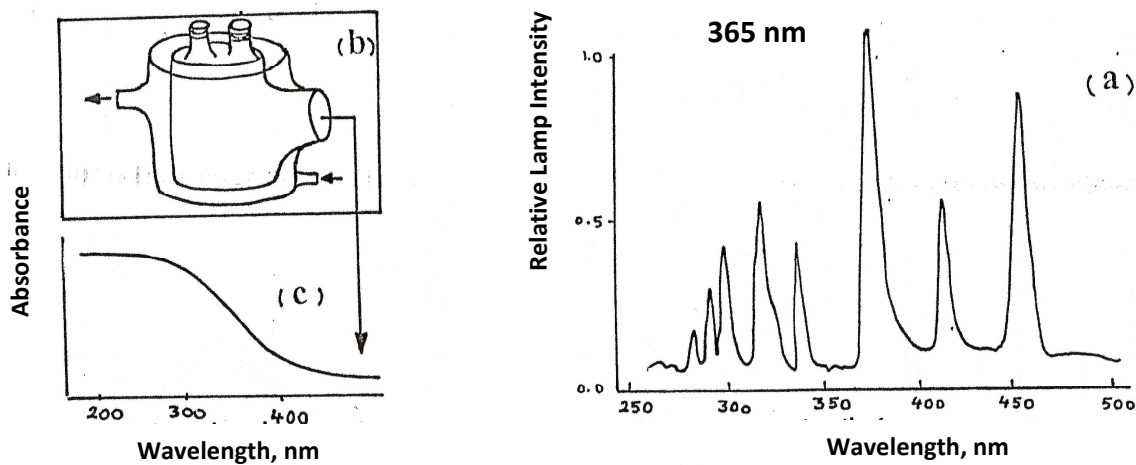


Figure (2-3): Schematic diagram for ; (a) emission spectra of the MPML; (b) photocatalysis cell; (c) absorption spectra of glass

### 2.3.2 Scanning Electron Microscopy (SEM)

The Hitachi S-4700 FE-SEM is a cold field emission high resolution scanning electron microscope. This SEM permits ultra high resolution imaging of thin films and semiconductor materials on exceptionally clean specimens (Image 2-2).



Image (2-2): Hitachi S-4700 FE-SEM (Georgia Institute of Technology, Atlanta, GA, USA)

### **2.3.3 Transmission Electron Microscopy (TEM)**

High resolution STEM for nanoscale analysis. Low magnification and wide field of view image observation for specimen/orientation and particle size analysis. All necessary STEM operations are embedded in the HT7700 including Bright Field (BF) and Dark Field (DF) detectors displaying BF-STEM and DF-STEM.

Images are supported by means of DF-STEM where Z-contrast imaging facilitates further chemical/structural analysis (Image 2-3).

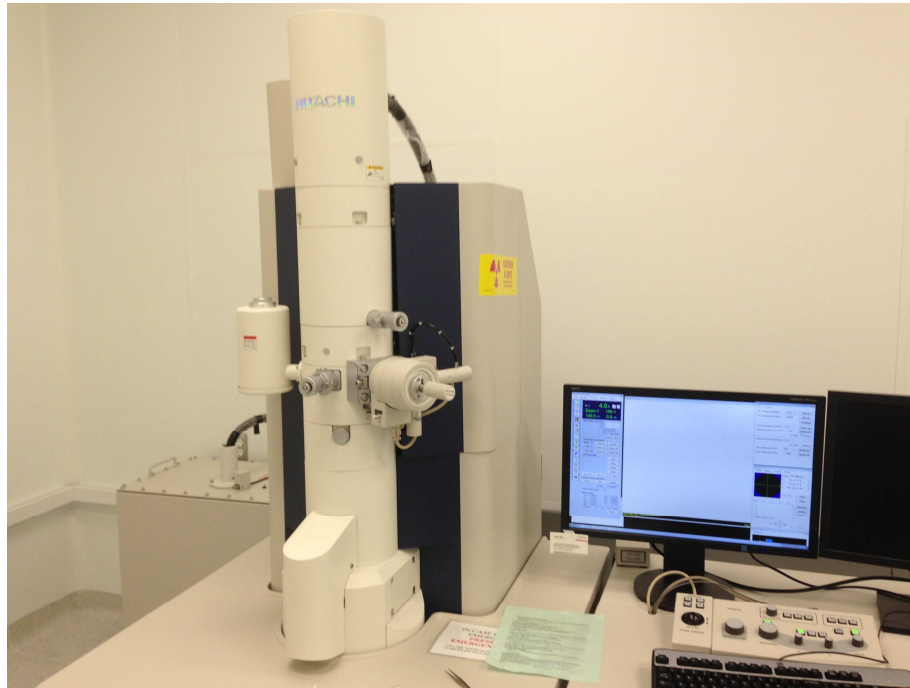


Image (2-3): Hitachi HT7700 STEM (Georgia Institute of Technology, Atlanta, GA, USA)

### **2.3.4 Energy Dispersive X-ray Spectroscopy (EDXS)**

The Hitachi S-700N variable pressure SEM features a low vacuum observation of 6-270 pa which enables imaging of non-conductive samples and moist samples without traditional drying or coating procedures. The Deben cool stage controls sample temperature between -23° C and 50° C to control sample vapor pressure. Magnification range X5-X300000 with resolution of 3 nm at 30 kV applied voltage (Image 2-4).

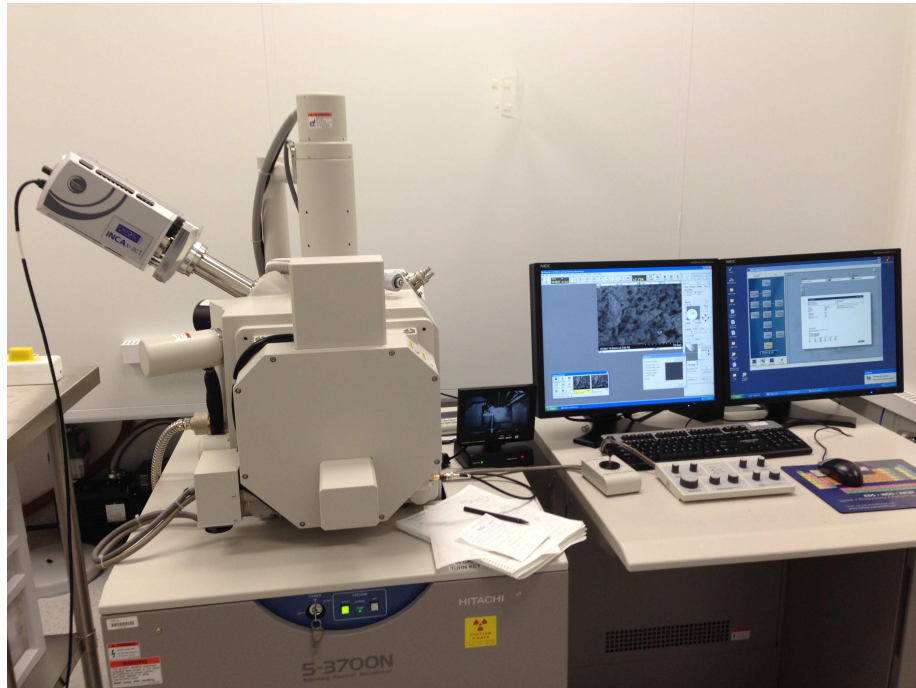


Image (2-4): Hitachi S-3700N VP-SEM(Georgia Institute of Technology, Atlanta, GA, USA)

### 2.3.5 X-ray Spectrometer

Pananalytical Philips diffractometer with Cu  $K\alpha$  radiation line of 0.15425 nm has been employed for the range of  $2\theta$  from  $20^\circ$  to  $40^\circ$  (Image 2-5).



Image (2-5): Pananalytical Philips diffractometer (Georgia Institute of Technology, Atlanta, GA, USA)

### **2.3.6 Raman Spectrometer**

Spex Ramalog 4 (Georgia Institute of Technology, Atlanta, GA, USA)

### **2.3.7 Brunauer Emmett Teller (BET)**

Bel Sorp 18 plus nitrogen adsorption apparatus (Georgia Institute of Technology, Atlanta, GA, USA)

### **2.3.8 Diffused Reflectance UV-VIS Spectrometer**

Avantes / Ava spec 2048 (Georgia Institute of Technology, Atlanta, GA, USA)

### **2.3.9 Ultra Violet-Visible Spectrophotometer (UV-VIS)**

Double beam shimadzu UV-1650 PC UV-VIS spectrophotometer has been used for spectrophotometric measurements (Image 2-6).



Image (2-6): Shimadzu UV-1650PC

### 2.3.10 Single beam VIS spectrophotometer

Apel PD-303 single beam spectrophotometer has been used for visible light absorption measurements (Image 2-7).



Image (2-7): Apel PD-303 single beam visible spectrophotometer

### 2.3.11 pH Meter

HANNA instruments

### 2.3.12 Muffle furnace

SX-5-12 BOX-Resistance Furnaces Controller Box

### 2.3.13 Drying cabinet

K Hot Air Sterilizer

### 2.3.14 Centrifuge

K centrifuge PLC series.

### 2.3.15 Hot Plate

Lab Tech Daihan Labtech. Co. Ltd.

## 2.3.16 Fourier Transform Infrared Spectroscopy (FTIR)

IR Prestige-21 Shimadzu



Image (2-8): IR Prestige-21 Shimadzu

# 1. Introduction

## 1.1 Advanced oxidation process (AOP)

Various chemicals are discharged into the aquatic environment as industrial liquid wastes. Some of them are not only toxic but also partly biodegradable; therefore they are not easily removed in biological wastewater treatment plants. That is why there is a need to develop effective methods for the degradation of organic pollutants, render into less harmful compounds (non aromatic) or to their complete mineralization [1].

Conventional processes to remove these pollutants involve physical, chemical, and biological methods. Nevertheless, the individual application of these techniques is generally limited and cannot degrade completely the recalcitrant organic matter [2]. Biological processes such as activated sludge and aerated lagoons are used to treat pulp mill effluents but these have limited ability to metabolize recalcitrant moieties because of their size and complex structure. Latest investigations on the degradation of organic pollutants are focused on the combination of biological and physical–chemical treatments. For example, advanced oxidation followed by biological treatment or vice versa has been studied to improve removal efficiencies and reduce process energy cost [3].

Chemical precipitation, filtration, electro-deposition, ion-exchange adsorption, and membrane systems are some of the conventional methods for water treatment and have found certain practical applications [4]. However, these methods may not be very effective, because they are either slow or non-destructive to some or most persistent organic pollutants. Besides, large scale implementations of these methods have some limitations, owing to the expensive equipments involved in these processes. It is therefore essential to investigate the use of efficient

catalytic materials to remove highly toxic compounds from potential sources of drinking water. Semiconductor heterogeneous photocatalysis is a popular technique that has the great potential to control the organic contaminants in water or air. This process which is also known as “Advanced Oxidation Process (AOP)” is suitable for the oxidation of recalcitrant contaminants such as dyes and phenolic compounds. Heterogeneous photocatalytic oxidation, developed in the 1970s, has attracted considerable attention particularly when used under solar light [2-4]. In the past decades, numerous studies have been carried out by researchers from all over the world on the application of heterogeneous photocatalytic oxidation process to decompose and mineralize certain recalcitrant contaminants [5].

Advanced oxidation processes (AOP), which involve the in situ generation of highly potential chemical oxidants such as hydroxyl radical  $\cdot\text{OH}$ , with oxidation potential 2.8 V [6] have recently emerged as an important class of technologies for accelerating the oxidation and destruction of a wide range of organic contaminants in polluted water and air [7]. Further, when these processes are applied on a right place, offer a good opportunity to reduce the contaminants concentration from several hundreds ppm (mg/L) to less than 5 ppb ( $\mu\text{g/L}$ ), therefore, they are called “the treatment processes of the 21st century” [1].

As a response, the development of newer eco-friendly methods of destroying these pollutants became an imperative task. Ultimately, research activities centred on advanced oxidation processes (AOPs) for the destruction of synthetic organic species resistant to conventional methods. AOPs rely on in situ generation of highly reactive radical species, mainly  $\cdot\text{OH}$  by using solar, chemical or other forms of energy. The most attractive feature of AOPs is that this highly potential and strongly oxidizing radical allows the destruction of a broad range of

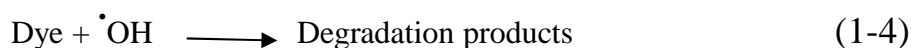
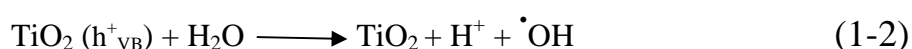
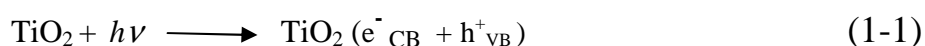
pollutants quickly and non selectively. Among AOPs, heterogeneous photocatalysis has proved to be of real interest as efficient tool for degrading both aquatic and atmospheric organic contaminants. Heterogeneous photocatalysis involve the acceleration of photoreaction in presence of semiconductor photocatalyst. One of the major applications of heterogeneous catalysis is photocatalytic oxidation (PCO) to promote partial or total mineralization of gas phase or liquid phase contaminants to benign substances. Even though degradation begins with a partial degradation, the term ‘photocatalytic degradation’ usually refers to complete photocatalytic oxidation or photomineralisation, essentially to  $\text{CO}_2$ ,  $\text{H}_2\text{O}$ ,  $\text{NO}_3^-$ ,  $\text{PO}_4^{3-}$  and halide ions [8].

In recent years advanced oxidation processes (AOPs) involving hydrogen peroxide, ozone and /or Fenton reagents, with or without a source of UV light have been reported to be useful for the photo-oxidation of organic pollutants in waste waters. It removes substantial amount of Chemical Oxygen Demand (COD) and Total Organic Carbon (TOC) from industrial effluents. However, these oxidation methods results in partial oxidation of organics and more often lead to the generation of potentially harmful chemicals. Total oxidation of organics by these technologies is both cost and energy intensive. Among the various AOPs, semiconductor mediated photocatalysis has been accorded great importance over the last few years due to its potential to destroy a wide range of organic and inorganic pollutants at ambient temperatures and pressures, without the production of harmful byproducts [9].

For the removal of dye pollutants, traditional physical techniques (adsorption on activated carbon, ultra filtration, reverse osmosis, coagulation by chemical agents, ion exchange on synthetic adsorbent resins... etc.) can generally be used efficiently [10]. Nevertheless, they are non-destructive, since they just transfer organic compounds from

water to another phase, thus causing secondary pollution. Consequently, regeneration of the adsorbent materials and post-treatment of solid-wastes, which are expensive operations, are needed. Due to the large degree of aromatics present in dye molecules and the stability of modern dyes, conventional biological treatment methods are ineffective for decolorization and degradation. Furthermore, the majority of dyes is only adsorbed on the sludge and is not degraded. Chlorination and ozonation are also being used for the removal of certain dyes but at slower rates as they have often high operating costs and limited effect on carbon content [11]. These are the reasons why advanced oxidation processes (AOPs) have been growing during the last decade since they are able to deal with the problem of dye destruction in aqueous systems. AOPs such as Fenton and photo-Fenton catalytic reactions, H<sub>2</sub>O<sub>2</sub>/UV processes and TiO<sub>2</sub> mediated photo-catalysis have been studied under a broad range of experimental conditions in order to reduce the color and organic load of dye containing effluent waste waters [10-12].

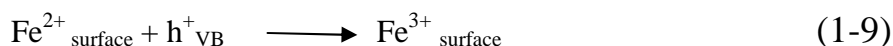
Formation of  $\cdot\text{OH}$  on surface of nano TiO<sub>2</sub> [10]:



Fenton reaction :

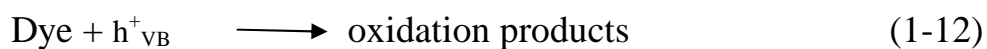
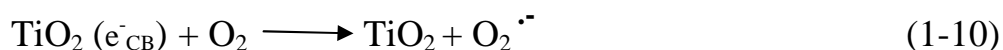


Photo-Fenton reaction [6] :



Intense research activity is seen in recent years in advancing the synthesis and functionalization of various sizes and shapes of semiconductor and metal nanoparticles. The goal of these activities are improving the performance and utilization of nanoparticles in various applications from sensing devices to photonic materials to molecular electronics and to advanced oxidation techniques (AOTs). The size and shape dependent optical and electronic properties of these nanoparticles make an interesting case for exploiting them in light induced chemical reactions. Nanoparticles are commonly employed as photocatalysts, in photodecomposition system of various ecotoxicants [13-14]. Maximizing the efficiency of photo induced charge separation in semiconductor systems remains to be a major challenge to the scientific community. Obtaining insight into charge transfer processes is important to improve the photo conversion efficiencies in semiconductor based nano assemblies. Quantizations and its effects on charge transfer, the processes that are induced by charge separation at the particle's surface are the focus of many of the current advances in the field and dual use of these materials as well as combination of AOTs is often attempted [13].

Formation of  $e^{-}h^{+}$  on nano  $\text{TiO}_2$  surface as shown in Figure (1-1) and following equations [10]:



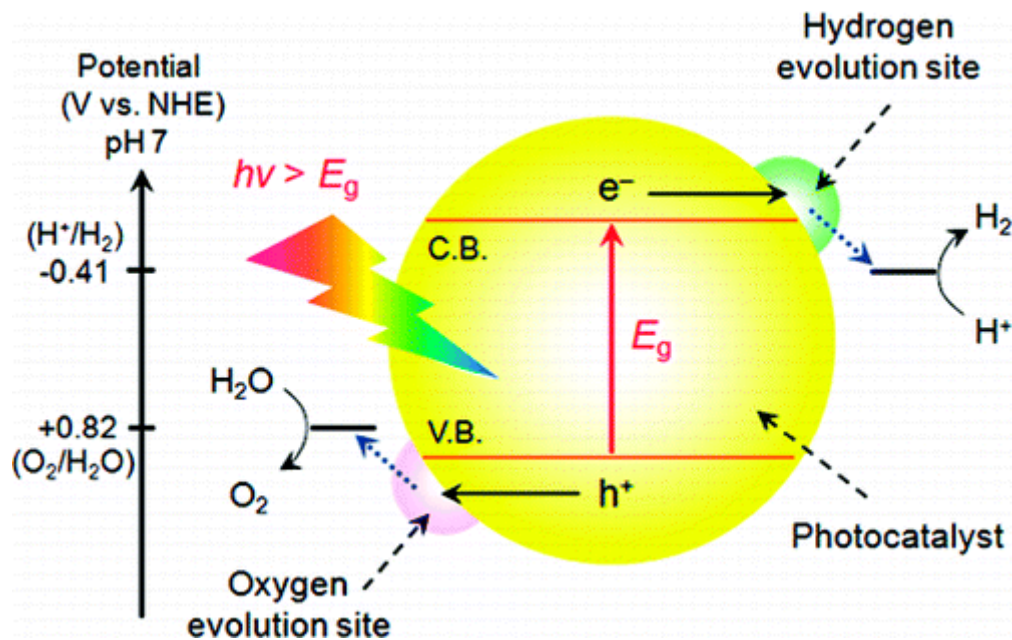


Figure (1-1): Formation of electron-hole pairs on TiO<sub>2</sub> surface

## 1.2 Dyes and phenolic compounds as water ecotoxigants

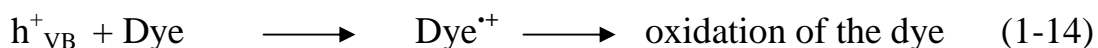
### 1.2.1 Dyes

Textile dyes and other industrial dyestuffs constitute one of the largest group of organic compounds that represent an increasing environmental danger. These contaminants are being continuously released into the aquatic environment through various anthropogenic activities. The detection of toxic organic compounds in storm and wastewater effluent is reported to be a major obstacle as regards wide ranging acceptance of water recycling. Furthermore, their variety, toxicity and persistence can directly impact the health of ecosystem and present a threat to humans through contamination of drinking water supplies e.g., surface and ground water. The response has been the drive to achieve

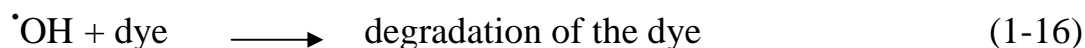
efficient removal of persistent organic pollutants from wastewater effluent to lessen the risk of pollution problems from such toxic chemicals to enable its reuse. Consequently, considerable efforts have been devoted to developing a suitable purification method that can easily destroy these bio-recalcitrant organic contaminants. Due to their incomplete removal during wastewater treatment, they are ubiquitous in secondary wastewater effluents at low concentration. Despite their low concentration, these contaminants have raised substantial health concern due to their extremely high endocrine disrupting potency and genotoxicity [15-16].

Dyes are usually the first contaminant to be recognized in wastewater because they are highly visible and undesirable in water, even in very small amounts (<1ppm for some dyes). Nevertheless, dyes are still widely used in many contemporary fields of technology. Over 100,000 commercially available dyes exist, and more than  $7 \times 10^5$  tones of dyes are produced annually. Dyes play a very important role in various branches of the textile industry; dyes used in this industry are often synthetic, usually derived from two sources: coal tar and petroleum-based intermediates. Synthetic dyes have become common water pollutants and are usually found in trace quantities in industrial wastewater owing to their good solubility in water [4]. A wide range of technologies have been developed to remove synthetic dyes from wastewaters so as to reduce their impact on the environment. Chemical precipitation, adsorption on organic or inorganic matrices, and decolorization by photocatalysis and/or by chemical oxidation processes are some of the technologies currently being used for the removal of synthetic dyes. The photocatalyzed decolorization of a dye in solution is initiated by the photoexcitation of the semiconductor, followed by the formation of electron–hole pair on the surface of catalyst, eq. (1-1). The high oxidative

potential of the hole ( $h^+_{vb}$ ) in the catalyst permits the direct oxidation of the dye to reactive intermediates eq. (1-14) [17].



Another reactive intermediate which is responsible for the degradation is hydroxyl radical ( $\cdot\text{OH}$ ), which is either formed by the decomposition of water eq. (1-2) or by reaction of the hole with  $\text{OH}^-$  eq.(1-15) [17].



### 1.2.2 Phenolic compounds

Important organic contaminants in industrial wastewaters are phenols and phenolic compounds [9]. Phenolic compounds are aromatic compounds with one or more hydroxyl groups attached to the aromatic ring. These compounds are usually found in wastewater discharged from a variety of industries [4]. The production and usage of chemicals in industry has led to the entry of many xenobiotics into the environment. During the industrial production of pesticides, herbicides, dyes, pigments, phenolic resins and paper, chlorinated phenols are used as intermediates compounds [3].

Phenolic compounds have high stability, high toxicity and a carcinogenic character, they have caused considerable damage and threat to the ecosystem in water bodies and human health. How to eliminate phenolics in wastewater effectively has been in urgent demand? [18]. Humans are generating and disposing more wastewater today than any other time. The disposal of toxic contaminants, such as dyes and phenolic compounds which are harmful to the environment, hazardous to humans, and difficult

to degrade by natural means, is pervasively associated with industrial development and these contaminants are frequently found in the industrial effluents [9, 18].

In response, it has become a challenge to achieve an effective removal of persistent dyes and phenolic organic pollutants from waste water effluent to minimize the risk of pollution problems from such toxic chemicals and to enable its reuse. Consequently, considerable efforts have been devoted to developing a suitable purification method that can easily destroy these biorecalcitrant organic contaminants. Due to their incomplete removal during wastewater treatment, they are ubiquitous in secondary wastewater effluents, rivers and lakes at low concentration. Despite their low concentration, these contaminants are a major health concern because of their extremely high genotoxicity [14].

### **1.3 Size effect of semiconductor particles**

When the size of semiconductor is extremely small, several characteristics may differ from bulk semiconductor. One of them is size quantization effect. This effect shows the shift of electronic energy levels [19-20]. Nanoparticles of different semiconductors, including  $\text{TiO}_2$ , have been widely studied during the last decade [21-22].

The absorption spectra normally (i.e., bandgap) shift to higher photon energy (toward the blue end of the spectrum) and develop a discrete character as the size of particles decrease. The theoretical concept of this quantum behavior has been developed by Brus [23-24], which is based on effective mass approximation. The dependence of the energy properties of nanoparticles of metals and semiconductors on their size has been analyzed [25].

For metals, the appearance of size dependent metallic properties is an important feature. Thus, for mercury clusters, a gradual metal insulator

transition take places between  $N=20$  and  $N=10^2$  atoms. An example of the external size effect is the collective electronic or lattice excitation known as the Mie resonance. Quantum size effects are associated with unusual spectra of electron energy levels arranged in a discrete fashion [26].

Figure (1-2) shows how the splitting of energetic levels into a filled and an empty region proceeds as the number of contributing MOs increases, and the extent of band structure depends on the size of the cluster. Simple molecular orbital show that the center of the band is developed first, where the separation between the bands are greater than  $E_g$  (bulk band gap energy) and consequently, it takes more energy to create  $e^-/h^+$  pair in the cluster than in the bulk sample. While the edges of the band approach a continuum only for the large cluster sizes. Hence, one can conclude that in large particles, the ensemble of energetic levels of conduction and valence bands becomes more dense than in nanosized particles, and the electronic transitions from highest occupied molecular orbitals (HOMO) to lowest unoccupied molecular orbitals (LUMO) for Q-sized particles require higher energy [6].

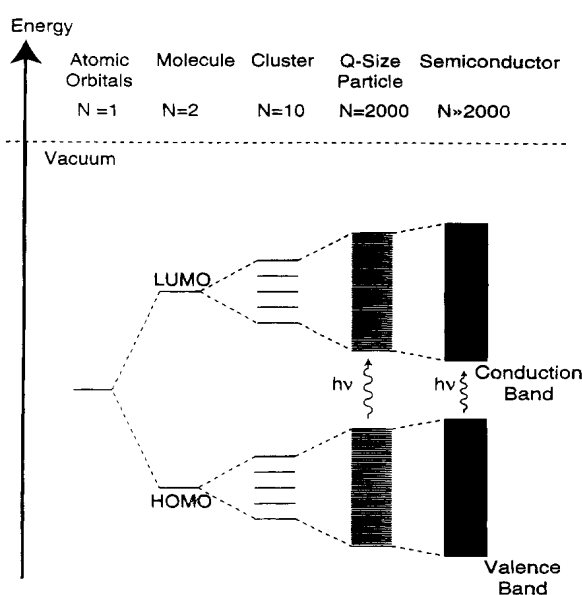


Figure (1-2): model for particle growth. The spacing of the energy levels (i.e. density states) varies among systems

Figure (1-3) illustrates the increase in effective bandgap when the size of the CdS particles is decreased from diameter  $> 10$  nm, signifying the dimensions of a bulk semiconductor, to  $d \approx 2.6$  nm where significant quantum size effects occur for CdS. In another investigation, Hoffman and co-workers noticed an increase in the bandgap energy of CdS nano particles from 2.5 eV to 3.07 eV as the diameter was changed from 6.9 nm to 3.2 nm respectively [6].

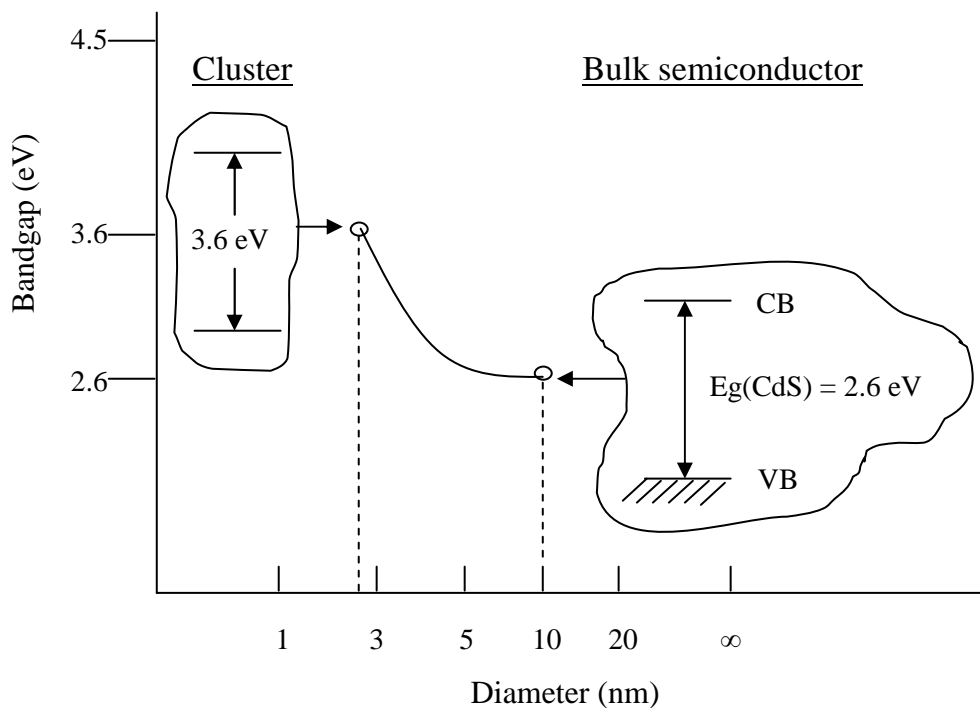


Figure ( 1-3 ): Quantum size effect on semiconductor bandgap

The quantization in the ultrafine particles arises from the confinements of charge carrier in semiconductors with potential wells of small geometrical dimensions (less than the De Broglie wavelength of the electrons and holes) [20]. Under these conditions the energy levels or electronic states available for the electrons and holes in the conduction and valence bands become discrete and the effective bandgap of the

semiconductor is increased. Such effects can change the photocatalytic properties and also the color of the material (due to the altered optical absorption maxima) [27].

Recombination of light induced charge gives rise to luminescence of nanoparticles, which is accompanied by a short wavelength shift with a decrease in the particle size. The inverse problem, namely, the determination of the particle size from its spectrum has not yet been solved. This requires further development of the theory. However, the studies in which the Plasmon line width versus particle size dependence were observed, using scanning electron microscope (SEM), and electron spectroscopy technique have already appeared [28].

The energy shift in the bandgap,  $\Delta E$ , as a function of particle size can be predicted by the three dimensional confinement model based on the effective mass approximation [23, 29-31]:

$$\Delta E = (\hbar^2 \pi^2 / 2R^2) [1/m_e^* + 1/m_h^*] - 1.786 e^2 / \epsilon_s R - 0.248 E_{RY} \quad (1-17)$$

Where R is the particle radius,  $m_e^*$  and  $m_h^*$  are the effective masses for the electrons and holes,  $\epsilon_s$  is the dielectric constant, and  $E_{RY}$  is the effective Rydberg energy given as  $e^4 / 2\epsilon_s^2 \hbar^2 (1/m_e^* + 1/m_h^*)$ .

The equation is characterized by the first term which represents the energy of localization, the second term which represents the coulombic attraction [23, 29] and the third term which represents the correlation effects [32].

When the crystalline dimension of a semiconductor particle falls below a critical radius of approximately 10 nm the charge carriers appear to behave quantum mechanically [33-35] as a simple particle in a box.

As a result of this confinement the bandgap increased and the band edges shift to yield larger redox potentials [36].

## 1.4 The nature of heterogeneous photocatalysis

Generally heterogeneous photocatalytic processes can be defined as catalytic processes during which one or more reaction steps occur by means of electron-hole pairs photogenerated on the surface of semiconductor materials illuminated by light of suitable energy. This general and wide definition implies that some steps of a photocatalytic process are redox reactions involving the photogenerated electron hole pairs [37].

The exact definition of the term heterogeneous photocatalysis is a difficult one especially as in many cases the detailed mechanism of the ongoing reactions is uncertain. However in all cases such a reaction scheme implies the previous formation of an interface between in general a solid photocatalysis and a liquid or a gas phase containing the reactants and/or the products of the photoreaction. The common case is that of a light absorbing semiconductor in contact with either a liquid or a gas phase [37].

Heterogeneously dispersed semiconductor surfaces provide both a fixed environment to influence the chemical reactivity of a wide range of adsorbate and a means to initiate light-induced redox reactivity in these weakly associated molecules. Upon photoexcitation of several semiconductors non homogeneously suspended in either aqueous or non aqueous solutions or in gaseous mixtures, simultaneous oxidation and reduction reaction occur. This conversation often accomplishes either a specific, selective oxidation or a complete oxidative degradation of an organic substrate present [38].

Photocatalysis has gained more and more attention by scientists all over the world and many books [39-40] reporting studies on several processes successfully carried out by using polycrystalline semiconductors as catalysts, both in gas-solid and in liquid-solid regimes,

have been published in the last years. The most widely used semiconductor is polycrystalline  $\text{TiO}_2$  in the anatase or rutile phase, due to its photostability, to the relatively moderate band-gap value (3.0 and 3.2 eV for rutile and anatase respectively) and to the fact that it doesn't present any toxicity [37].

The knowledge of the main thermodynamic and kinetic factors influencing the photoreactivity is essential in order to make predictions on the feasibility of photoprocesses and to explain why some solids are active and others are not. Moreover the same solids can be active in a particular system for a particular photo reaction and not active in different experimental conditions or for different reactions. Therefore, thermodynamic and kinetic factors governing the photocatalytic processes should be carefully considered in order to choose the best experimental conditions for their occurrence [37].

## **1.5 Characteristic aspects of the photo induced $\text{TiO}_2$**

Considerable attention has been paid over the last two decades on the synthesis and application of nanocrystalline materials, because of their novel and spectacular physical and chemical properties. These particular properties are resulted from the ultrafine structures (i.e., grain sizes smaller than 50 nm) of these materials and can be classified in two categories: properties that are relative to the bulk and to the surface [41]. Over the years, a large number of semiconductors have been used as photocatalysts. The most commonly studied catalyst are  $\text{TiO}_2$ , ZnO and CdS [9].  $\text{TiO}_2$  is the most suitable because of its high oxidizing ability, long-term stability, low cost and nontoxicity. However,  $\text{TiO}_2$  can only be activated by ultraviolet (UV) light because it is a large band gap semiconductor (3.2 eV for anatase, 3.0 eV for rutile), and thus only utilizes ~5% of the solar spectrum. Another current bottle neck in  $\text{TiO}_2$

photocatalysis is the low quantum yield. The high recombination rate of the photogenerated electron–hole pairs in  $\text{TiO}_2$  hinders its further application [42].

Titanium dioxide ( $\text{TiO}_2$ ) is a natural occurring oxide of titanium; it is also named as titania or titanium(IV) oxide. In nature,  $\text{TiO}_2$  exists in five different forms, i.e. rutile, anatase, brookite, monoclinic and orthorhombic. However, monoclinic and orthorhombic phase of  $\text{TiO}_2$  are two exceptions found only in shocked granet gneisses from Ries crater in Germany [4]. Rutile appears to be the most common form of  $\text{TiO}_2$ , while anatase and brookite forms of  $\text{TiO}_2$  tend to convert into rutile form upon heating at high temperature. Calcinated  $\text{TiO}_2$ , especially in rutile form is very stable and insoluble in water; it is also insoluble or only moderately soluble in concentrated and hot acids.  $\text{TiO}_2$  is well known for its widespread applications in paints, sunscreens, environmental treatment and purification purposes. These widespread applications of  $\text{TiO}_2$  are credited to its high level of photoconductivity, ready availability, low toxicity, inertness, low cost as well as high photo efficiency and activity.  $\text{TiO}_2$  has drawn great attentions of researchers in photovoltaic and photocatalysis fields since Fujishima and Honda first discovered the ability of  $\text{TiO}_2$  in splitting of water under ultraviolet (UV) light. Crystalline structure of  $\text{TiO}_2$  has been reported as one of the factors affecting its photocatalytic activity. Anatase form of  $\text{TiO}_2$  has the best photocatalytic activity, followed by rutile form.  $\text{TiO}_2$  can utilize natural UV radiation from sunlight for photocatalysis because it has suitable energetic separation between its conduction and valence band. Band-gap energy of  $\text{TiO}_2$  (3.2 eV for anatase; 3.03 for rutile) is relatively smaller compared to other semiconductors, such as ZnO (3.35 eV) and SnO<sub>2</sub> (3.6 eV). Therefore,  $\text{TiO}_2$  is able to absorb photons energy in the near UV range (wave length < 387 nm) [4, 43].

For the preparation of nanocrystalline particles, wet chemical synthesis routes including sol–gel, hydrothermal, and precipitation methods are widely used. For the past two decades, the sol–gel routes have become an appropriate method for the preparation of nanocrystalline materials. During  $\text{TiO}_2$  sol–gel synthesis temperature of calcinations (and pH value) influences the type of phase. Anatase nanopowders obtained by sol–gel method are amorphous in phase, but with increasing the temperature up to  $350^\circ\text{C}$  or higher the transition from amorphous to anatase phase happens. The metal ions which are found to inhibit the anatase to rutile phase transformation are Si, W, Nb, Ta, and Cr while the metal ions which are reported to promote the phase transformation are Ni, Co, Mn, Fe, Cu, V and Ag [10]. Sol–gel process is highly potential as appropriate process for preparing nanostructure materials because the particle size, morphology and porosity can be controlled by adjusting preparation parameters [41].

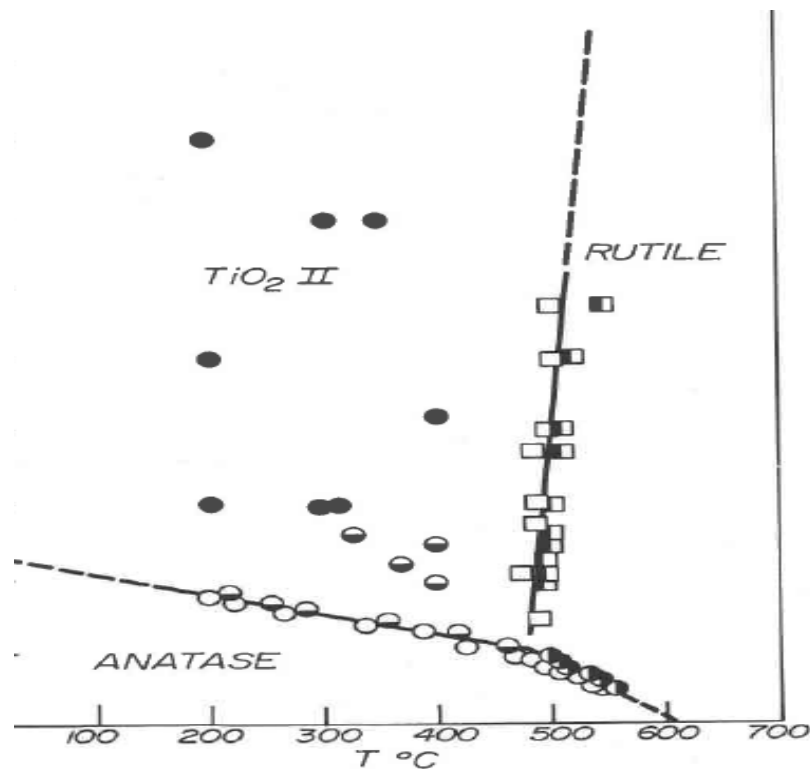


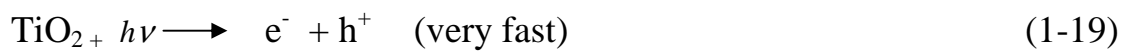
Figure (1-4) : Effect of temperature on  $\text{TiO}_2$  allotropes

Photoexcitation of TiO<sub>2</sub> with light of an energy equal to or greater than the bandgap, results in the promotion of an electron from the filled valence band to the empty conduction band, creating an electronic vacancy or hole (h<sup>+</sup>) at the valence band as in the following equation [44]:



There are four steps could occur on TiO<sub>2</sub> surface including the generation of an e\h pair, as in the following equations [8]:

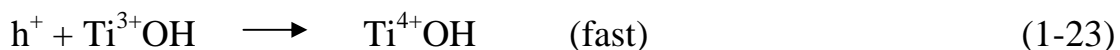
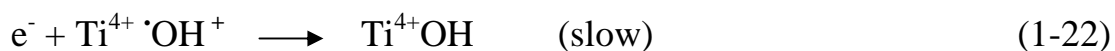
- charge carrier generation :



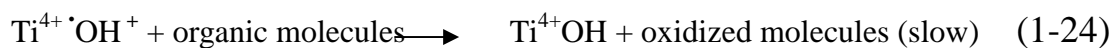
- charge carrier trapping



- charge carrier recombination



- interfacial charge transfer



In generated conduction band electrons and valence band holes, migrate rapidly within a few nanoseconds [27, 36], to the surface of the catalyst where they take part in a series of redox reactions, illustrated in Figure (1-5) [36, 45-46].

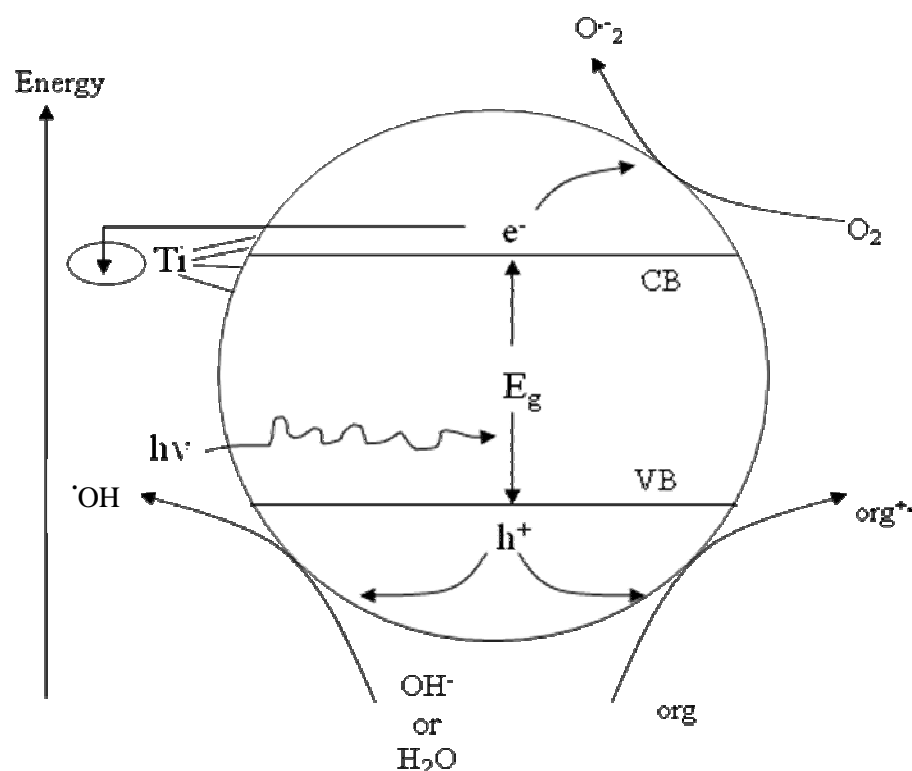


Figure (1-5) : Initial charge transfer pathways for TiO<sub>2</sub> photoelectro- chemical mechanism

The development of titanium oxide photocatalysts that can utilize the solar or indoor artificial light for the degradation of pollutants is of great importance. Most of these studies are aimed at decreasing the band gap of the material and hydroxyl content on the surface of the catalyst [47].

The photocatalytic activity of various forms of TiO<sub>2</sub>, such as TiO<sub>2</sub> film, TiO<sub>2</sub> powders, TiO<sub>2</sub> nanotubes, supported TiO<sub>2</sub> and doped TiO<sub>2</sub> have been evaluated through degradation of dyes and/or phenolic compounds under light irradiation. Results of these studies showed that TiO<sub>2</sub> was effective for removing dyes and phenolic compounds from aqueous solutions [4].

## 1.6 Photocatalytic degradation of phenols in aqueous TiO<sub>2</sub> suspension

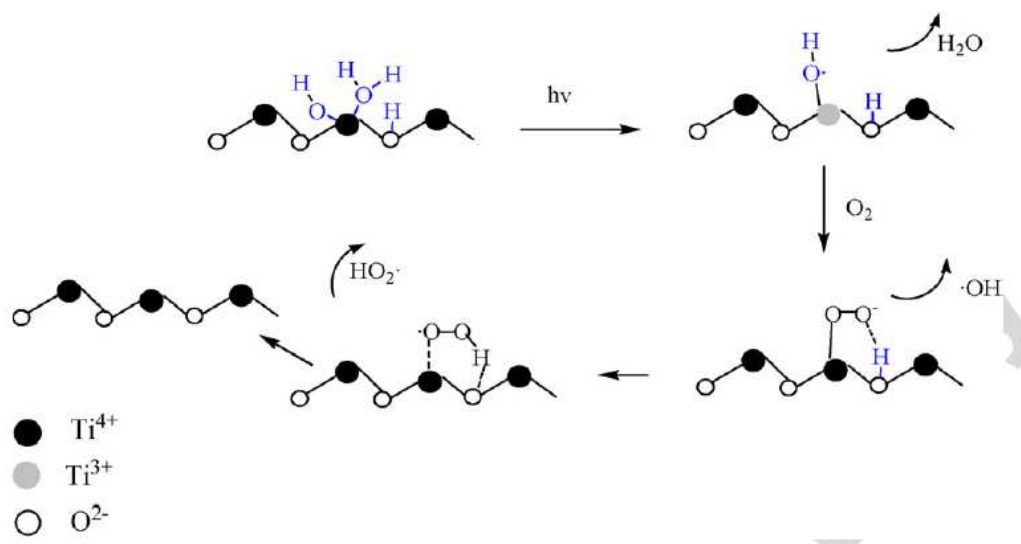
Many toxic and harmful phenols directly or indirectly enter water bodies, soil and atmosphere. This is due to an ever increasing deterioration of environment quality and is threatening to human health and safety. In the scheme of pollution abatement, the effective elimination of these phenols becomes an essential priority [48].

Regarding the serious pollution problems, one of the important tasks is the removal of the pollutants of low concentration from water. Photocatalytic process which contribute significantly in this removal task has the following advantages [49] :

1. Complete oxidation of organic pollutants within a few hours.
2. Without production of polycyclized products.
3. Oxidation of pollutants in ppb range.

The application of catalytic techniques to waste treatment demands a deep knowledge of catalyst surface features, such as surface area, hydroxylation degree, crystallinity or pore size. Additionally, in photocatalytic process, the proximity between adsorption and photoactive centers also determines reaction rate. As adsorption seems to be specific, different molecules can adsorb at different centers. In fact, degradation depends on the molecule interaction as determined by its functional groups. This suggests that the photocatalytic behavior of phenols may not be easily predicted. It has been indicated that certain adsorbates can interact with active centers such as hydroxyl groups or bridging oxygen on TiO<sub>2</sub> surface, resulting in a different catalytic activity [50]. For example, it has been indicated that catechol can adsorb at different centres. Ti<sup>4+</sup> atoms present on the TiO<sub>2</sub> hydrated surface must be completely coordinated by hydroxyl groups and water molecules in an

approximate proportion of 50%. Under these conditions, there are no voids for oxygen fixation. Thus,  $\bullet\text{OH}$  radical formation on  $\text{TiO}_2$  surface can be illustrated as in Scheme (1-1) [50].



Scheme (1-1): The mechanism of  $\bullet\text{OH}$  radical formation on  $\text{TiO}_2$  surface

The first process step would consist of the hydroxyl reaction with photogenerated holes. It has been indicated that strongly basic, isolated hydroxyls are the most photoactive, though photoactivity of other less basic hydroxyls or even adsorbed water molecule is not discarded [50].

It was concluded that the organic molecules possessing donor groups with the highest ionic contribution to bonding adsorb to greatest extent, due to the high ionic properties of  $\text{TiO}_2$  surface. This conclusion was confirmed by many authors whose results have shown a higher percentage of degradation, through the direct ligand to metal charge transfer (LMCT) oxidation process induced by visible light, for 4-chlorocatechol on  $\text{TiO}_2$  surface than for 4-chlorophenol (4-CP), because catechol is adsorbed through two donor groups. While 4-CP is adsorbed only through single hydroxyl group as it is illustrated in Figure (1-6) [6]

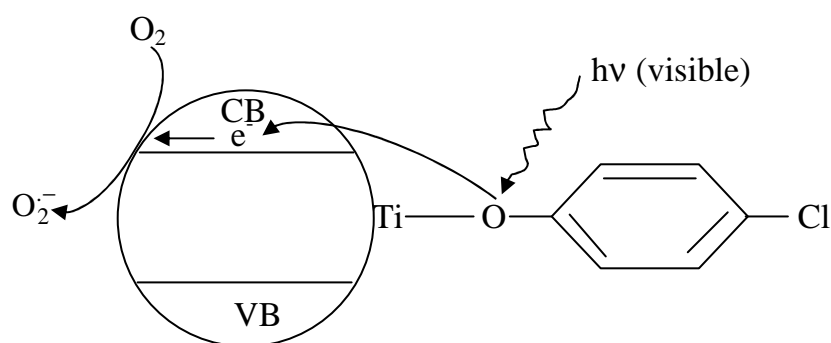


Figure ( 1-6 ): Surface complex mediated photodegradation of 4-CP on pure  $\text{TiO}_2$  under visible light

The primary step of the photocatalytic treatment involves the irradiation of suitable semiconductor particles with light energy greater than the band-gap, with the production of charge carriers (electrons and holes) which can either recombine or migrate to the particle surface where various redox reaction can occur with different species (adsorbed substrate, oxygen and hydroxyl groups, water and dissolved molecules... etc.). These reactions give rise to the production of highly reactive oxidizing or reducing products, in turn capable of attack the organic pollutants [51].

On the other hand, in some surface promoted photocatalytic degradation reaction, oxidation is initiated by direct electron transfer, which generates organic cationic radicals, and not by hydroxyl radical mediated attack. Furthermore, the ring-opening reactions are induced by single electron transfer, in which the hole plays a significant role rather than hydroxyl-type chemistry, as it is illustrated in Figure (1-7). Consequently the reaction of the organic cationic radicals with the superoxide radical species may be responsible for the complete mineralization of aromatic pollutants [6].

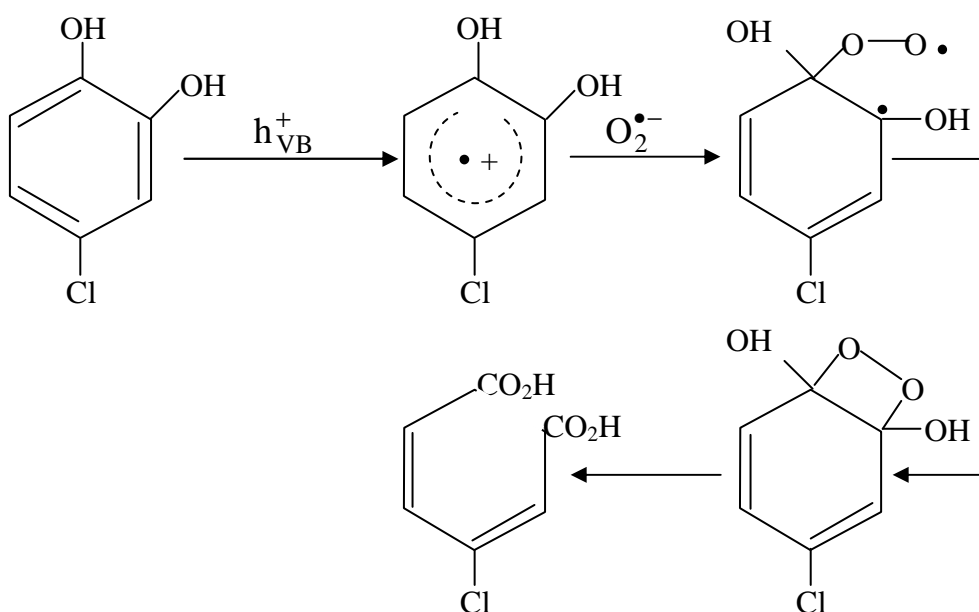


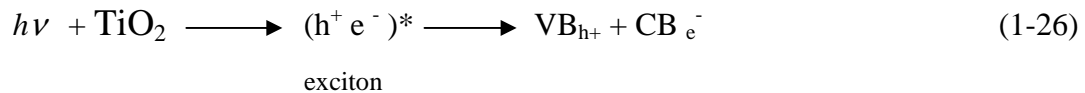
Figure (1-7 ): Single electron transfer mechanism for ring opening of chlorocatechol

pH values are considered as one of the most important parameters in The photocatalytic degradation of phenols in aqueous  $TiO_2$  suspension in which, differences in removal ratio between the best and worst conditions are 26, 40 and 51%, respectively for the three isomers of cresol(ortho, meta and para), while those of nitrophenol are 7, 12 and 12%, respectively under different pH values. It is indicated that the decomposition of both cresols and nitrophenols is affected by pH, and such effect is more significant on cresol [48].

The surface functional groups of  $TiO_2$  in water may be  $TiOH_2^+$ ,  $TiOH$  and  $TiO^-$ , and the  $pH_{zpc}$  of  $TiO_2$  is one of the important factors determining the distribution of surface functional groups. At  $pH > pH_{zpc}$ ,  $TiO^-$  is the predominant species, while  $TiOH_2^+$  plays the role as  $pH < pH_{zpc}$  [48].

## 1.7 Mechanism of exciton formation on TiO<sub>2</sub> surface

In terms of the band theory for electrical conductivity, pure stoichiometric TiO<sub>2</sub> is an insulating oxide with a full valence band and an empty conduction band. TiO<sub>2</sub> absorbs strongly in the ultraviolet (UV) region of the electromagnetic spectrum; anatase at wavelengths < 400nm and rutile at wavelengths < 420nm. Companion and Wyatt [52] reported that absorption edges of 3.23eV and 3.0eV were observed in the reflectance spectra of TiO<sub>2</sub> samples. These values correspond to the band gap energies of anatase and rutile respectively, and represent the photo-induced promotion of electrons from the valence band to the conduction band. In many instances, the electron-hole pair generated by photon absorption does not dissociate immediately, but remains bound in a pre-ionisation state known as an exciton. Excitons can be readily produced by irradiation with light of wavelength close to the tail of the fundamental absorption band. Dissociation of excitons gives rise to mobile electrons and valence holes, which are independent of each other, as represented by the following equation [53]:



Thus, irradiation of TiO<sub>2</sub> with light of wavelength < 400nm, corresponding to an energy equal to, or greater than, the band gap energy, results in an increase in the electron population of the conduction band. Electron-hole pair generation is a non-equilibrium process which cannot occur indefinitely and a steady-state situation soon arises in which the rate of formation of electron-hole pairs equals the rate of their destruction by recombination and trapping processes. Wakim [54] studied the wavelength dependence of the time required for the photocurrent in TiO<sub>2</sub> to saturate and found that it increased with decreasing wavelength. It was proposed that when shorter wavelength light is used, penetration of

photons into the bulk lattice falls due to an increase in electron-hole recombination at the surface.

Recombination of electron-hole pairs can occur in three ways:

- 1) direct recombination, in which an excited electron in the conduction band falls directly to an unoccupied level within the valence band,
- 2) recombination at trap levels, which first capture an excited electron and then electrostatically attract a positive hole and,
- 3) surface recombination, in which the electrons and holes have migrated through the lattice to the surface where they recombine.

The energy generated by electron-hole recombination is dissipated either by photon and/or phonon emissions, or given to a third body in what is termed an Auger recombination [55].

## **1.8 Literature survey**

Advanced oxidation processes deal with the environmental problems stemmed by a broad range of organic pollutants, particularly phenolic contaminants, exploiting the nano  $\text{TiO}_2$  heterogeneous photocatalysis [10]. Phenolics which are aromatic compounds with one or more hydroxyl groups attached to the aromatic ring, are common persistent organic contaminants that pose serious risks to the environment once discharged into natural water, therefore, are considered as EPA's priority pollutants [4, 56]. Sivalingam et al. [47] have reported, in their photocatalytic degradation of phenol, chlorophenols and methylphenols in the presence of synthesized  $\text{TiO}_2$ , that the concentration continuously decreased with time and no intermediate compounds were observed. This trend is in a good accordance with findings of other researchers [9] who studied the photocatalytic degradation of phenols over 40–100 ppm concentration range.

Ahmed et al. [16] and Ibrahim et al. [8] reported that various operating parameters such as photocatalyst type, light intensity, initial concentration, catalyst amount, initial pH of the reaction medium, oxidizing agents/electron acceptors, and the presence of ionic components in solution can significantly influence the photocatalytic degradation rate of pesticides and phenols. Furthermore, González et al. [3] showed a good capability to remove chlorophenols at low pH. However, Lathasree et al. [9] found that the degradation rate of phenol was favourable in the neutral pH range, whereas, the o-chlorophenol and p-chlorophenol were found to undergo degradation at a faster rate at lower pH values. Moreover, experimental results indicated that initial rate of photodegradation increased with increase in catalyst weight up to an optimum loading. Further increase in the catalyst weight showed a negative effect. The degradation of phenols was found to follow first-order kinetics and further, the apparent rate constant values obtained were found to decrease with increase in the initial concentration [9].

## **1.9 Scope of the present work**

in the present work it is intended to investigate several operational parameters such as pH, illumination time, initial concentration of the pollutant, TiO<sub>2</sub> photocatalyst loading, UV light source intensity, added oxidants, nanocatalyst particle size and temperature. Furthermore, a special attention has been given to the characterization of the synthesized nano anatase TiO<sub>2</sub>. The prepared material was characterized by structural (XRD and EDXS), morphological (TEM, BET and SEM) and optical (UV/VIS reflection and Raman) techniques. The kinetic and thermodynamic studies have also been one of the objectives of this research work as well.

## References

- [1]. G. Anna, "Advanced oxidation process for water purification and soil remediation", factually of Chemical and Materials Technology Department of Chemical Engineering ,Tallinn university of technology. thesis on chemistry and chemical engineering. Dissertation was accepted for the commencement of the degree of Doctor of Philosophy in Engineering on March 30, 2005.
- [2]. A. Dixit, A. J. Tirpude, A. K. Mungray, M. Chakraborty, "Degradation of 2,4 DCP by sequential biological-advanced oxidation process using UASB and UV/TiO<sub>2</sub>/H<sub>2</sub>O<sub>2</sub>", *Desalination* 272 (2011) 265-269.
- [3]. L. F. González, V. Sarria, O. F. Sánchez, "Degradation of chlorophenols by sequential biological-advanced oxidative process using *Trametes pubescens* and TiO<sub>2</sub>/UV", *Bioresource Technol.* 101 (2010) 3493–3499.
- [4]. C. M. Teh, A. Mohamed, "Roles of titanium dioxide and ion-doped titanium dioxide on photocatalytic degradation of organic pollutants (phenolic compounds and dyes) in aqueous solutions": A review, *J. Alloy. Compd.* 509 (2011) 1648–1660.
- [5]. M. S. Dieckmann, K. A. Gray, "A comparison of the degradation of 4-Nitrophenol via direct and sensitized photocatalysis in TiO<sub>2</sub> slurries", *Pergamon* 30 (1996) 1169-1183.

- [6]. H. S. Wahab, "Computational study of the induced photocatalytic degradation of the chlorinated aromatic compounds on nanocrystalline TiO<sub>2</sub> particles", Ph. D. thesis, Al-Mustansiriya university, 2006.
- [7]. W. H. Glaze, J. W. Kang, D. H. Chapin, "The chemistry of water treatment involving ozone, hydrogen peroxide and ultraviolet radiation, Ozone: Science & Engineering", The Journal of the International Ozone Association 9 (1987) 335-342.
- [8]. G. U. Ibrahim, A. H. Abdullah, "Heterogeneous photocatalytic degradation of organic contaminants over titanium dioxide: A review of fundamentals, progress and problems", J. Photochem. Photobiol. C: Photochemistry Reviews 9 (2008) 1–12.
- [9]. S. Lathasree, A. N. Rao, B. SivaSankar, V. Sadasivam, K. Rengaraj, "Heterogeneous photocatalytic mineralisation of phenols in aqueous solutions", J. mol. Catal. A: Chemical 223 (2004) 101–105.
- [10]. I. K. Konstantinou, T. A. Albanis, "TiO<sub>2</sub>-assisted photocatalytic degradation of azo dyes in aqueous solution: kinetic and mechanistic investigations A review", Appl. Catal. B: Environmental 49 (2004) 1–14.

- [11]. R. Hu, C. Li, X. Wang, Y. Sun, H. Jia, H. Su, Y. Zhang, "Photocatalytic activities of  $\text{LaFeO}_3$  and  $\text{La}_2\text{FeTiO}_6$  in p-chlorophenol degradation under visible light", *Catal. Comm.* 29 (2012) 35-39.
- [12]. G. Pecchi, P. Reyes, P. Sanhueza, J. Villasenor, "Photocatalytic degradation of pentachlorophenol on  $\text{TiO}_2$  sol-gel catalysts", *Chemosphere* 43 (2001) 141-146.
- [13]. V. Kamat, Dan Meisel, "Nanoparticles in advanced oxidation processes", *Curr. Opin. Colloid. In.* 7 (2002). 282-287.
- [14]. G. Ewelina, R. Joanna, Z. Adriana, "Mechanism of phenol photodegradation in the presence of pure and modified- $\text{TiO}_2$ : A review", *water Res.* 46 (2012) 5453-5471.
- [15]. J. Arana, V. M. Rodriguez Lopez, J. M. Dona Rodriguez, J. A. Herrera Melian, J. P. Pena, "The effect of aliphatic carboxylic acids on the photocatalytic degradation of p-nitrophenol", *Catal. Today* 129 (2007) 185–193.
- [16]. S. Ahmed, M. G. Rasul, R. Brown, M. A. Hashib, "Influence of parameters on the heterogeneous photocatalytic degradation of pesticides and phenolic contaminants in waste water: A short review", *J. Environ. Manage.* 92 (2011) 311-330.

- [17]. R. Chauhan , A. Kumar , R. P. Chaudhary, "Structural and photocatalytic studies of Mn doped TiO<sub>2</sub> nanoparticles", *Spectrochim. Acta Mol. Biomol. Spectros.* 98 (2012) 256–264.
- [18]. Z. Guo, R. Ma, G. Li, "Degradation of phenol by nanomaterial TiO<sub>2</sub> in wastewater", *Chem. Eng. J.* 119 (2006) 55–59.
- [19]. Y. Nosaka, N. Ohta, H. Miyama, "Photochemical kinetics of ultrasmall semiconductor particles in solution: effect of size on the quantum yield of electron transfer", *J. Phys. Chem.* 94 (1990) 3752-3755.
- [20]. P. V. Kamat, "Photochemistry on nonreactive and reactive (semiconductor) surfaces", *Chem. Rev* 93 (1993) 267-300.
- [21]. S. Monticone, R. Tufeu, A. V. Kanaev, E. Scolan, C. Sanchez, "Quantum size effect in TiO<sub>2</sub> nanoparticles: does it exist?", *Appl. Surf. Sci.* 162-163 (2000) 565-570.
- [22]. K. M. Reddy, C. V. Reddy, S. V. Manorama, "Preparation, Characterization, and Spectral Studies on Nanocrystalline Anatase TiO<sub>2</sub> ", *J. Solid State Chem.* 158 (2001) 180-186.
- [23]. L. E. Brus, "A simple model for the ionization potential, electron affinity, and aqueous redox potentials of small semiconductor crystallites", *J. Chem. Phys.* 79 (1983) 5566-5571.

- [24]. L. E. Brus, "Electronic wave functions in semiconductor clusters: experiment and theory", *J. Chem. Phys.* 90 (1986) 2555-2560.
- [25]. K. Sattler, "In Handbook of thin films materials" , H.S. Nalwa, ,Ed, Academic Press, New York, (2002) 61-97.
- [26]. G. B. Sergeev, K. J. Klabunde, " Nanochemistry" , 2nd ed. , Elsevier, 2013, Oxford, UK.
- [27]. A. L. Linsebigler, G. Lu, J. T. Yates, "Photocatalysis on TiO<sub>2</sub> Surfaces: Principles, Mechanisms, and Selected Results", *Chem. Rev.* 95 (1995) 735-758.
- [28]. H. J. Freund, "Clusters and islands on oxides: from catalysis via electronics and magnetism to optics", *Surf. Sci.* 500 (2002) 271-299.
- [29]. L. E. Brus, "Electron–electron and electron hole interactions in small semiconductor crystallites: The size dependence of the lowest excited electronic state", *J. Chem. Phys.* 80 (1984) 4403-4412.
- [30]. A. Foitik, H. Weller, U. Koch, "A. Henglein, Photo-chemistry of colloidal metal sulfides. 8. Photophysics of extremely small CdS particles – Q-state CdS and magic agglomeration numbers" *Chem. Phys.* 88 (1984) 969-977.

- [31]. H. M. Schmidt, H. Weller, "Quantum size effects in semiconductor crystallites: Calculation of the energy spectrum for the confined exciton", Chem. Phys. Lett. 129 (1986) 615-618.
- [32]. Y. Kayanuma, "Quantum-size effects of interacting electrons and holes in semiconductor microcrystals with spherical shape", Phys. Rev. B 38 (1988) 797-805.
- [33]. P. V. Kamat, "Photochemistry on nonreactive and reactive (semiconductor) surfaces", Chem. Rev. 93 (1993) 267-300.
- [34]. L. Brus, "Quantum crystallites and nonlinear optics", Appl. Phys. A 53 (1991) 465-474.
- [35]. M. G. Bawendi, P. J. Carroll, W. L. Wilson, "Luminescence properties of cadmium selenide quantum crystallites: resonance between interior and surface localized states", J. Chem. Phys. 96 (1992) 946-954.
- [36]. M. R. Hoffmann, S. T. Martin, W. Choi, D. W. Bahnemann, "Environmental Application of Semiconductor Photocatalysis", Chem. Rev. 95 (1995) 69-96.
- [37]. Heterogeneous Photocatalysis handbook, vol 3, Wiley series in Photo science and Photo engineering, chap 1.
- [38]. M. A. Fox, M. T. Dulay, "Heterogeneous photocatalysis", Chem. Rev. 93 (1993) 341-357.

- [39]. Photoelectrochemistry , photocatalysis and photoreactors, Fundamentals and developments, M. Schiavello (Ed.) Reidel, Dordrecht, 1985.
- [40]. J. E. Valladares and J. R. Bolton in photocatalysis purification and treatment of water and air; D. F. Ollis and H. Al-Ekabi (Eds.) Elsevier, New York, (1993) 111.
- [41]. J. Jiu, S. Isoda, M. Adachi, F. Wang, "Preparation of TiO<sub>2</sub> nanocrystalline with 3–5 nm and application for dye-sensitized solar cell", Journal of Photochemistry and Photobiology A: Chemistry 189 (2007) 314–321.
- [42]. S. Song, F. Hong, Z. He, Q. Cai, J. Chen," AgIO<sub>3</sub>-modified AgI/TiO<sub>2</sub> composites for photocatalytic degradation of p-chlorophenol under visible light irradiation", J. Colloid. Interf. Sci. 378 (2012) 159–166.
- [43]. D. Chen, Q. Zhu, Z. Lv, X. Deng, F. Zhou, Y. Deng, "Microstructural and photocatalytic properties of Eu-doped mesoporous titanium dioxide nanoparticles by sol–gel method", Mater. Res. Bull. 47 (2012) 3129–3134.
- [44]. M. A. Fox, “ Icosahedral carborane derivatives” Top. Curr. Chem. 142 (1991) 71-77.

- [45]. C. Chen, P. Lei, H. Ji, W. Ma, J. Zhao, "Photocatalysis by Titanium Dioxide and Polyoxometalate/TiO<sub>2</sub> Cocatalysts. Intermediates and Mechanistic Study", *Environ. Sci. Technol.* 38 (2004) 329-337.
- [46]. J. Ryu, W. Choi, "Effects of TiO<sub>2</sub> surface modifications on photocatalytic oxidation of arsenite: the role of superoxides", *Environ. Sci. Technol.* 38 (2004) 2928-2933.
- [47]. G. Sivalingam, M. H. Priya, G. Madras, "Kinetics of the photodegradation of substituted phenols by solution combustion synthesized TiO<sub>2</sub>", *Appl. Catal. B-Environ.* 51 (2004) 67-76.
- [48]. K. H. Wang, Y. H. Hsieh, L. J. Chen, "The heterogeneous photocatalytic degradation, intermediates and mineralization for the aqueous solution of cresols and nitrophenols", *J. Hazard. Mater.* 59 (1998) 251-260.
- [49]. D. F. Ollis, E. Pelizzetti, N. Sperone, in: N. Sperone, E. Pelizzetti (Eds.), "Photocatalysis-fundamentals and applications", Wiley, Chichester (1989) 603.
- [50]. J. Arana, E. P. Melian, V. M. R. Lopez, A. P. Alonso, J. M. D. Rodriguez, O. G. Diaz, J. P. Pena, "Photocatalytic degradation of phenol and phenolic compounds", Part 1. Adsorption and FTIR study, *J. Hazard. Mater.* 146 (2007) 520-528.

- [51]. D. Fabbri, A. B. Prevot, E. Pramauro, "Effect of surfactant microstructures on photocatalytic degradation of phenol and chlorophenol", *Appl. Catal. B-Enviro.* 62 (2006) 21-27.
- [52]. A. L. Companion, R. E. Wyatt; "The diffuse reflectance spectra of some titanium oxides", *J. Phys. Chem. Solids*; 24 (1963) 1025-1028.
- [53]. K. Smallwood, "Catalysis and photocatalysis by platinized titanium dioxide and other catalyst", Thesis submitted to the University of Nottingham for the Degree of Doctor of Philosophy, April, 1993.
- [54]. F. G. Wakim, "Some effects of trapping on the photoelectronic properties of TiO<sub>2</sub> single crystals", *Phys. Status Solidi B* 1 (1970) 479-485.
- [55]. A. K. Ghosh, F. G. Wakim, R. R. Addiss Jr; "Photoelectronic Processes in Rutile", *Phys. Rev.*; 184 (1969) 979-988.
- [56]. K. Naeem, P. Weiqian, F. Ouyang, "Thermodynamic parameters of activation for photodegradation of phenolics", *Chem. Eng. J.* 156 (2010) 505-509.
- [57]. C. G. Hatchard and C. A. Parker, "A New Sensitive Chemical Actinometer II. Potassium Ferrioxalate as a Standard Chemical Actinometer" , *Proc. R. Soc. Lond. A* 1956 235, 518-536 doi: 10.1098/rspa.1956.0102.

- [58]. H. I. Abdullah, "Spectroscopic photochemical studies of some new vanadium (v) Schiff base complexes", College of science Al Mustansiriya university 1997.
- [59]. Z. Tamura, M. Maeda, "Differences between phthaleins and sulfonphthaleins (in Japanese)". *Yakugaku Zasshi* 117 (1997) 764–770.
- [60]. J. C. Yu, L. Zhang, W. Ho, "Enhancing effects of water content and ultrasonic irradiation on the photocatalytic activity of nano-sized TiO<sub>2</sub> powders", *J. photochem. Photobiol. A: Chem.* 148 (2002) 263-271.
- [61]. W. Zhao, Z. Wu, H. Shi, D. Wang, "UV photodegradation of azo dye Diacryl Red X-GRL", *J. Photochem. Photobiol. A: Chem.* 171 (2005) 97-106.
- [62]. E. Vulliet, C. Emmelin, J. M. Chovelon, C. Guillard, J. M. Hermann, "Photocatalytic degradation of the herbicides cinosulfuron in aqueous TiO<sub>2</sub> suspension", *Environ. Chem. Lett.* 1 (2003) 62-67.
- [63]. D. Chen, A. K. Ray, "Photodegradation kinetics of 4- nitrophenol in TiO<sub>2</sub> suspension" *Wat. Res.* 32 ( 1998) 3223-3234.
- [64]. L. Y. Cherif, I. Yahiaoui, F. A. Benissad, K. Madi, N. Benmehdi, F. Fourcade, A. Amrane, "Heat Attachment Method for the

Immobilization of TiO<sub>2</sub> on Glass Plates: Application to Photodegradation of Basic Yellow Dye and Optimization of Operating Parameters, Using Response Surface Methodology", *Ind. Eng. Chem. Res.* 53 (2014) 3813–3819.

[65]. A. M. Asiri , M. S. Al-Amoudi , T. A. Al-Talhi , A. D. Al-Talhi, "Photodegradation of Rhodamine 6G and phenol red by nanosized TiO<sub>2</sub> under solar irradiation", *J. Saudi Chem. Soc.* 15 (2011) 121–128.

[66]. K. M. Oghenejoboh, F. A. Aisien, N. Ihoeghian, "Photocatalytic Degradation of Chlorobenzene in Aqueous Solutions–Comparison of TiO<sub>2</sub> with Periwinkle and Snail Shells' Powder as Photo Catalyst", *British J. Appl. Sci. technol.* 4 ( 2014) 808-822.

[67]. [http://en.wikipedia.org/wiki/Phenol\\_red#cite\\_note-4](http://en.wikipedia.org/wiki/Phenol_red#cite_note-4).

[68]. Y. Zhang , R. Selvaraj , M. Sillanpää , Y. Kim , C. W. Tai, "The influence of operating parameters on heterogeneous photocatalytic mineralization of phenol over BiPO<sub>4</sub> ", *Chem. Eng. J.* 245 (2014) 117-123.

[69]. S. Malato , P. Fernandez-Ibanez , M. I. Maldonado , J. Blanco , W. Gernjak , "Decontamination and disinfection of water by solar photocatalysis: Recent overview and trends", *Catal. Today* 147 (2009) 1-59.

- [70]. P. R. Gogate, A. B. Pandit, "A review of imperative technologies for wastewater treatment I: Oxidation technologies at ambient conditions", *Adv. Environ.al Research*, 8 (2004)501-551.
- [71]. J. Hermann, "Heterogeneous photocatalysis: Fundamentals and applications to the removal of various types of aqueous pollutants", *Catal. Today* 53 (1999) 115-129.
- [72]. Y. Shih, C. Lin, "Effect of particle size of titanium dioxide nanoparticle aggregates on the degradation of one azo dye", *Environ. Sci. Pollut. Res.* 19 (2012)1652-1658.
- [73]. S. Sakthivel, B. Neppolian, M. V. Shankar, B. Arabindoo, M. Palanichamy, V. Murugesan, "Solar photocatalytic degradation of azo dye: comparison of photocatalytic efficiency of ZnO and TiO<sub>2</sub>",*Solar Energy Mater. Solar Cells* 77 (2003) 65-82.
- [74]. M. A. Behnajady, N. Modirshahla, M. Shokri, H. Elham, A. Zeininezhad, "The effect of particle size and crystal structure of titanium dioxide nanoparticles on the photocatalytic properties", *J Environ. Sci. Heal. A* 43 (2008) 460-467.
- [75]. T. Viraraghavan, F. de Maria Alfaro, "Adsorption of phenol from wastewater by peat, fly ash and bentonite", *J. Hazard. Mater.* 57 (1998) 59-70.

- [76]. A. A. Adesina, "Industrial exploitation of photocatalysis: progress, perspectives and prospects" *Catalysis surveys from Asia* 8 (2004) 265-273.
- [77]. L. Andronic, A. Enesca, C. Vladuta, A. Duta, "Photocatalytic activity of cadmium doped TiO<sub>2</sub> films for photocatalytic degradation of dyes", *Chem. Eng. J.* 152 (2009) 64-71.
- [78]. N. Daneshvar, D. Salari, A. R. Khataee, "Photocatalytic degradation of azo dye acid red 14 in water: investigation of the effect of operational parameters", *J. Photochem. Photobiol .A: Chem.* 157 (2003) 111-116.
- [79]. B. Neppolian , H. C. Choi , S. Sakthivel, B. Arabindoo , V. Murugesan, "Solar light induced and TiO<sub>2</sub> assisted degradation of textile dye reactive blue 4", *Chemosphere* 46(2002) 1173-1181.
- [80]. C. H. Chio, C. Y. Wu, R. S. Juang, "Photocatalytic Degradation of Phenol and M-Nitrophenol using Irradiated TiO<sub>2</sub> in Aqueous Solutions", *Separation and purification technol.* 62 (2008)559-564.
- [81]. K. Selvam, M. Muruganandham, I. Muthuvel, M. Swaminathan, "The Influence of Inorganic Oxidants and Metal Ions on Semiconductor

Sensitized Photodegradation of 4-Fluorophenol", Chem. Eng. J. 128 (2007)51-57.

- [82]. Y. Su, L. Deng, N. Zhang, X. Wang, X. Zhu, "Photocatalytic Degradation of C.I. Acid Blue 80 in Aqueous Suspensions of Titanium Dioxide under Sunlight", React. Kinet. Catal. Lett. 98(2008) 228-230.
- [83]. F. H. Hussein "Photochemical Treatments of Textile Industries Wastewater" in "Advances in Treating Textile Effluent" Prof. Peter Hauser (Ed.), Intech publishing company, Croatia, 2011, chapter 6, p.117.
- [84]. S. B. Khan, M. Faisal, M. M. Rahman, K. Akhtar, A. M. Asiri, A. Khan, K. A. Alamry, "Effect of Particle Size on the Photocatalytic Activity and Sensing Properties of CeO<sub>2</sub> Nanoparticles", Int. J. Electrochem. Sci., 8 (2013) 7284-7297.
- [85]. P. Pichat, G. Guillard, C. Maillard, L. Amatric, J. C. Doliveira, in D. F. Ollis and H. El-Ekabi (Eds) "Photocatalytic purification of water and air", Elsevier science publishers B.V., Amsterdam, 1993, p.207.
- [86]. M. Ksibi, A. Zemezmi, R. Boukchina, "Photocatalytic degradability of substituted phenols over UV irradiated TiO<sub>2</sub> ", J. Photochem. Photobiol. A: Chemistry 159 (2003) 61-70.

- [87]. T. Cordero, C. Duchamp, J. M. Chovelon, C. Ferronato, J. Matos, "Influence of Ltype activated carbons on photocatalytic activity of TiO<sub>2</sub> in 4-chlorophenol photodegradation", *J. Photochem. Photobiol. A: Chem.* 191 (2007) 122-131.
- [88]. E. Evgenidou, E. Bizani, C. Christophoridos, K. Fytianos, "Heterogeneous photocatalytic degradation of prometryn in aqueous solution under UV–vis irradiation", *Chemosphere* 68 (2007) 1887-1882.
- [89]. A. Bianco-Prevot, C. Baiocchi, M. C. Brussino, E. Pramauro, P. Savarino, V. Augugliaro, G. Marci, L. Palmisano, "Photocatalytic degradation of acid blue 80 in aqueous solutions containing TiO<sub>2</sub> suspensions", *Environ. Sci. Technol.* 35 (2001) 971-976.
- [90]. C. S. Turchi, D. F. Ollis "Photocatalytic degradation of organic water contaminants: mechanisms involving hydroxyl radical attack" *J. Catal.* 122 (1990)178-192.
- [91]. D. Monllor-Satoca, R. Gomez, M. Gonzalez-Hidalgo, P. Salvador, "The "Direct–Indirect" model: an alternative kinetic approach in heterogeneous photocatalysis based on the degree of interaction of dissolved pollutant species with the semiconductor surface", *Catal. Today* 129 (2007) 247-255.

- [92]. C. Minero, "Kinetic analysis of photoinduced reactions at the water semiconductor interface", *Catal. Today* 54 (1999) 205-216.
- [93]. E. Kusvuran, O. Gulnaz, A. Samil, O. Yildirim, "Decolorization of malachite green, decolorization kinetics and stoichiometry of ozone-malachite green and removal of antibacterial activity with ozonation processes", *J. Hazard. Mater.* 186 (2011) 133-143.
- [94]. B. H. Hameed, T. W. Lee, "Degradation of malachite green in aqueous solution by Fenton process", *J. Hazard. Mater.* 164 (2009) 468-472.
- [95]. M. A. El-Ries, E. Khaled, F. I. Zidane, S. A. Ibrahim, M. S. Abdelmonem "Catalytic spectrophotometric determination of iodide in pharmaceutical preparations and edible salt" *Drug Test. Anal.* 4 (2012) 129-135.
- [96]. T. K. Lau, W. Chu, N. J. D. Graham, "The aqueous degradation of butylated hydroxyanisole by UV/S<sub>2</sub>O<sub>8</sub><sup>2-</sup>: study of reaction mechanisms via dimerization and mineralization", *Environ. Sci. Technol.* 41 (2007) 613-619.
- [97]. Y. T. Lin, C. Liang, J. H. Chen, "Feasibility study of ultraviolet activated persulfate oxidation of phenol", *Chemosphere* 82 (2011) 1168-1172.

- [98]. S. Malato, J. Blanco, M. I. Maldonado, P. Fernandez-Ibanez, A. Campos, "Optimising solar photocatalytic mineralisation of pesticides by adding inorganic oxidising species; application to the recycling of pesticide containers", *Appl. Catal. B: Environ.* 28 (2000) 163-174.
- [99]. S. Lodha, D. Vaya, R. Ameta, P. B. Punjabi, "Photocatalytic degradation of Phenol Red using complexes of some transition metals and hydrogen peroxide", *J. Serb. Chem. Soc.* 73 (2008) 631-639.
- [100]. L. M. A. Fayoumi, M. A. Ezzedine, H. H. Akel, M. M. El Jamal, "Kinetic Study of the Degradation of Crystal Violet by  $K_2S_2O_8$ . Comparison with Malachite Green", *Port. Electrochim. Acta* 30 (2012) 121-133.
- [101]. J. C. Garcia, J. L. Oliveira, A. E. C. Silva, C. C. Oliveira, J. Nozaki, N.E. de Souza, "Comparative study of the degradation of real textile effluents by photocatalytic reactions involving UV/TiO<sub>2</sub>/H<sub>2</sub>O<sub>2</sub> and UV/Fe<sup>2+</sup>/H<sub>2</sub>O<sub>2</sub> systems", *J. Hazard. Mater.* 147 (2007) 105-110.
- [102]. Y. Ding, L. Zhu, J. Yan, "Spectrophotometric determination of persulfate by oxidative decolorization of azo dyes for wastewater treatment", *J. Environ. Monit.* 13 (2011) 3057-3063.
- [103]. D. C. Harris, *Quantitative Chemical Analysis*, 4th Edition, W.H. Freeman and Company, New York, 1995.

- [104]. S. Y. Oh, H. W. Kim, J. M. Park, "Oxidation of polyvinyl alcohol by persulfate activated with heat,  $\text{Fe}^{2+}$ , and zero-valent iron", *J. Hazard. Mater.* 168 (2009) 346-351.
- [105]. X. R. Xu, X. Z. Li, "Degradation of azo dye Orange G in aqueous solutions by persulfate with ferrous ion", *Sep. Purific. Technol.* 72 (2010) 105-111.
- [106]. V. Augugliaro, C. Baiocchi, A. B. Prevot, E. G. Lopez, V. Loddo, S. Malato, G. Marci, L. Palmisano, M. Pazzi, E. Pramauro, "Azo-dyes photocatalytic degradation in aqueous suspension of  $\text{TiO}_2$  under solar irradiation", *Chemosphere*, 49 (2002)1223-1230.
- [107]. G. Anipsitakis, D. Dionysiou, "Degradation of organic contaminants in water with sulphate radicals generated by the conjunction of peroxymonosulphate with cobalt", *Environ. Sci. Technol.* 37 (2003) 4790-4797.
- [108]. M. Movahedi, A. R. Mahjoub, S. Janitabar-Darzi, "Photodegradation of Congo Red in Aqueous Solution on ZnO as an Alternative Catalyst to  $\text{TiO}_2$ ", *J. Iran. Chem. Soc.*, 6 (2009) 570-577.
- [109]. <http://www.chem.ucla.edu/~webspectra/irtable.html>.

- [110]. A. Kathiravan, R. Renganathan, "Effect of anchoring group on the photosensitization of colloidal TiO<sub>2</sub> nanoparticles with porphyrins", *J. Colloid. Interface Sci.* 331 (2009) 401-407.
- [111]. H. S. Wahab, T. Bredow, S. M. Aliwi, "A Computational study on the adsorption and ring cleavage of para-chlorophenol on anatase TiO<sub>2</sub> surface", *Surf. Sci.* 603 (2009) 664-669.
- [112]. H. S. Wahab, T. Bredow, S. M. Aliwi, "Computational modeling of the adsorption and photodegradation of 4-chlorophenol on anatase TiO<sub>2</sub> particles", *J. Molecul. Struct. :THEOCHEM* 863 (2008) 84-90.
- [113]. K. Laidler, J. Meisler, B. Sanctuary "Physical Chemistry" 4th ed., Houghton Mifflin Co., N.Y., 2003, pp.390-394.
- [114]. G. Garsoux, J. Lamotte, C. Geraday, G. Feller, "Kinetic and structural optimization to catalysis at low temperatures in a psychrophilic cellulase from the Antarctic bacterium *Pseudoalteromonas haloplanktis*", *Biochem. J.* 384 (2004) 247–253.
- [115]. T. Lonhienne, C. Gerday, G. Feller, "Psychrophilic enzymes : revisiting the thermodynamic parameters of activation may explain local flexibility", *Biochim. Biophys. Acta* 1543 (2000) 1-10.

- [116]. X. Fu, L. A. Clark, W. A. Zeltner, M. A. Anderson, "Effects of reaction temperature and water vapor content on the heterogeneous photocatalytic oxidation of ethylene", *J. Photochem. Photobiol. A: Chemistry* 97 (1996) 181–186.
- [117]. E. T. Soares, M. A. Lansarin, C. C. Moro, "A study of process variables for the photocatalytic degradation of Rhodamine B", *Braz. J. Chem. Eng.* 24 (2007) 29-36.

# Chapter Three

## Results and Discussion

### 3.1 UV-VIS spectroscopic feature of phenol red

The model phenolic dye pollutant, phenol red, whose chemical structure is shown in Figure (3-1), has been scanned UV-VIS spectrophotometrically in the range 200-1100 nm (Figure 3-2).

The molar extinction coefficient (absorptivity,  $\epsilon$ ) of 10 and 20 ppm of phenol red in NFDW was measured at the maximum absorption wavelength, 432 nm, using Beer-lambert equation ( $A = \epsilon bc$ ), where  $A$  = absorbance,  $b$  = absorption light path, 1 cm,  $c$  = molar concentration of phenol red. The absorptivity ( $\epsilon$ ) has been  $0.1258 \times 10^5 \text{ mol}^{-1} \cdot \text{L} \cdot \text{cm}^{-1}$  and  $0.1197 \times 10^5 \text{ mol}^{-1} \cdot \text{L} \cdot \text{cm}^{-1}$  for molar concentrations of  $2.822 \times 10^{-5}$  and  $5.644 \times 10^{-5}$  mole/L, respectively.

Figure (3-3) presents typical UV-VIS spectra of three absorption bands located at 263, 432 and 590 nm. The main two visible region bands (432 and 590nm) are impacted by the pH of the media, where in crystalline form, and in solution under very acidic conditions (low pH), the phenol red exists as a zwitterion as in the structure shown below (Figure 3-1), with the sulfate group negatively charged, and the ketone group carrying an additional proton. If the pH is increased ( $pK_a = 1.2$ ), the proton from the ketone group is lost, resulting in the yellow color phenol red. At still higher pH ( $pK_a = 7.7$ ), the phenol's hydroxide group loses its proton, resulting in the red color phenol red. Figure (3-3) shows the standard UV-VIS scan for phenol red at different pH [59].

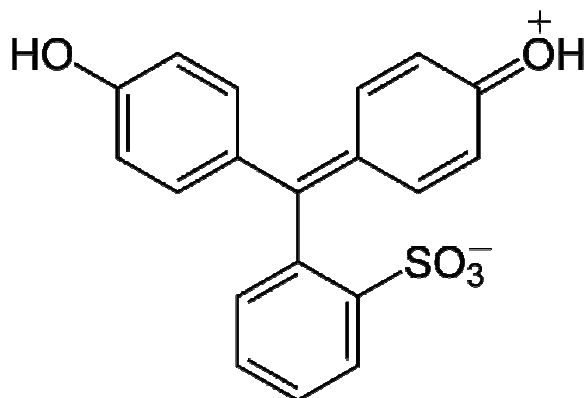


Figure (3-1): Chemical structure of phenol red

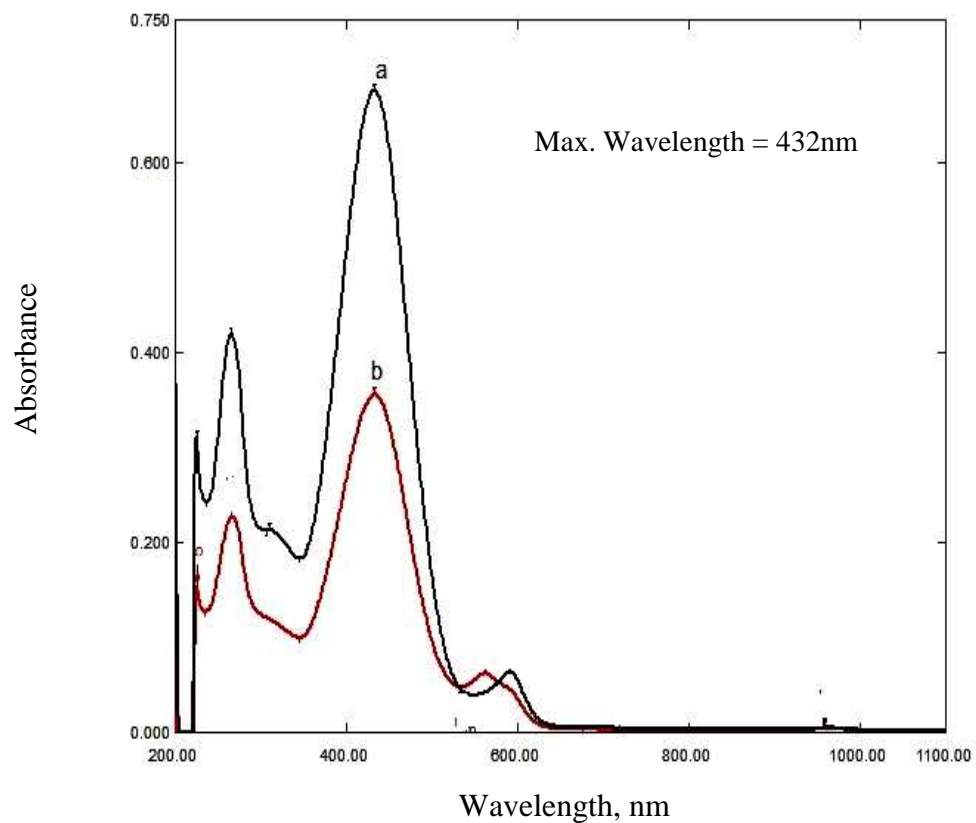


Figure (3-2): UV-VIS spectrum of phenol red; (a) 20 ppm (b) 10 ppm

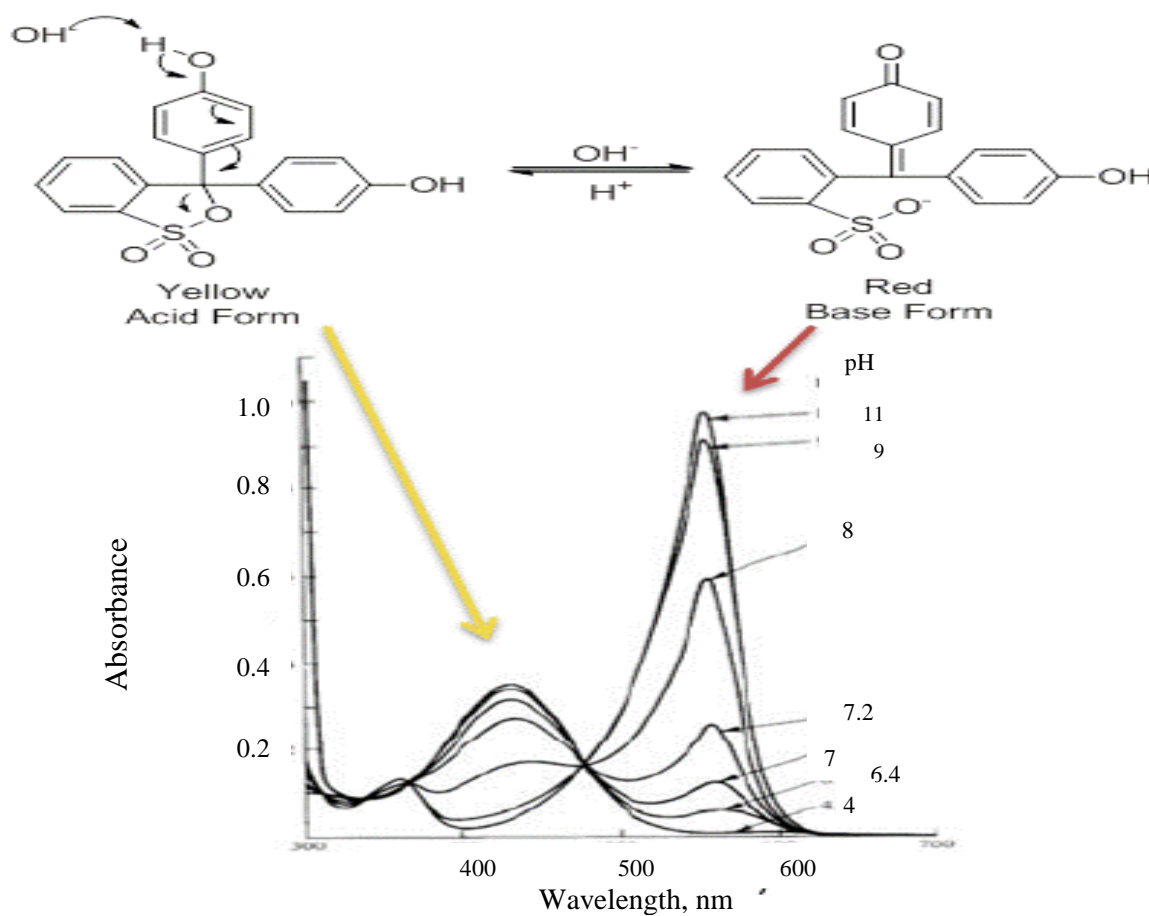


Figure (3-3): Standard scan of phenol red at different pH values

When the pH of the scanned solution is  $\approx 5$ , the peak at 432 nm has been at highest intensity (Figure 3-2), whereas, with increasing the pH of solution there are increasing in the intensity of the peak at 590 nm and decrease in peak intensity at 432 nm (Figure 3-3), due to the keto structure formation which consequently leads to the red shift (higher wavelength).

The calibration (standard) curve for phenol red has been drawn (Figure 3-4) using various standard solutions ranged from 3 to 15 ppm measured at the optimum (maximum) wavelength.

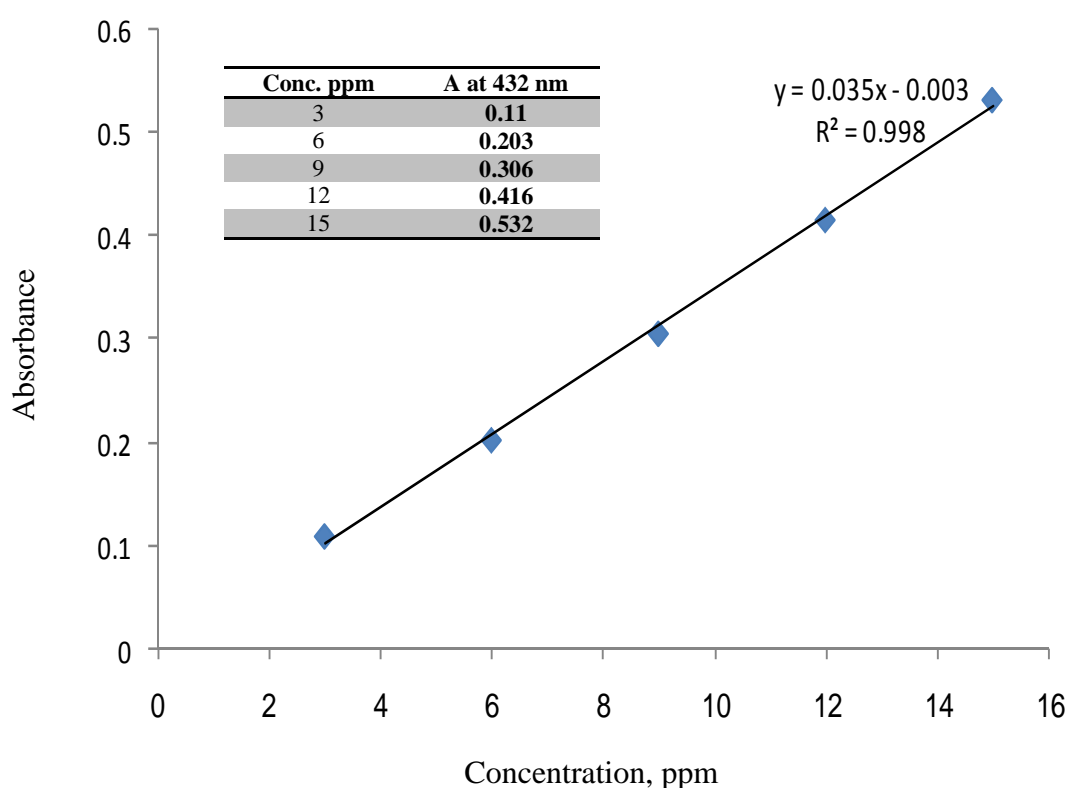


Figure (3-4): Calibration curve for phenol red together with the inset which presents the absorbances at relevant concentrations

## **3.2 Characterization of the synthesized nano anatase TiO<sub>2</sub> particles**

### **3.2.1 Surface morphology**

The surface morphology of anatase nano TiO<sub>2</sub> was characterized by a cold field emission high resolution scanning electron microscope (SEM). Some micrographs at different magnifications with very smooth and homogeneous surfaces are shown in Image (3-1). The shape of the particles is very similar.

The surface has also been explored by high resolution Scanning Transmission Electron Microscope (STEM) for nanoscale analysis. The nanocrystals have an irregular spherical shape and excellent dispersivity (Image 3-2). On the other hand it should be noted that the necking regions between the particles are benefit for the formation of network structure as observed in SEM and TEM images which is expected to be advantageous for the transport of electron in the skeleton [41]. Based on the above results, we may report here that the relatively low calcination temperature (400 C<sup>o</sup>) is beneficial in preserving the particle size at nano scale.

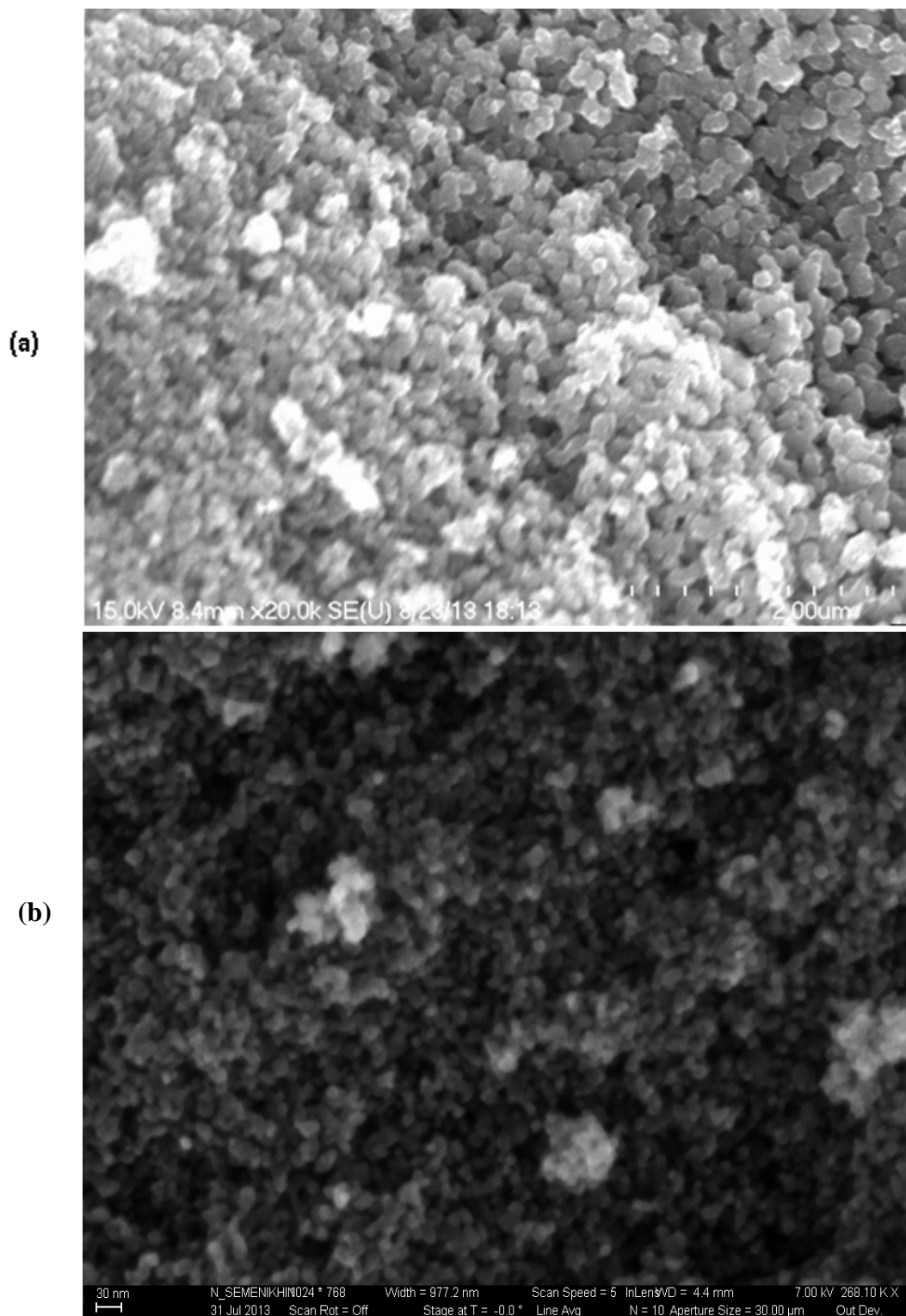


Image (3-1): Scanning Electron Microscope (SEM) micrographs anatase  $\text{TiO}_2$  with different magnifications; (a) 200 $\mu\text{m}$  (b) 30 nm

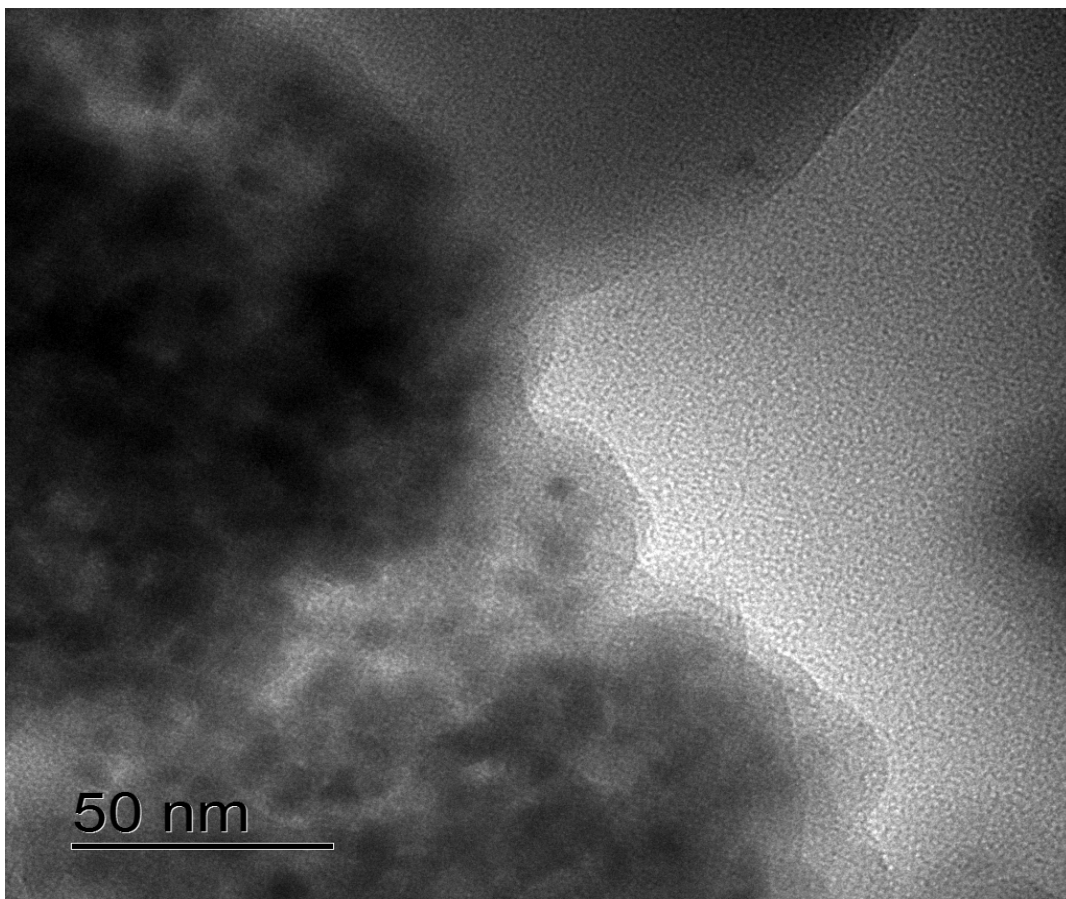


Image (3-2): Transmission Electron Microscope (TEM) micrograph of nano anatase TiO<sub>2</sub> particles

### 3.2.2 Energy and composition perspectives

Ground state diffused reflectance absorption spectra of solid powder for both the standard nanopowder anatase TiO<sub>2</sub> reference specimen and synthesized nanopowder anatase TiO<sub>2</sub> were measured. Figure (3-5) depicts explicitly the excellent accordance of absorption thresholds for both the reference and synthesized specimen at 350 nm which subsequently refer to band gap energy (E<sub>g</sub>) of 3.4 eV.

The X-ray diffraction (XRD) patterns of the nanoparticles that are presented in Figure (3-6) obtained on x-ray diffractometer using Cu K $\alpha$  radiation (0.15425 nm) in the range of  $2\theta$  from 20 to 40 with scan rate of  $2\theta = 0.10 \text{ s}^{-1}$ . These patterns were used to determine the identity of any phase present. Diffraction signal assigned to the anatase (101) structure at  $25.3^\circ$  ( $25.7^\circ$ - $25.8^\circ$  in this work) is clearly observed in TiO<sub>2</sub> [41]. The diffraction signal at  $27.5^\circ$  due to the rutile

phase (110) is not observed in TiO<sub>2</sub> powder. On the basis of the above findings, one can conclude that the absence of the diffraction due to the rutile phase in synthesized TiO<sub>2</sub> nano powder proved that the calcination at 400° might be the appropriate temperature for anatase TiO<sub>2</sub> preparation.

For further scrutinization, Raman measurements have also been performed. Figure (3-7) exhibits a clear matching between the spectra of prepared nano anatase TiO<sub>2</sub> (Figure 3-7b) and the reference specimen (Figure 3-7a). The Raman spectra were obtained with an argon-ion laser operating at 4880 Å and 5145 Å with incident power 50 mW. Light scattered at 90° to the incident beam was passed through a double-grating monochromator and detected photoelectrically. Moreover, the wavelength calibration was made using the neon and mercury emission lines.

Prior to the application of the synthesized anatase nano powder on the photo decomposition process of a model pollutant, Phenol Red, the composition of the synthesized nano anatase TiO<sub>2</sub> was verified using Energy Dispersive X-ray Spectrometer (EDXS). The spectra shown in Image (3-3b) for the prepared nano anatase TiO<sub>2</sub> is to an excellent extent similar to that of reference sample which is shown in Image (3-3a).

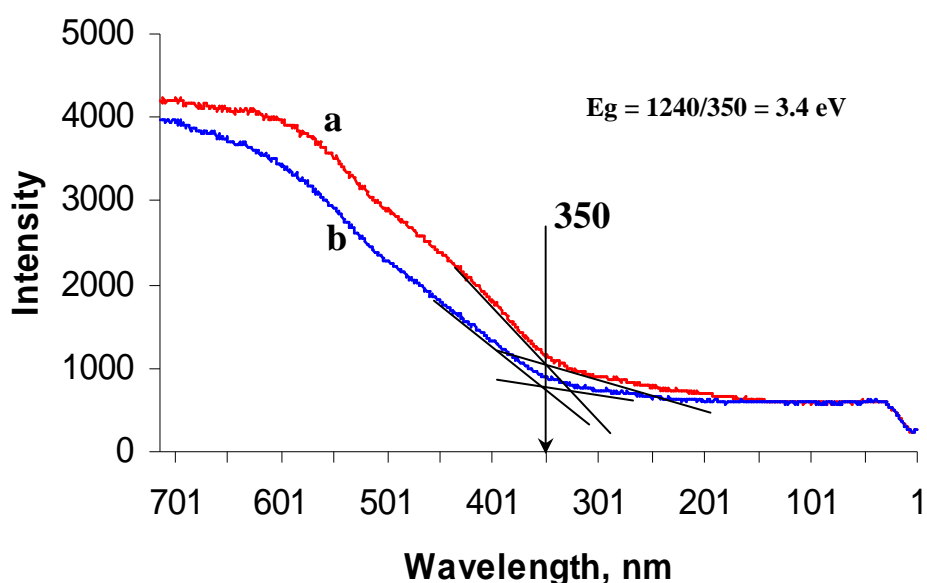


Figure (3-5): Diffused reflectance UV-VIS absorption threshold for  
 (a) standard nanopowder anatase TiO<sub>2</sub> reference specimen;  
 (b) synthesized nanopowder anatase TiO<sub>2</sub>

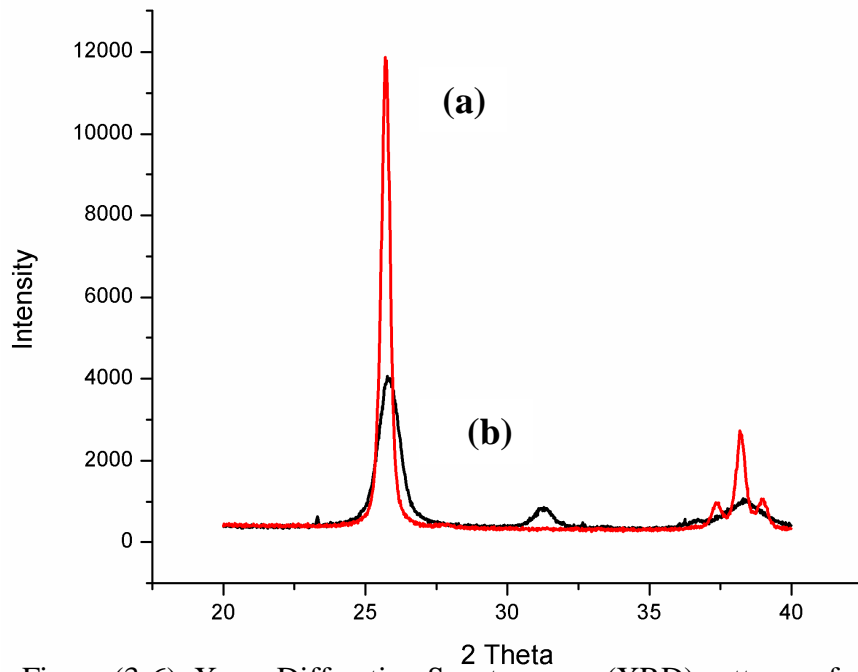


Figure (3-6): X-ray Diffraction Spectroscopy (XRD) patterns of (a) standard nanopowder anatase TiO<sub>2</sub> reference specimen; (b) synthesized nanopowder anatase TiO<sub>2</sub>

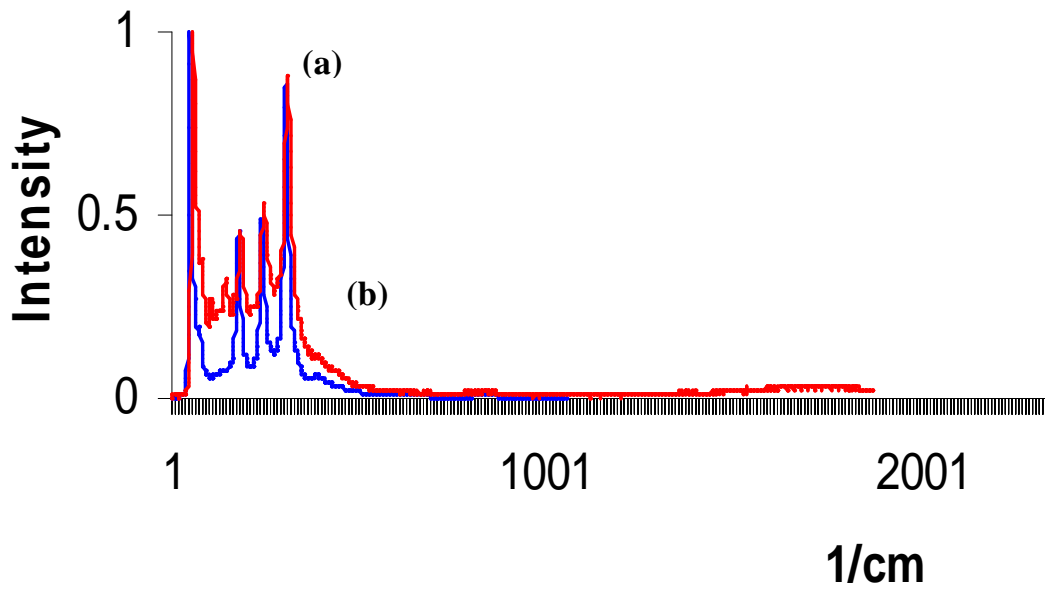


Figure (3-7): Raman spectra for (a) standard nanopowder anatase TiO<sub>2</sub> reference specimen; (b) synthesized nanopowder anatase TiO<sub>2</sub>

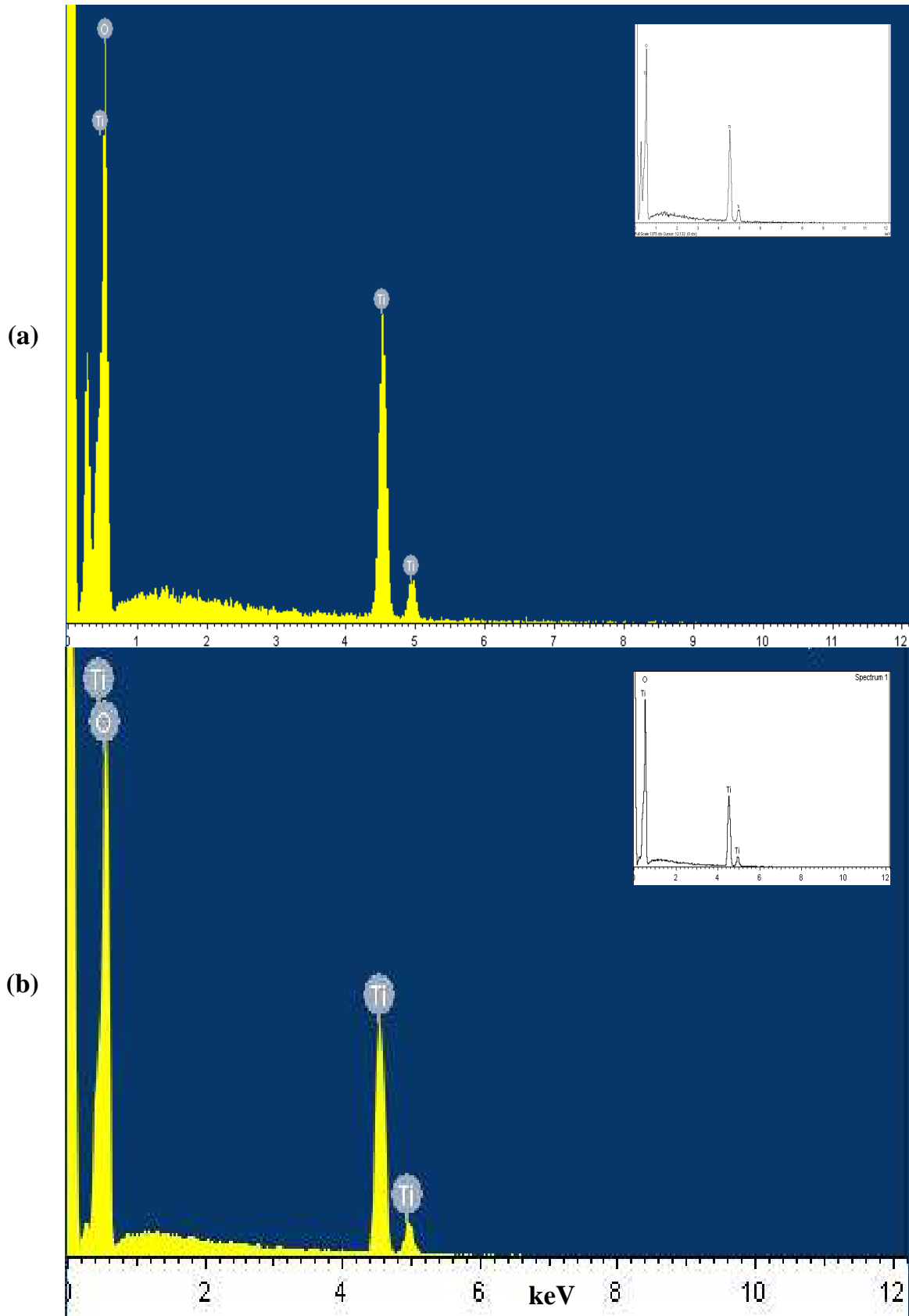


Image (3-3): Energy Dispersive X-ray Spectroscopy (EDXS) image of  
(a) standard nanopowder anatase  $\text{TiO}_2$  reference specimen;  
(b) synthesized nanopowder anatase  $\text{TiO}_2$

### 3.2.3 Surface area, pore size and particle size aspects

The surface area and pore size of the synthesized anatase TiO<sub>2</sub> nanoparticles are measured employing (BET) methodology. Figure (3-8a) illustrates the adsorption-desorption isotherm plot which results in surface area of 48 m<sup>2</sup>/g. Further, Figure (3-8b) shows the maxima at pore size of 3.7 nm, which indicates the mesoporosity of the prepared nano anatase TiO<sub>2</sub> particles. Ya et al. [60] reported in their study about the photocatalytic activity of nano-sized TiO<sub>2</sub> powders that the mesoporous pores (0.2-50 nm) allow rapid diffusion of various reactants and products during photocatalytic reaction and consequently enhance the speed of photocatalytic reaction.

Image (3-4) exhibits the approximate particle size (11nm) of the meso- porous TiO<sub>2</sub> which was measured by SEM. TEM was also used to investigate the size of the sol-gel synthesized nano anatase TiO<sub>2</sub>. A small amounts of dry powder was dispersed in ethanol by ultrasonic agitation. Two droplets of the suspension were placed on a carbon-coated copper grid and analysed by means of field emission gun microscope. Image (3-5) presents the average particle size of 9 nm, which is in accordance with that measured by SEM (Image 3-4).

The average grain size was also calculated employing Sherrer's equation using the XRD line broadening method [29]. The crystal size  $D = 0.9 \lambda / (\beta \cos \theta)$ ; where  $\lambda$  represents the wavelength of X-ray,  $\beta$  the FWHM and the  $\theta$  diffraction angle. By using the experimental data, an average grain size of 9.95 nm was derived. The peak width inversely proportional with particle size in which by increasing the peak width the size of nano TiO<sub>2</sub> decreases. Accordingly, a closer look at (Figure 3-6) confirms this phenomenon in which the synthesized nano TiO<sub>2</sub> band (Figure 3-6b) shows more broadening than the reference TiO<sub>2</sub> band (Figure 3-6a) whose grain size is consequently ( $\approx 25$  nm) higher than that of the prepared nano TiO<sub>2</sub> (9.95 nm). Based on the above results, the value determined from XRD (9.95 nm) is an excellent agreement with the average particle size derived from TEM analysis (9 nm).

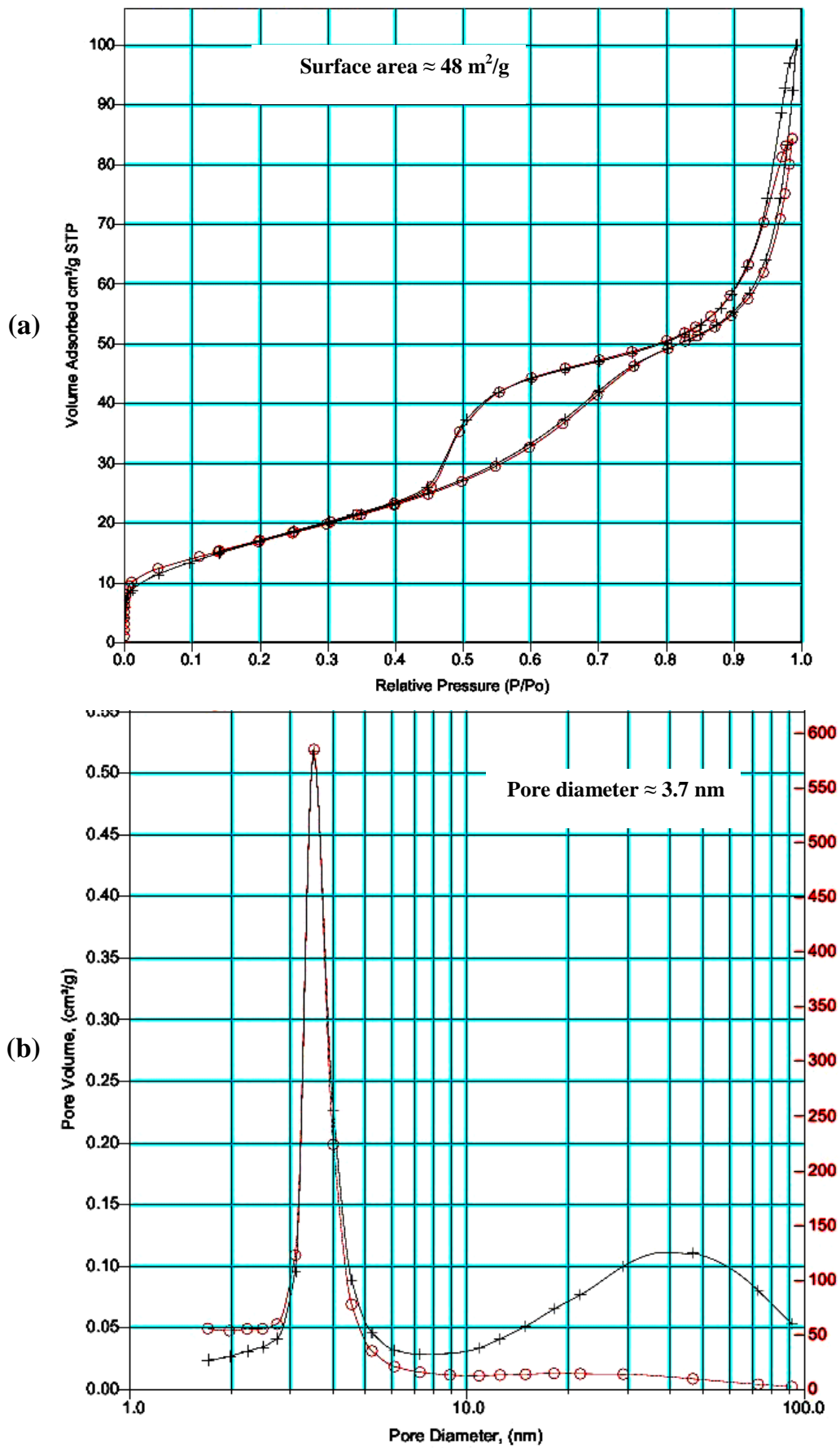


Figure (3-8): BET measurements for nano anatase  $\text{TiO}_2$  ;  
 (a) Isotherm plot ; (b) pore size plot

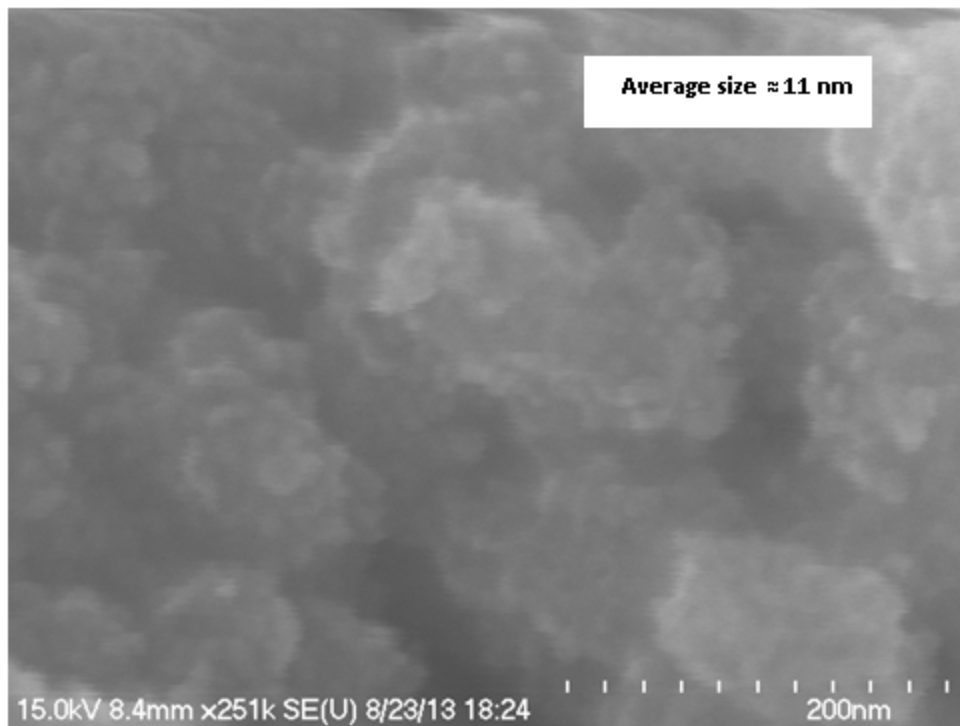


Image (3-4): Scanning Electron Microscope (SEM) micrographs anatase TiO<sub>2</sub>

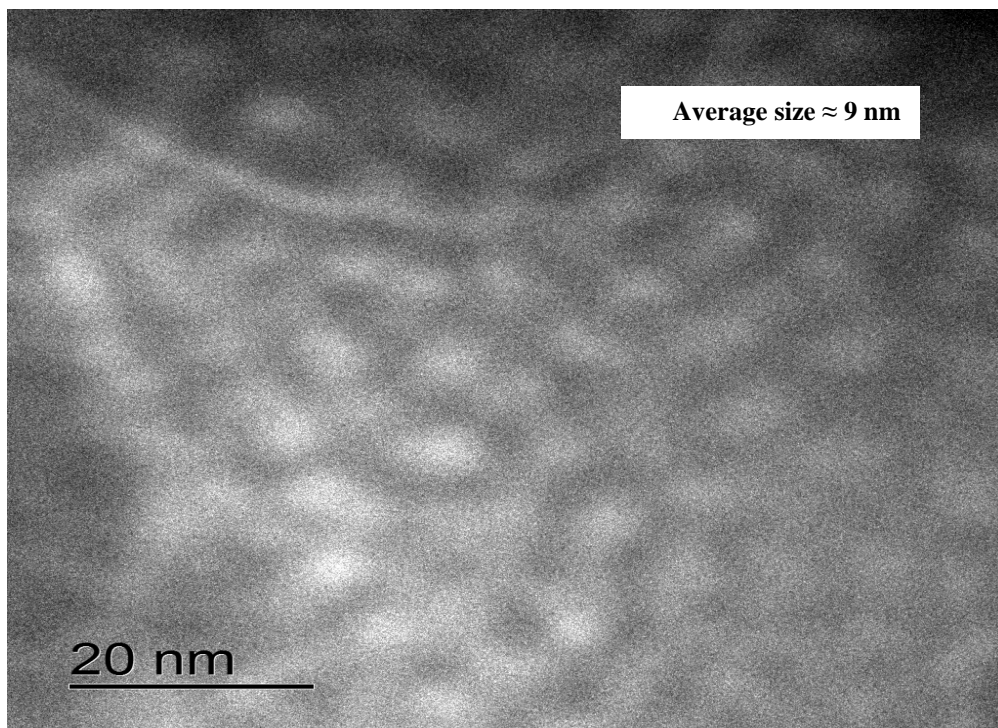


Image (3-5): Transmission Electron Microscope (TEM) image of nano anatase TiO<sub>2</sub> particles

### 3.3 Control experiments

Prior to employment of synthesized nano anatase  $\text{TiO}_2$  for the photodecolorization of phenol red, a series of control experiments were carried out since some phenolic dyes are degraded by direct UV illumination [61] and further, to check parameters that primarily influence the process. To eliminate the effects of adsorption, the reaction solution was magnetically agitated for 3 hours with samples collected and analyzed by means of a visible spectrophotometer regularly. One set was performed with phenol red solution exposed to  $\text{TiO}_2$  without UV light irradiation (in dark). The second set was implemented by exposing phenol red to UV light source with absence of  $\text{TiO}_2$  photocatalyst. The last set was accomplished in the presence of UV light and  $\text{TiO}_2$  semiconductor, which represents the photocatalysis circumstances. As shown in Figure(3-9), a very small change in the concentration of phenol red was observed when only UV light is present or when only  $\text{TiO}_2$  is used in dark. However, phenol red could be degraded quickly by UV source illuminated  $\text{TiO}_2$ . Accordingly, these experiments demonstrated that both UV irradiation and the  $\text{TiO}_2$  photocatalyst are needed for the effective photolysis of phenol red dye. This conclusion was also reported by several researchers for different phenolic pollutants [56,62-63].

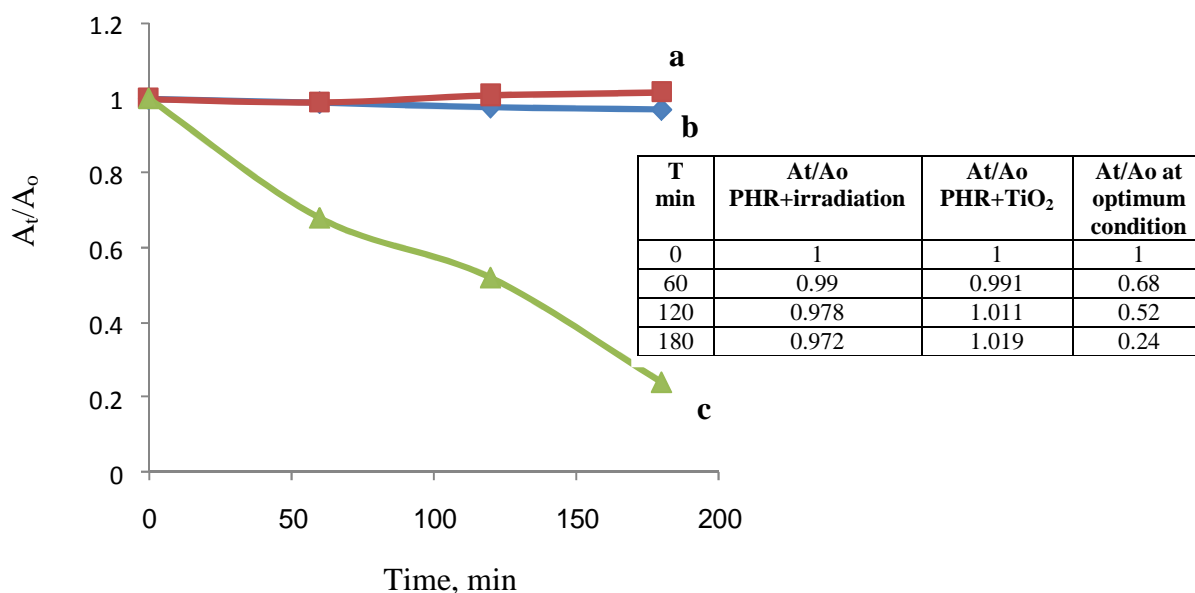


Figure (3- 9): The relative decrease in absorption intensity of phenol red as a function of irradiation time: (a) TiO<sub>2</sub> in dark; (b) UV irradiation in absence of TiO<sub>2</sub>; (c) UV illumination in presence of TiO<sub>2</sub>

### 3.4 Experimental optimization of photocatalysis parameters

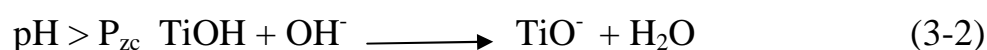
The rate of photocatalysis and degradation yield are normally impacted by several operational parameters namely, pH of photolysis media, TiO<sub>2</sub> dosage, initial dye concentration, light source intensity, photocatalyst particle size, type and occurrence of the oxidants....etc. These experimental variables play a significant role in the optimization of the photodegradation process via various chemical and physical phenomena based on the properties of the dye moiety and the type of photocatalyst.

#### 3.4.1 Effect of varying the pH on the rate of photocatalysis

An important parameter in the photocatalytic reactions taking place on particulate surfaces is the pH of the solution, since it dictates the surface charge properties of the photocatalyst, can play a key role in the adsorption and photocatalytic oxidation of organic molecules and size of aggregates it forms [8]. Cherif et al. [64] have reported that the point of zero charge (pzc) of the TiO<sub>2</sub> has been at pH 6.5 and, hence, TiO<sub>2</sub> surface is positively charged in acidic

medium (pH <6.5) and negatively charged in alkaline medium (pH >6.5). On the other hand, Asiri and his collaborators [65] stated that phenol red molecule exists in different molecular structures with different charge distribution (Figure 3-10) depending on the pH of the solution. Whereas, Tamura and Maeda [59] have stated that the phenol red in crystalline form and in solution under acidic conditions (low pH), the compound exists as a zwitterion as in the structure (b) , with the sulfate group negatively charged, and the ketone group carrying an additional proton. This form is sometimes symbolically written as  $H_2^+PS^-$  and is orange-red. If the pH is increased, the proton from the ketone group is lost, resulting in the yellow negatively charged ion denoted as  $HPS^-$  as in the structure (a). At still higher pH, the phenol's hydroxide group loses its proton, resulting in the red ion denoted as  $PS^{2-}$  as in the structure (c). Therefore, pH changes can influence the adsorption of phenol red dye molecules onto the  $TiO_2$  surfaces, an important step for the photocatalytic oxidation to take place. In order to optimize the pH of the phenol red degradation process, experiments were conducted with pH range 2-8 at a fixed catalyst dosage of 0.5 g/l and initial dye concentration of 10 ppm. We observed that phenol red degradation was favorable at mild acidic solution (pH=4.5) as shown in Figure (3-11). Accordingly, on the basis of this result, pH of 4.5 was taken as the optimum pH for the optimization processes. Similar results were reported by Asiri et al. [65] for the maximum photodegradation of phenol red on  $TiO_2$  under solar irradiation at value of pH that included in 4.4 and Oghenejoboh et al. [66] in their study of the photodegradation of chlorobenzene at pH=3 on  $TiO_2$ .

The surface functional groups of  $TiO_2$  in water may be  $TiOH_2^+$ ,  $TiOH$  and  $TiO^-$ . At  $pH > pH_{zpc}$  ,  $TiO^-$  is the predominant species, while  $TiOH_2^+$  plays the role as  $pH < pH_{zpc}$  according to the following reactions [4, 53]:



Wang et al. [48] have reported that the state of the chemical species presented in water is not affected only by pH, but is also closely related to the dissociation constant of the species. When pH is lower than the  $pK_a$  of the species, it primarily presents in molecular state, whereas, at pH greater than the  $pK_a$  it exists as ionic state. The  $pH_{zpc}$  of  $TiO_2$  used in this study is about 6.5 and the  $pK_a$ 's phenol red is 8 [67].

Accordingly, under moderate acidity conditions ( $pH=4.5$ ) and based on above debate, we predict that  $TiOH_2^+$  is the predominant species for  $TiO_2$  and the structure (a) of phenol red is the primary species, which contributes appreciably in the elevation of the amount of adsorption and as a result, enhances the degradation rate.

Figure (3-12) which reveals the influence of pH variation on the degradation percentage of phenol red, follows similar trend of pH impact on reaction rate (Figure 3-11), in which the degradation rate and yield are relatively low in  $pH < 4.5$ . This could be ascribed to the well known agglomeration phenomenon of the  $TiO_2$  particles under acidic conditions and consequently, the surface area available for dye adsorption and photon absorption would be reduced [38].

Based on the above outcomes, we conclude that the optimum value of photodegradation is found to be at pH 4.5 for phenol red, due to a strong adsorption of the phenol red on  $TiO_2$  as a result of the electrostatic force attraction of the positively charged  $TiO_2$  with the fully ionized sulfonic group (structure a).

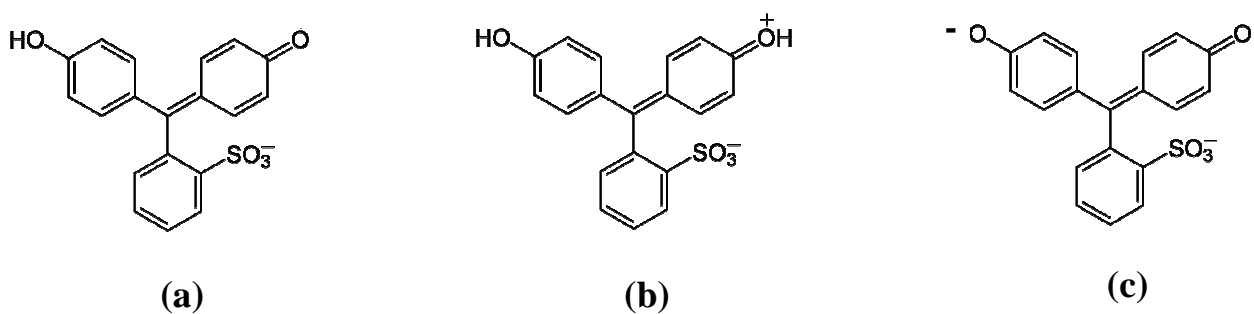


Figure (3-10): Variation of phenol red molecular structure at different pH values; (a) low pH; (b) moderate pH : (c) high pH

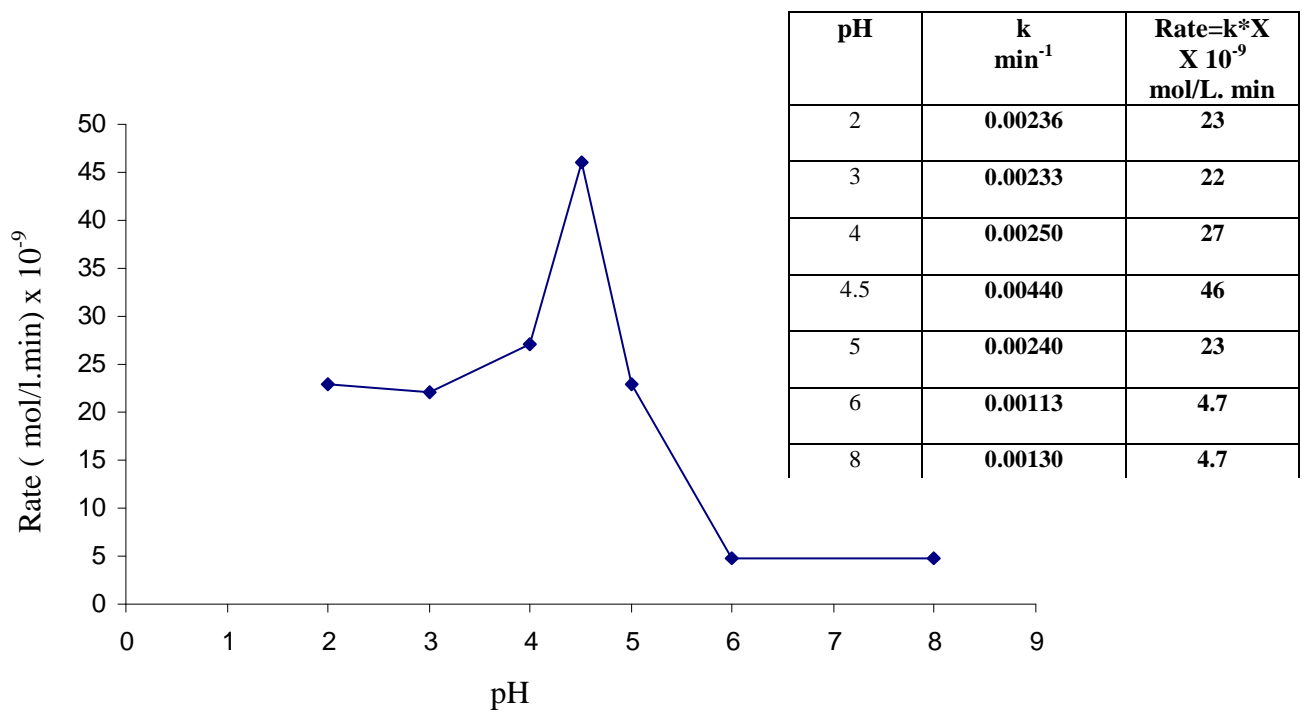


Figure (3-11): Effect of pH variation on the rate of photocatalysis of phenol red

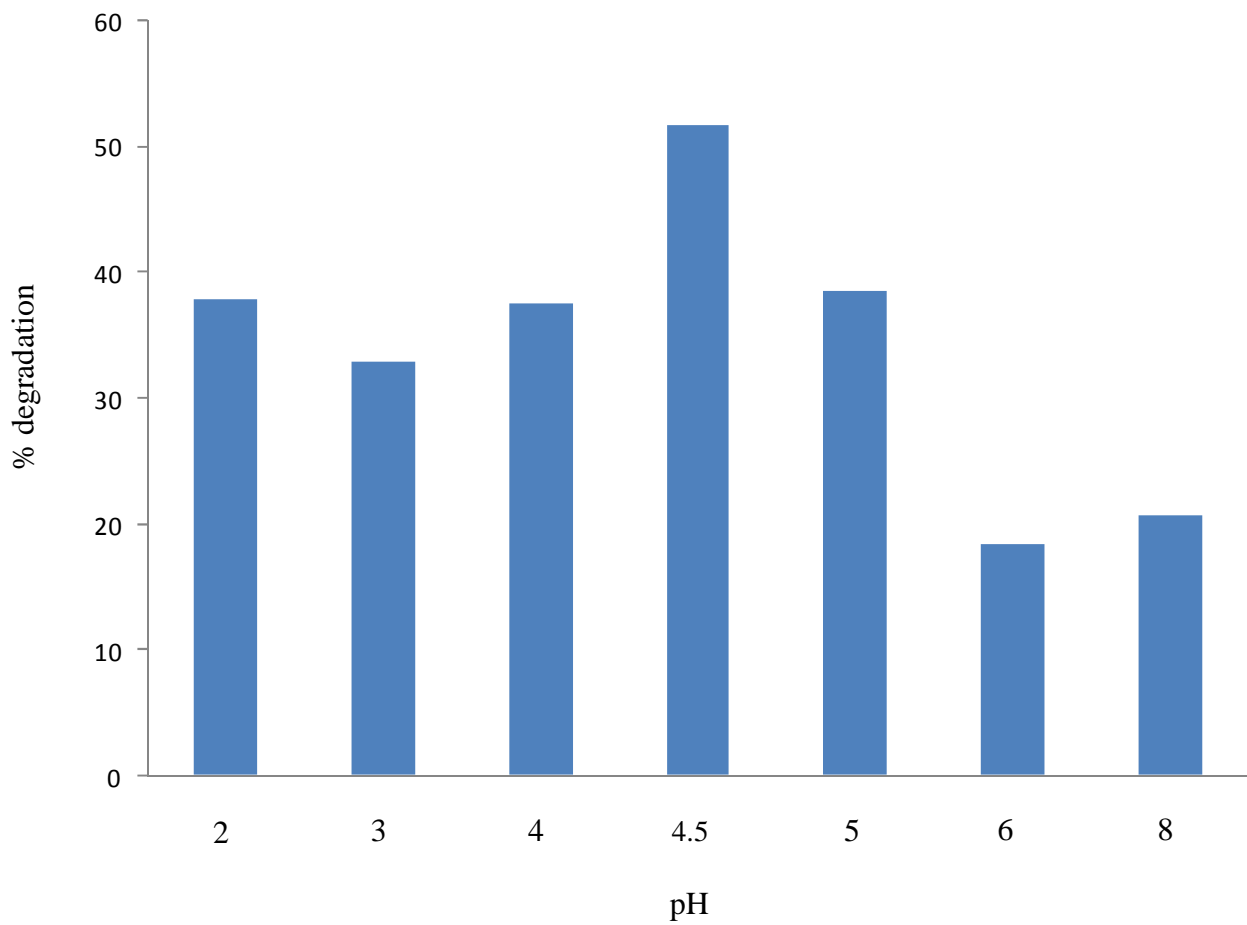


Figure (3-12): Effect of pH variation on the degradation yield of phenol red

### 3.4.2 Influence of nano anatase TiO<sub>2</sub> loading

The loading amount of catalyst is a significant factor in the photocatalytic degradation process, because the efficiency could be strongly affected by the number of active sites and photo-adsorption ability of the catalyst used, as extensively demonstrated in previous studies [68,9].

Furhermore, Malato and his collaborators [69] have stated that in any given application, this optimum catalyst mass has to be found in order to avoid excess catalyst and ensure total absorption of efficient photons.

Therefore a TiO<sub>2</sub> load ranging from 10 to 100 mg was used to investigate its influence on the photocatalytic degradation rate and degradation yield of phenol red and find out the optimal loading amount. Figure (3-13) reveals the variation in degradation rate of phenol red against the dosage of nano anatase TiO<sub>2</sub>. The results obtained support the behavior described by some authors [70-71]. These studies evaluate the increase in reaction rate with catalyst loading as evidence that the process is photoactivated. The enhancement of the photodegradation rates was observed from Figure (3-13) with the increase of TiO<sub>2</sub> dosage from 10 to 40 mg (0.13 to 0.53 g/l). This direct proportional of initial reaction rates with catalyst loading is indicating evidently the heterogeneous regime [72]. However, a further increase in loading amount had negative effect on the photocatalytic degradation of phenol red. This outcome is in a good accordance with most of studies in the literature which reported enhanced degradation rates for TiO<sub>2</sub> catalyst loading up to 400–500 mg/l [10,73] This can be attributed to the fact that increased number of TiO<sub>2</sub> particles will increase the availability of active sites of TiO<sub>2</sub> surface and number of photons absorbed. Beyond the optimal limiting value of TiO<sub>2</sub> loading (40 mg), the dropping in the photo-degradation rate mainly results from following two factors [63] (a) aggregation (particle-particle interaction) of TiO<sub>2</sub> particles at high loadings, causing a decrease in the number of surface active sites, and (b) increase in opacity and light scattering of

TiO<sub>2</sub> particles leading to a decrease in the passage of irradiation through the sample. In addition, the decreased penetration of UV light irradiation in a high TiO<sub>2</sub> loading attributable to light scattering and screening could result in the reduction of TiO<sub>2</sub> specific activity, and this approach is consistent with the observation by Behnajady et al. [74]. The final degradation percent and photomineralization rate were compared as a function of loading amount. The trend in Figure (3-14) clearly shows that the loading of photocatalyst (TiO<sub>2</sub>) has a similar influence on phenol red degradation rate and yield. The explanation could be that the adequate photocatalyst particles increased the generation of electron/hole pairs, and thus the affluent formation of OH radicals, resulting in enhanced photodegradation rate and yield [68]. Yet a further increase in the dosage of TiO<sub>2</sub> exhibited a negative influence on the photocatalytic degradation yield and rate of phenol red. The screening effect of the suspended particles is the main cause of this phenomenon, because the overloaded photocatalyst particles may reduce the incident light intensity by reflection, despite the large number of active sites present [75-76].

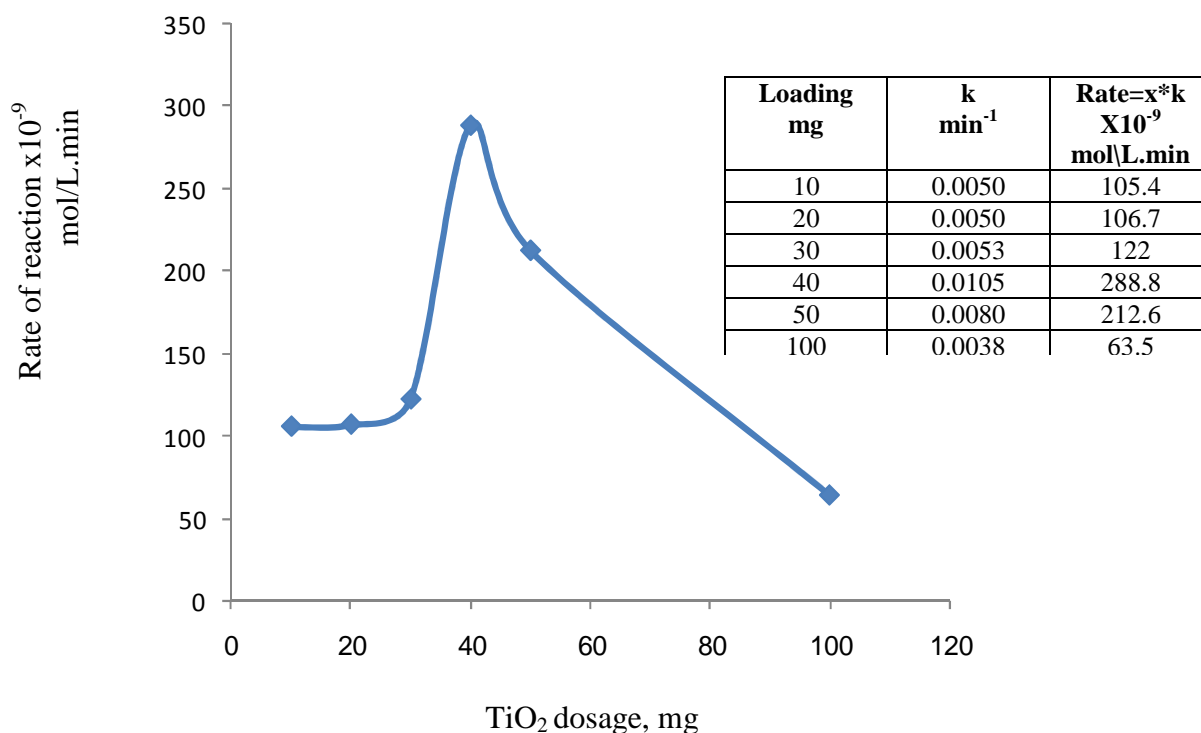


Figure (3-13): Degradation of phenol red at different TiO<sub>2</sub> loading

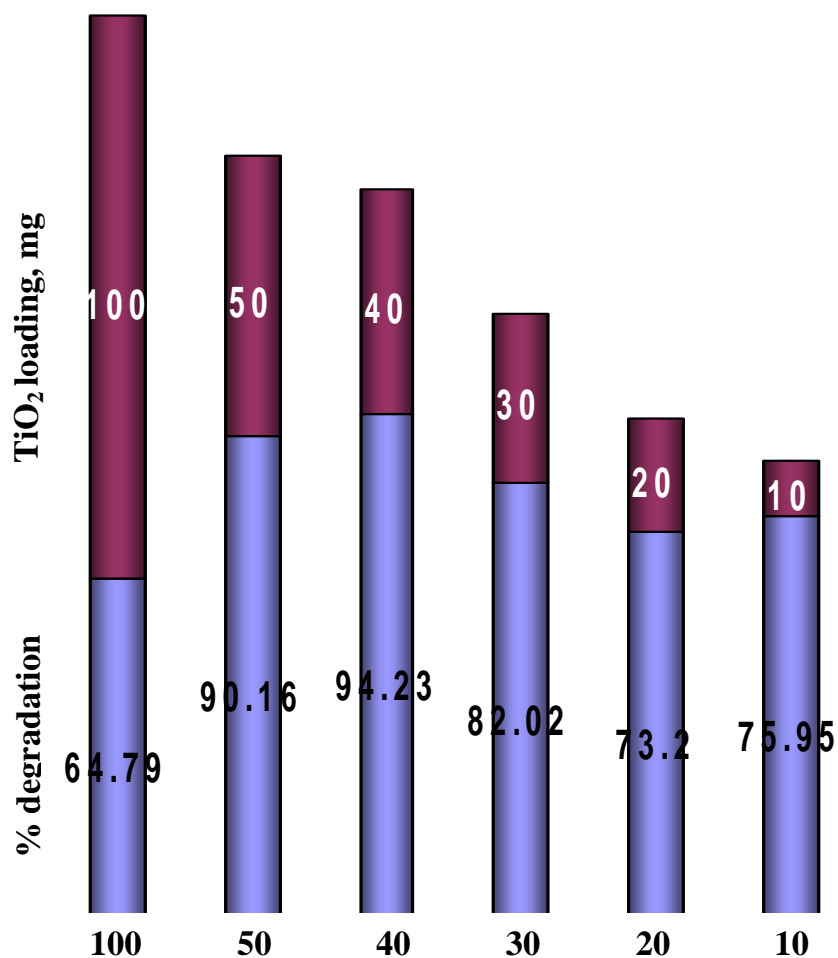


Figure (3-14): Effect of TiO<sub>2</sub> catalyst loading on the degradation yield of phenol red; blue columns represent % degradation and red columns represent TiO<sub>2</sub> dosage

### 3.4.3 Impact of initial phenol red concentration

It is important both from a mechanistic and from application perspectives to study the dependence of the photocatalytic process rate and degradation yield on the phenol red initial concentration. As a result of this, the initial dye concentration was optimized by varying the concentration of phenol red between 5 and 25 ppm at a catalyst dosage of 0.5 g/l and pH of 4.5. The effect of initial concentration on the photocatalytic degradation rate of phenol red is shown in

Figure (3-15), which illustrates different concentration profiles during the degradation of different initial concentrations.

From Figure (3-16), it is noted that the degradation yield and rate increase with the increase in phenol red concentration to a certain level and a further increase in dye concentration leads to decrease the percentage degradation and decolorization rate of the dye. Similar phenomenon has also been reported by several researchers [64, 66, 68]. Konstantinou and Albanis [10] stated that the rate of degradation relates to the probability of  $\cdot\text{OH}$  radicals formation on the catalyst surface and to the probability of  $\cdot\text{OH}$  radicals reacting with dye molecules. Accordingly, as the initial concentrations of the dye increase, the probability of reaction between dye molecules and oxidizing species also increases, leading to an enhancement in the decolorization rate. On the contrary, the degradation efficiency of the dye decreases as the dye concentration increases further. The presumed reason is that at high dye concentrations the generation of  $\cdot\text{OH}$  radicals on the surface of catalyst are reduced since the active sites are covered by dye ions. This possible explanation for this behavior was verified by Andronic et al. [77] who reported that, for increasing initial dye concentrations, more organic substances are adsorbed on the surface of  $\text{TiO}_2$ , while fewer photons are available to reach the  $\text{TiO}_2$  surface and, therefore, less hydroxyl radicals are formed, causing a decrease of the degradation efficiency. Daneshvar et al. [78] concluded, in their work on azo dye acid red photocatalytic degradation, that a possible cause for such phenomenon is the UV-screening effect of the dye itself. At a high dye concentration, a significant amount of UV may be absorbed by the dye molecules rather than the  $\text{TiO}_2$  particles and that reduces the efficiency of the catalytic reaction because the concentrations of  $\cdot\text{OH}$  and  $\text{O}_2^{\cdot-}$  decrease. Further elucidation was published by Neppolian et al. [79] who explained that the major portion of degradation occurs in the region near to the irradiated side (termed as reaction zone) where the irradiation intensity is much higher than in the other side. Thus at higher dye concentration, degradation decreases at sufficiently long distances from the light

source or the reaction zone due to the retardation in the penetration of light. Hence, it is concluded that as initial concentration of the dye increases, the requirement of catalyst surface needed for the degradation also increases.

Also from Figure (3-16), we observe that more than 95% of phenol red was photomineralized within 5 h UV-light irradiation and using the optimal photocatalyst loading amount when the initial concentration was 10 ppm.

On the basis of the above debate, we can conclude that as phenol red dye concentration increases beyond the optimum (10 ppm), the percentage degradation decreases and the degradation rate is proportional to the concentration. Similar conclusion has also made by others working on the photocatalytic degradation of 4-fluorophenol, phenol and m-nitrophenol as well as acid blue 80 using  $\text{TiO}_2$  and  $\text{ZnO}$  under solar irradiation [80-82].

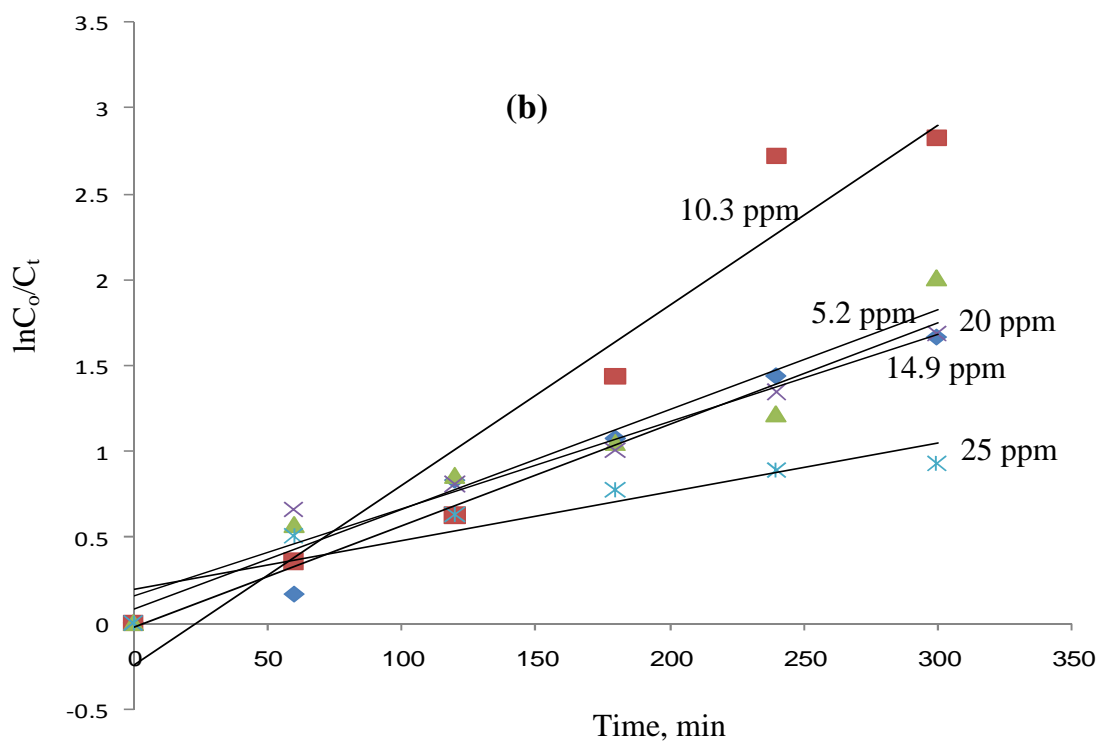
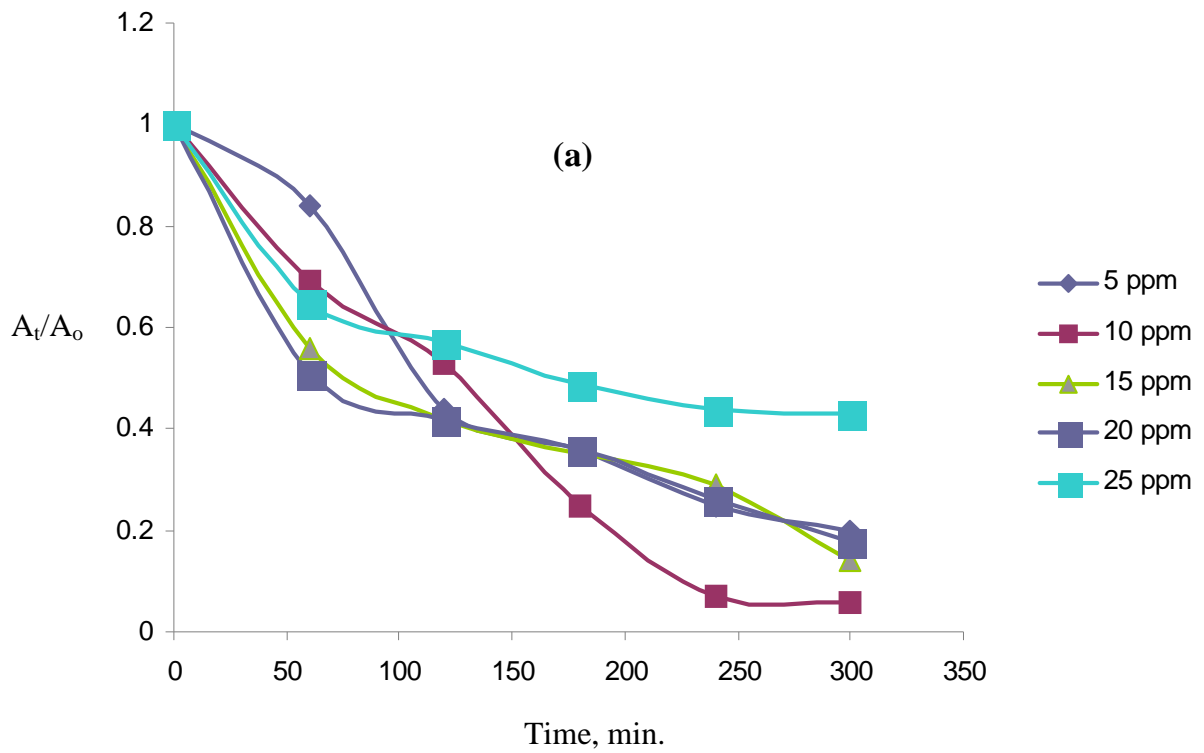


Figure (3-15): Effect of initial concentration of phenol red on the (a) remaining concentration and (b) degradation rate; pH = 4.5; catalyst dosage of 0.5 g/l

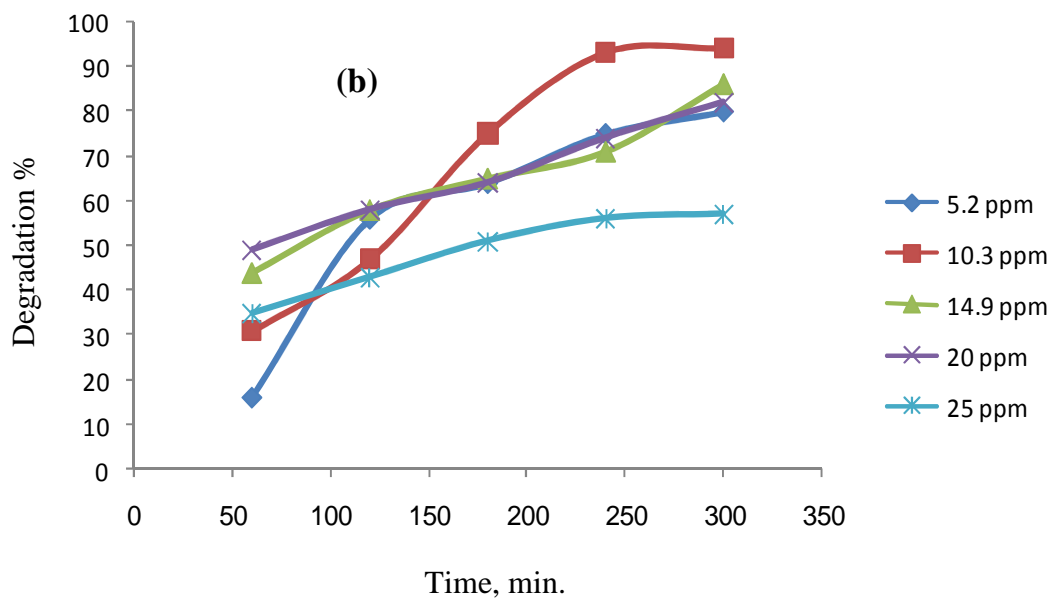
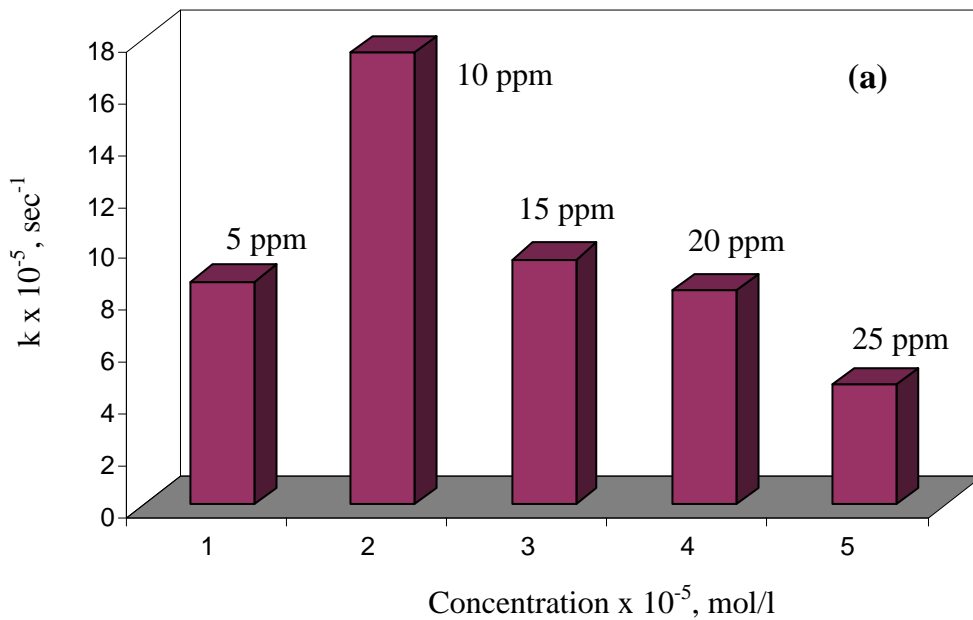


Figure (3-16): (a) Variation of rate constant with phenol red initial concentration and (b) Variation of degradation percent of phenol red with its initial concentration;  $\text{TiO}_2$  dosage = 0.5 g/l, pH = 4.5; irradiation period = 5 hours.

### 3.4.4 Influence of nano anatase TiO<sub>2</sub> particle size

The investigation of the photocatalyst surface area effect on the photolysis of phenol red is a significant operational parameter as long as the photodegradation process is running on the anatase TiO<sub>2</sub> surface. The surface area is directly related to particle size of the photocatalyst. For implementation the impact of this parameter on the photolysis rate and degradation yield, five different particle size anatase TiO<sub>2</sub> powders have been employed as photocatalysts.

The approach that we have found to be most useful is representation of the kinetic data for contaminant degradation on a semi-log plot of particle size versus the corresponding rate constants. The results which are shown in Figure (3-17) indicate that the rate of phenol red photocatalysis is steadily decreased with particle size increase. Furthermore, Figure (3-18) depicts obviously that the rate of photoreactivity of TiO<sub>2</sub> decreased with the increase of the average particle sizes from 10 to 150,000 nm. The rate constants are 0.0105, 0.0075, 0.0036, 0.0020 and 0.00120 min<sup>-1</sup> for the average particle size of 10, 25, 100, 75000 and 150000 nm, respectively.

This could be elucidated by the possibility of the photoelectrons and photoholes generation in the bulk would in smaller particles have fewer traps and recombination centers to overcome before reaching the surface [83]. The particle sizes of TiO<sub>2</sub> seem to affect the photocatalytic degradation percent of phenol red under UV light irradiation as well, as it is clearly presented in Figure (3-19). This prediction has been verified as the degradation percent of the phenolic moiety is significantly promoted when the available active surface area for the photolysis process is higher.

Some researchers [72, 84-85] have also observed similar impacts of particle size on kinetics and degradation yield in photooxidation processes. Shih and Lin [72] concluded that the effect of average particle size of TiO<sub>2</sub> nanoparticle aggregates for the degradation of azo dye has a special limit, while, Pichat et al. [85] reported that the rate of photodegradation of organic moieties is directly

proportional with the surface area of  $\text{TiO}_2$  nanoparticles and further, Khan and his colleagues [84] concluded that the lower particle sizes of  $\text{CeO}_2$  are responsible for their higher sensitivity and photo-catalytic activity.

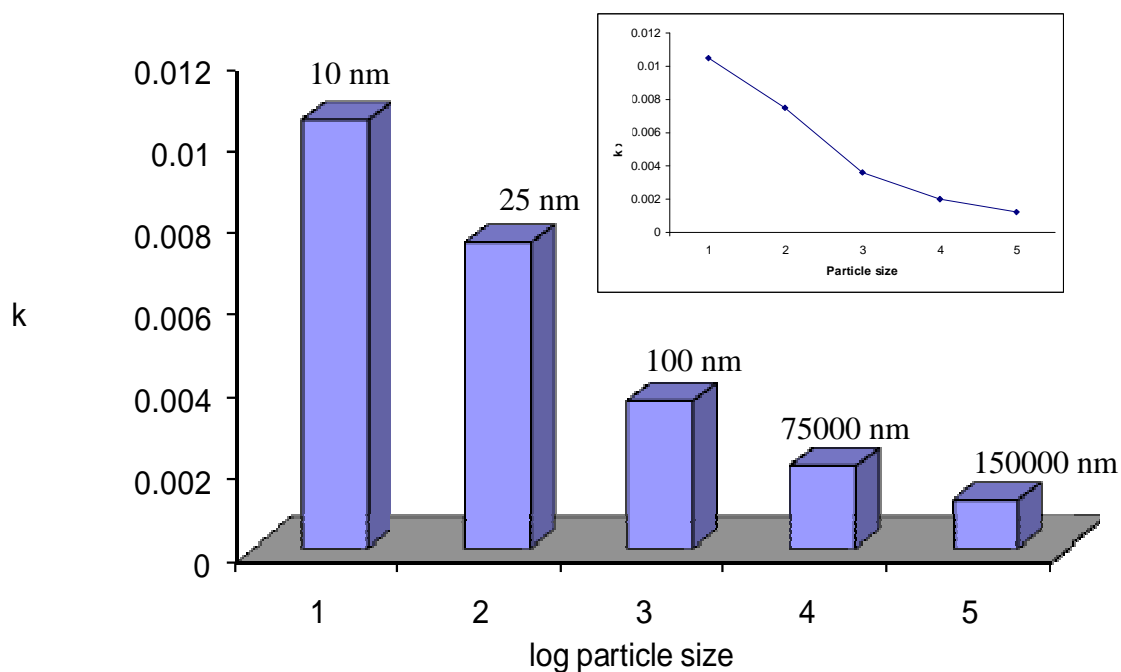


Figure (3-17): Influence of  $\text{TiO}_2$  particle size on the rate of photolysis

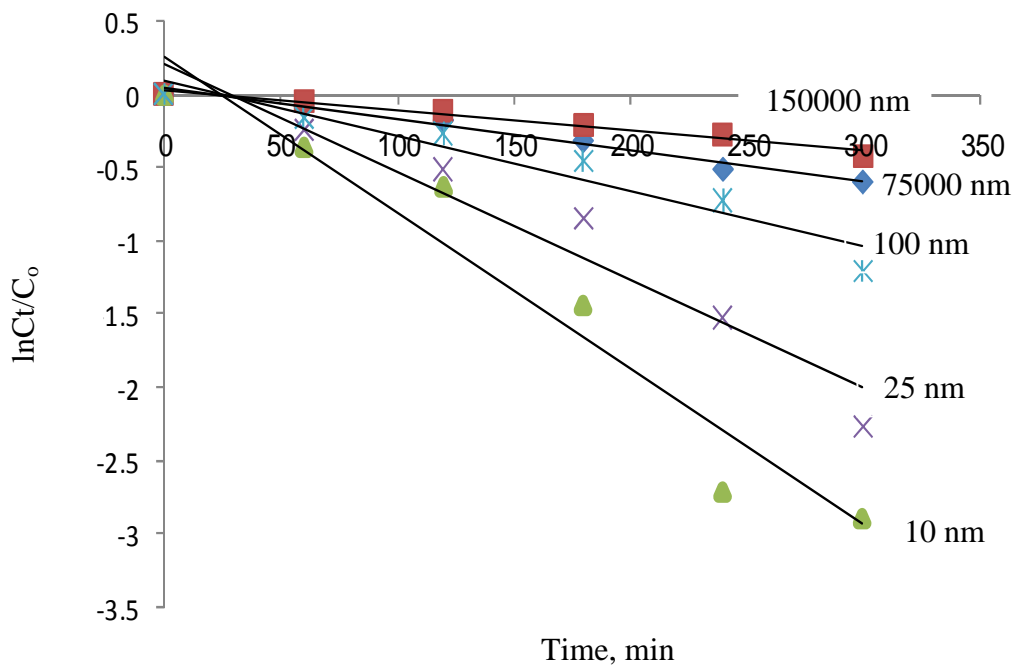


Figure (3-18): Rate of photoreactivity of TiO<sub>2</sub> with the average particle sizes

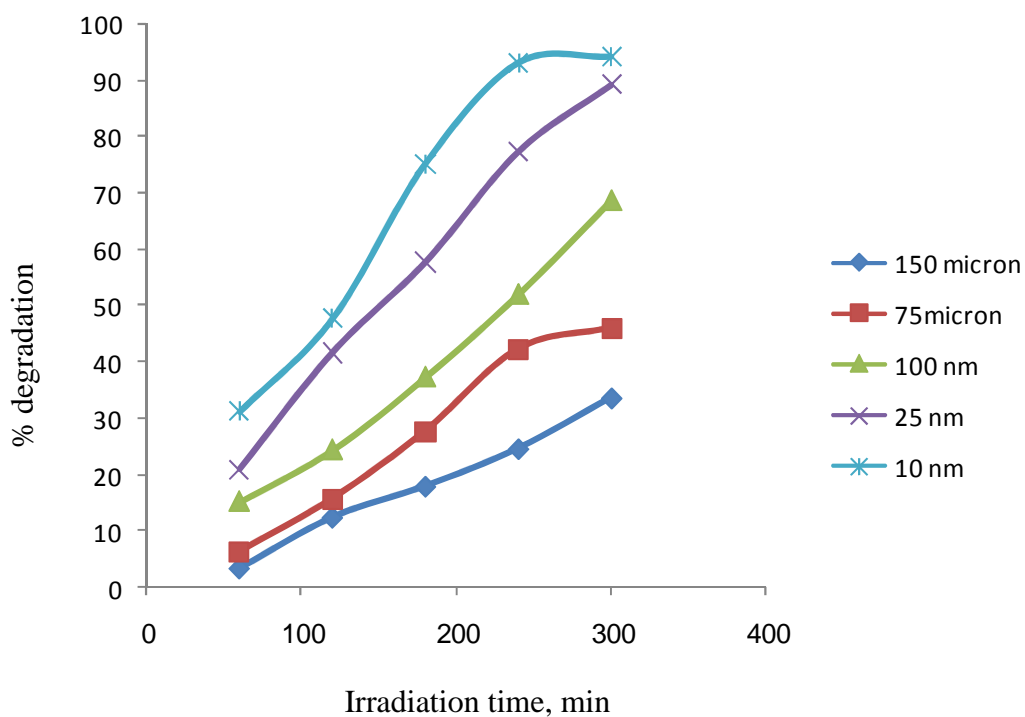


Figure (3-19): Degradation of phenol red at different size on nano TiO<sub>2</sub> particles.

## 3.5 Impacts of the photochemical parameters

### 3.5.1 The role of UV light source intensity

Photocatalytic reaction rate depends largely on the radiation absorption of the photocatalyst [8], where the increase in light intensity enhances the degradation rate and yield in photocatalytic degradation. Vulliet et al. [62] have reported in their work on the photodegradation of cinosulfuron in aqueous TiO<sub>2</sub> suspension that there are two distinguished domains in this aspect: in the first one, at low light intensities (0–14 mW/cm<sup>2</sup>), the rate would increase linearly with increasing light intensity (first order), whereas at intermediate light intensities, above 14 mW cm<sup>-2</sup> the rate would depend on the square root of the light intensity (half order). This is likely because at low light intensity reactions involving electron–hole formation are predominant and electron–hole recombination is negligible. However, at increased light intensity electron–hole pair separation competes with recombination, thereby causing lower effect on the reaction rate.

Figure (3-20) which shows the result of the effect of UV light intensity on the initial degradation rate of phenol red in this study is in a good accordance with the above approach. This enhancement of the rate of photodecolorization as the light intensity increased was also observed by other researchers [73, 79]. In accordance with Vulliet et al. [62], Konstantinou and Albanis [10] have stated that at low light intensities (0–20 mW/cm<sup>2</sup>), the rate would increase linearly with increasing light intensity (first order) and at intermediate light intensities beyond a certain value (approximately 25 mW/cm<sup>2</sup>) the rate would depend on the square root of the light intensity (half order), whereas, at high light intensities the rate is independent of light intensity. Malato et al. [69] have reported in their overview and trends for the solar photocatalysis of water that the typical Solar UV-flux of 20–30Wm<sup>-2</sup> is equivalent to 0.2–0.3 mol photons (Einstein) m<sup>-2</sup> h<sup>-1</sup> in the 300–400 nm range. Accordingly, the intensity magnitudes which are employed in this work (shown in Table 3-1) correspond to 0.97, 2.23 and 10.8 mW/cm<sup>-2</sup> and the rates, consequently, are increasing with

increasing light intensity, which is a stand alone verification for the first order process. These tentative findings are explicitly concerted with the published outcomes of other researchers [10, 62].

For further scrutinization and better evaluation the efficiency of the photocatalytic and photobleaching processes, we estimated the quantum yield  $\Phi$ , which is defined as the ratio of the number of converted molecules per second to the number of efficient photons reaching the surface per second. The values of  $\Phi$  are reported in Table (3-1). The maximum quantum yields are obtained for the lower light intensities, which are inline with the foregoing literature trend.

On the basis of above outcomes, it is evident that the percentage of decolorization and photodegradation increases with increase in irradiation time. The reaction rate decreases with irradiation time since it follows apparent first-order kinetics, however, it increases with increasing the light intensity (Figure 3-20) and additionally a competition for degradation between the reactant and the intermediate products should also be taken into consideration.

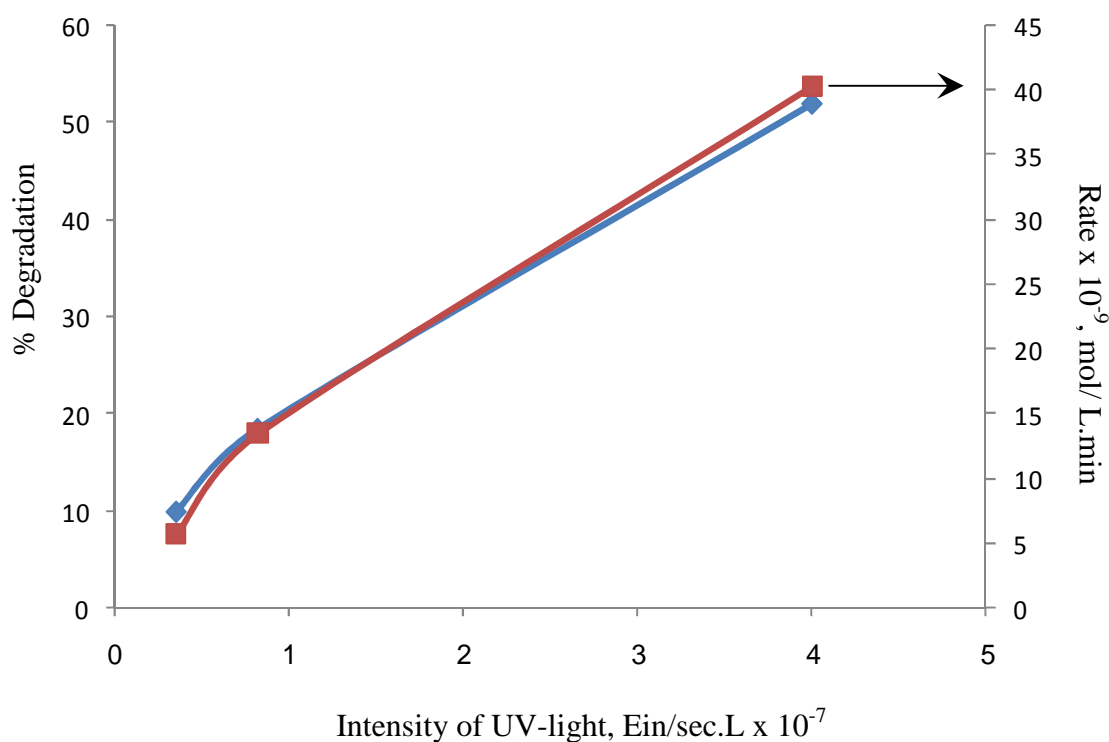


Figure (3-20): Variations of the initial rate and degradation yield as a function of light source intensity

Table (3-1) :Quantum yields of photodegradation of phenol red obtained at different intensities

<b>Intensity (E/L.sec) x10<sup>-7</sup></b>	<b>Rate (mol/L.sec) x10<sup>-9</sup></b>	<b>Quantum yield Φ%</b>
0.36	0.094	0.26
0.826	0.223	0.27
4	0.67	0.16

### 3.5.2 Rationalization of apparent quantum yield with some experimental variables

The quantum yield of a photochemical process is defined as the amount of substrate degraded or produced per photon, and is generally used as a measure of the efficiency of a photochemical process [8].

In homogeneous photochemistry, the quantification of quantum yield is a usual practice and extensively used as it provides a means of comparing two or more photochemical events. By contrast, a similar description in heterogeneous photochemistry is further complicated by many fundamental unknown quantities [63]. The problems in heterogeneous photolysis systems are normally stemmed due to the light scattering by the photocatalyst particles. Therefore, the quantum yields are not indicated in most photocatalysis studies or in few are indicated as apparent or pseudo-quantum yield.

In this work, the apparent or pseudo-quantum yield which is defined as the number of molecules converted relative to the total number of photons incident on the photolysis cell window, i.e.

$\Phi = \text{rate of reaction (mol L}^{-1}\text{s}^{-1}) / \text{rate of photon incident on window (mol L}^{-1}\text{s}^{-1})$   
 was measured following Valladares and Bolton [40]. In one set of experiment,

the incident light intensity, which is 100% absorbed by the TiO<sub>2</sub> / phenol red system, calculated by Hatchard and Parker [57] ferrioxalate actinometry method which is previously mentioned in details in this thesis. The average value of several measurements at 14 cm cell-light source distance is  $I_0 = 0.485 \times 10^{-7}$  Ein / Sec. L. The rate of photolysis of phenol red determined under the conditions employed (initial phenol red concentration of  $2.82 \times 10^{-5}$  mol / L, pH = 4.5 and TiO<sub>2</sub> dosage = 0.5 g/l) is  $4.813 \times 10^{-9}$  mol / L. Sec. The apparent quantum yield is consequently equals 0.1 according to;

$$\begin{aligned} \text{Quantum yield} &= \text{rate of reaction} / I_0 \\ &= 4.813 \times 10^{-9} / 0.485 \times 10^{-7} \\ &= 0.1 \end{aligned}$$

It has been figured out that the apparent quantum yield in the present system is influenced by some operational parameters namely; the TiO<sub>2</sub> dosage, initial phenol red concentration and the pH values.

Figure (3-21) depicts that the quantum yield increases with increasing TiO<sub>2</sub> loading and approaching a limiting value at 40 mg, (0.5 g/l), then starts declining. This limiting value mainly results from two factors:

(a) aggregation of TiO<sub>2</sub> particles at high concentrations, causing a decrease in the number of surface active sites, and (b) increase in opacity and light scattering of TiO<sub>2</sub> particles at high concentration leading to a decrease in the passage of irradiation through the sample [63].

The initial phenol red concentration is also impacted the value of quantum yield and the latter increases (Figure 3-22a) with initial concentration increase in the range  $1.4 \times 10^{-5} - 5.6 \times 10^{-5}$  mol/l (5-20 ppm). This might be explained by the fact that with increasing phenol red concentration the amount of the adsorbed dye on TiO<sub>2</sub> surface increases and hence the amount of decomposed dye is increased.

As it was mentioned earlier in this thesis (paragraph 3.4.1) that the rate of degradation of phenol red in aqueous TiO<sub>2</sub> suspension is higher in acidic medium (pH = 4.5). Accordingly the influence of pH on the variation of

apparent quantum yield has also been examined. Figure (3-22b) exhibits the variation of the apparent quantum yield with varying pH values.

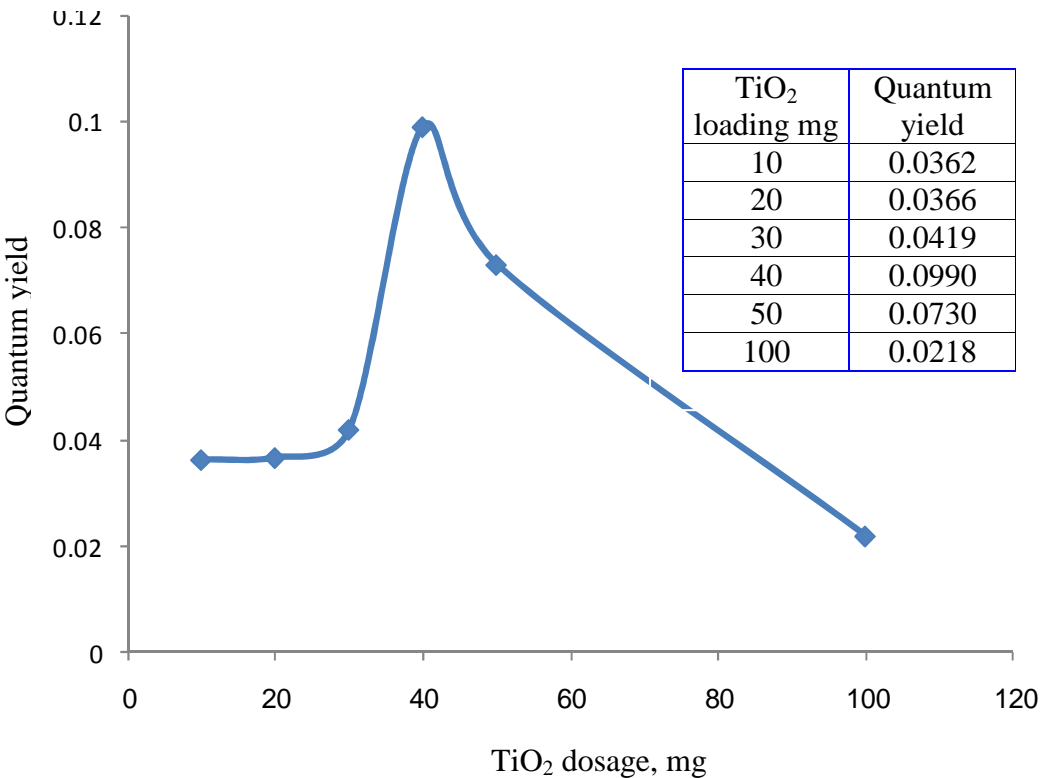


Figure (3-21): Effect of loading of TiO<sub>2</sub> on quantum yield

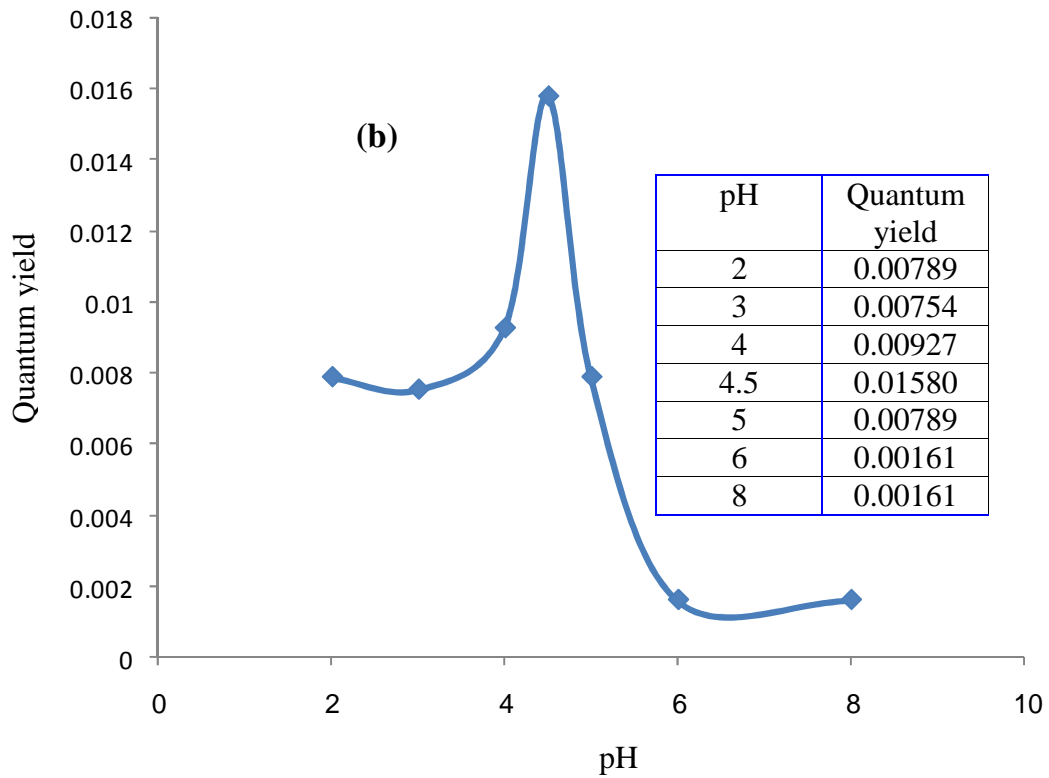
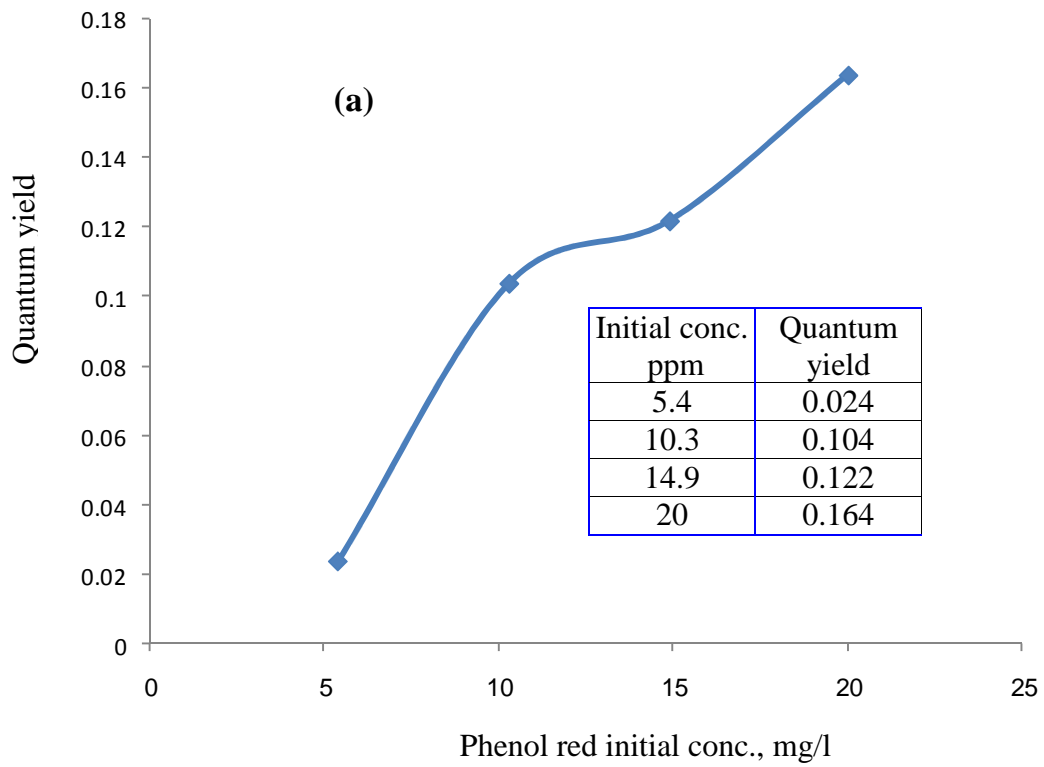


Figure (3-22): Impacts of (a) phenol red initial concentration and (b) pH of photolysis media, on the quantum yield of the process

### 3.6 Kinetics study

#### 3.6.1 Effect of irradiation time on the rate of photocatalysis

The kinetics of the photooxidative degradation of several phenolic compounds on TiO<sub>2</sub> surface have been investigated by many authors [86, 63, 56]. On regular basis, the order of photocatalytic decomposition reaction of phenols has been found to follow first order under normal conditions.

In the present investigation, the chemical kinetics of phenol red has been explored under the operational conditions described earlier in chapter two.

The rates of photolysis of the model compound were monitored spectrophotometrically in the wavelength 432 nm, at which it shows a maximum absorption.

Graphical method has been employed to anticipate the order of the photocatalysis reaction. Figure (3-23) describes the relative decrease in absorption intensity ( $A_t/A_0$ ) of  $2.9 \times 10^{-5}$  mol /l phenol red as a function of irradiation time. From kinetics point of view, it is useful to find out a rate equation that fits the experimental rate data. According to some researchers, generally, the photocatalytic degradation of organic pollutants is described by pseudo-first order kinetics [87-88].

$$-dC/dt = k_{app}C \dots\dots\dots(3-3)$$

Integrating the eq. (3-3) with the boundary conditions that at the start of irradiation ( $t = 0$ ), the concentration is the initial one,  $C_t = C_o$ , results in the following expression:

$$-\ln (C_t/ C_o) = k_{app}t \dots\dots\dots(3-4)$$

where  $k_{app}$  is the apparent first order rate constant ( $\text{min}^{-1}$  or  $\text{sec}^{-1}$ ) and  $C_o$  and  $C_t$  is the concentration of phenol red at a given irradiation time,  $t$  (min). Kinetic studies were monitored by the change in phenol red concentration at certain interval of time ( $C_t$ ). Apparent first order rate constant ( $k_{app}$ ) was evaluated using equation (3-4) from the plot of natural logarithm ( $\ln C_o/C_t$ ) change in phenol red concentration versus irradiation time,  $t$  (Figure 3- 24). The  $k_{app}$  was determined

by calculating the slope of the line obtained. This suggests, consequently, the first order kinetics of the primary photolysis process. The value of  $k_{app}$  obtained when the initial phenol red concentration has been  $2.9 \times 10^{-5} \text{ mol/l}$  (10.3 ppm) is  $0.01052 \text{ min}^{-1}$  ( $17.53 \times 10^{-5} \text{ sec}^{-1}$ ). The half life of the reaction accordingly computed from the expression  $t_{1/2} = 0.693/k_{app}$ , which has been equal to 1.098 hours.

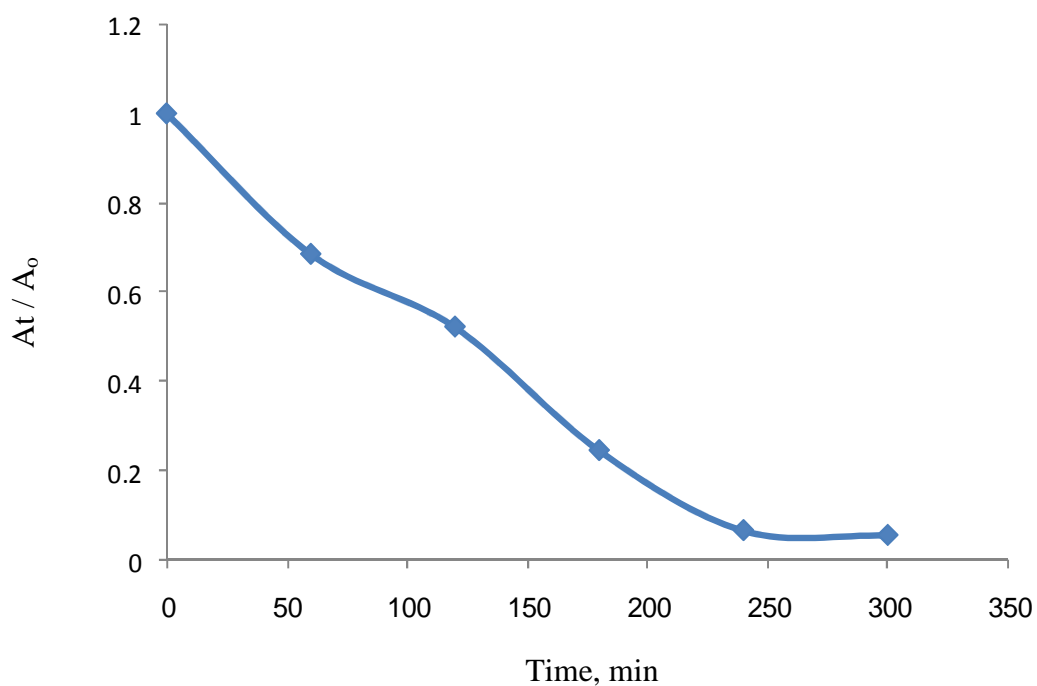


Figure (3-23): Rate of degradation of phenol red at optimum condition

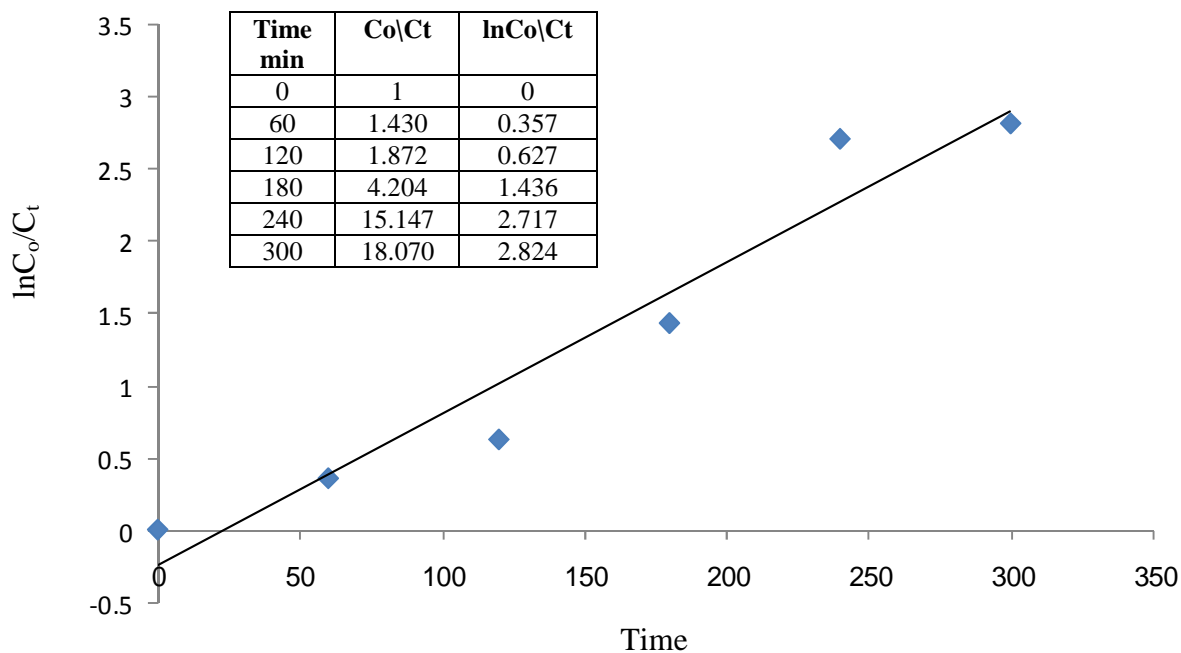


Figure (3-24): Degradation of phenol red at optimum condition

### 3.6.2 Initial concentration and Langmuir-Hinshelwood model

In recent years the Langmuir-Hinshelwood rate expression has been used successfully for heterogeneous photocatalytic degradation to elucidate the relationship between initial degradation rate and initial concentration[63]. Furthermore, the Langmuir–Hinshelwood model is usually used to describe the kinetics of photocatalytic process [68]. The derivation is based on the degradation rate ( $r$ ), which is expressed as follows:

$$r = - dC_0/ dt = (k_r K_{ad} C_0) / (1+ K_{ad} C_0) \dots\dots\dots(3- 5)$$

Where  $r$  represents the initial rate of photooxidation (mol or mg/l min),  $C_0$  the concentration of the reactant (mol or mg/l,  $t$  the irradiation time,  $k_r$  the rate constant of the reaction (mol or mg/l min) and  $K_{ad}$  is the adsorption equilibrium coefficient of the reactant (l/mg or mol). Assuming that adsorption is weak and

the concentration of the organic moiety is low, the equation (3-5) can be simplified to the first-order kinetics expression with an apparent rate constant ( $k_{app}$ ) [10]:

$$\ln (C_0/C_t) = kK_t = K_{app}t \dots\dots(3-6)$$

or

$$C_t = C_o e^{-k_{app} \cdot t} \dots\dots\dots(3-7)$$

From the perspective of linear algebra, the plot of  $\ln (C_t/C_o)$  as a function of reaction time,  $t$ , should have linear relationship and its slope is the apparent rate constant.

Hence, the plot of  $\ln(C_t/C_o)$  versus reaction time  $t$  with different initial phenol red concentrations,  $C_o$ , is shown in Figure (3-25). It was found that the linear relationship was good and rate constant  $k_{app}$  declined generally with increasing initial concentrations of phenol red.

Most authors agree that, with minor doubts, the expression for the rate of photodecomposition of organic dyes with irradiated  $TiO_2$  follows the Langmuir–Hinshelwood (L–H) law for the four possible situations; (a) the reaction takes place between two adsorbed substances, (b) the reaction occurs between a radical in solution and an adsorbed substrate molecule, (c) the reaction takes place between a radical linked to the surface and a substrate molecule in solution, and (d) the reaction occurs with the both of species being in solution. In all cases, the expression for the rate equation is similar to that derived from the L–H model, which has been useful in modeling the process. However, from kinetic studies only, it is not possible to find out whether the process takes place on surface or in solution[89].

Equation (3-5) could be modified to linear type equation as presented in equation (3-8);

$$1/r = 1/k_r + 1/ k_r K_{ad} C_0 \dots\dots\dots(3-8)$$

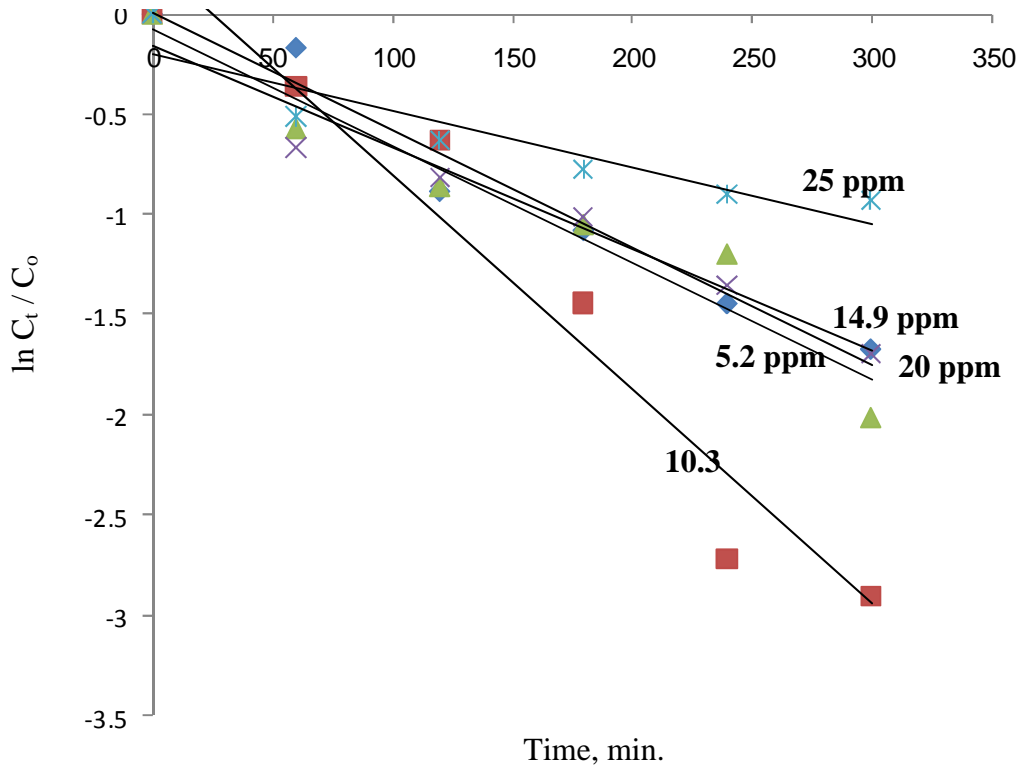


Figure (3-25): Plot of  $\ln(C_t/C_0)$  vs. reaction time at different initial concentrations of phenol red; (Catalyst loading = 0.5 g/L; pH = 4.5 )

Plot of reciprocal reaction rate  $1/r$  versus reciprocal initial concentration  $1/C_0$  (from equation (3-8) is presented in Figure (3-26). A reasonable fit of this equation was obtained with values of  $0.0045\mu\text{M}^{-1}$  ( $0.0127\text{ ppm}^{-1}$ ) and  $0.0333\mu\text{M sec}^{-1}$  for  $K_{ad}$  and  $k_r$  respectively. This indicates that the degradation of phenol red occurred mainly on the surface of  $\text{TiO}_2$ . However, Turchi and Ollis [90] investigated the photodegradation of organic pollutants in illuminated  $\text{TiO}_2$  slurries and found it plausible that the reaction occurs not only on the  $\text{TiO}_2$  surface but also in solution.

The foregoing value of  $K_{ad}$  refers to the strong adsorption of phenol red moiety onto the electrophilic ( $\text{Ti}^{+4}$ ) sites at the  $\text{TiO}_2$  surface. Asiri et al. [65]

have reported that the adsorption linkages of phenol red onto  $\text{TiO}_2$  surface bridged through sulphonato and phenolic anchoring groups as it is depicted in Figure (3-27).

Malato and his collaborators [69] stated that a quasi-exhaustive consideration of photodestruction studies of organic contaminants proved that the first order rate equation above holds true. Moreover, at any rate, Langmuir–Hinshelwood model serves as a basis for the photodegradation of organic compounds even if it could not directly give adequate fitting. Whereas, other researchers [91-92] concluded that the L–H model is not a perfect explanation of the mechanism of the photocatalytic process, it has been useful in modeling a process, however, it is generally agreed that both rate constants and orders are only “apparent” and they serve to describe the rate of degradation, but they have no physical meaning, and may not be used to identify surface processes. On the other hand, the value of  $K$  derived from a kinetic study is not directly equivalent to the Langmuir adsorption coefficient for an organic molecule on  $\text{TiO}_2$  in the dark as adsorption–desorption phenomena are different in the dark in comparison to those under illumination.

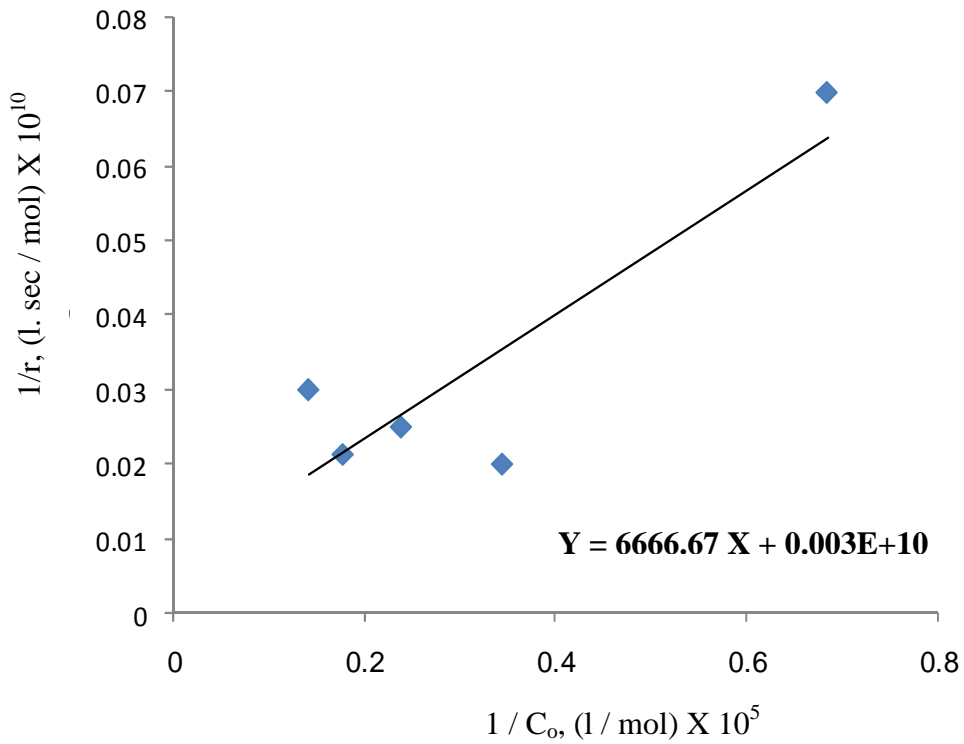


Figure (3- 26): Langmuir-Hinshelwood model outcomes for the disappearance of phenol red at different initial concentrations; TiO<sub>2</sub> loading= 0.5 g/l; pH = 4.5

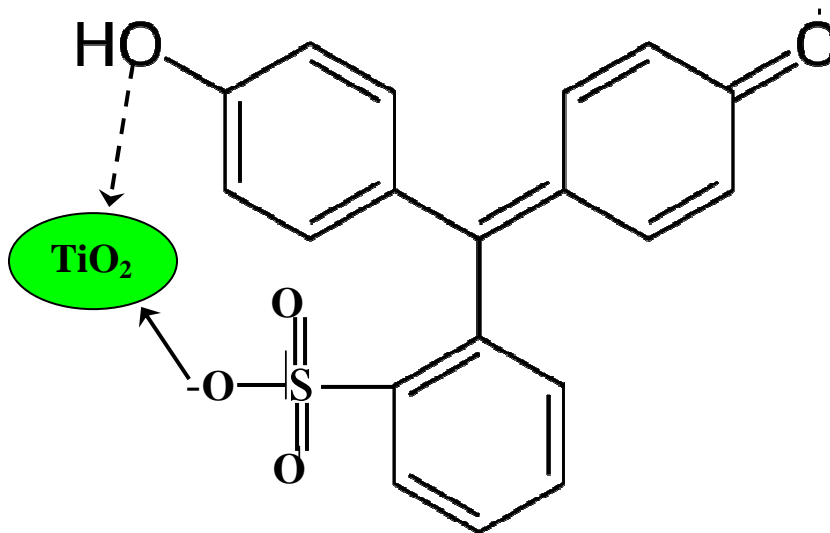


Figure (3-27): Virtual adsorption geometry of phenol red onto TiO<sub>2</sub> particle

### 3.7 Contribution of the added oxidants

Chemical oxidation of organic pollutants by various oxidants has been investigated by several authors over the last decades to develop novel remediation technologies. The oxidants, O<sub>3</sub> [93], Fenton's reagent [94], H<sub>2</sub>O<sub>2</sub> [95] and persulfate (K<sub>2</sub>S<sub>2</sub>O<sub>8</sub>) [96-97] have been widely tested in laboratory work and used for the remediation of wastewater and groundwater contaminated by organic compounds.

#### 3.7.1 Effect of H<sub>2</sub>O<sub>2</sub> on photocatalysis of phenol red

The electron / hole (e<sup>-</sup> / h<sup>+</sup>) recombination is considered as one of the main problems in the application of TiO<sub>2</sub> photocatalysis. Accordingly, Malato and his colleagues [98] have reported that one of the most accepted strategies for inhibiting e<sup>-</sup> / h<sup>+</sup> recombination has been the addition of other electron acceptors to the reaction. The addition of other oxidizing species could have several different impacts like; (a) increase the number of trapped conduction band e<sup>-</sup> in e<sup>-</sup>/h<sup>+</sup> pairs and, consequently avoid recombination; (b) generate more hydroxyl radical, ·OH, and other oxidizing species and (c) avoid problems stemmed due to O<sub>2</sub> gas starvation.

Molecular oxygen is generally used as an electron acceptor in heterogeneous photocatalytic reaction [4]. However, Figure (3-28) exhibits only about 60% photobleaching of phenol red in the presence of O<sub>2</sub> gas solely, at absence of H<sub>2</sub>O<sub>2</sub>, whereas the photodegradation yield has been found to be enhanced dramatically (>91%) by using hydrogen peroxide as an alternative electron acceptor. This is in accordance with the findings of Oghenejoboh et al. [66] who stated that the photo catalytic degradation of water effluent pollutants could be enhanced by addition of H<sub>2</sub>O<sub>2</sub> because it is a better electron acceptor than oxygen.

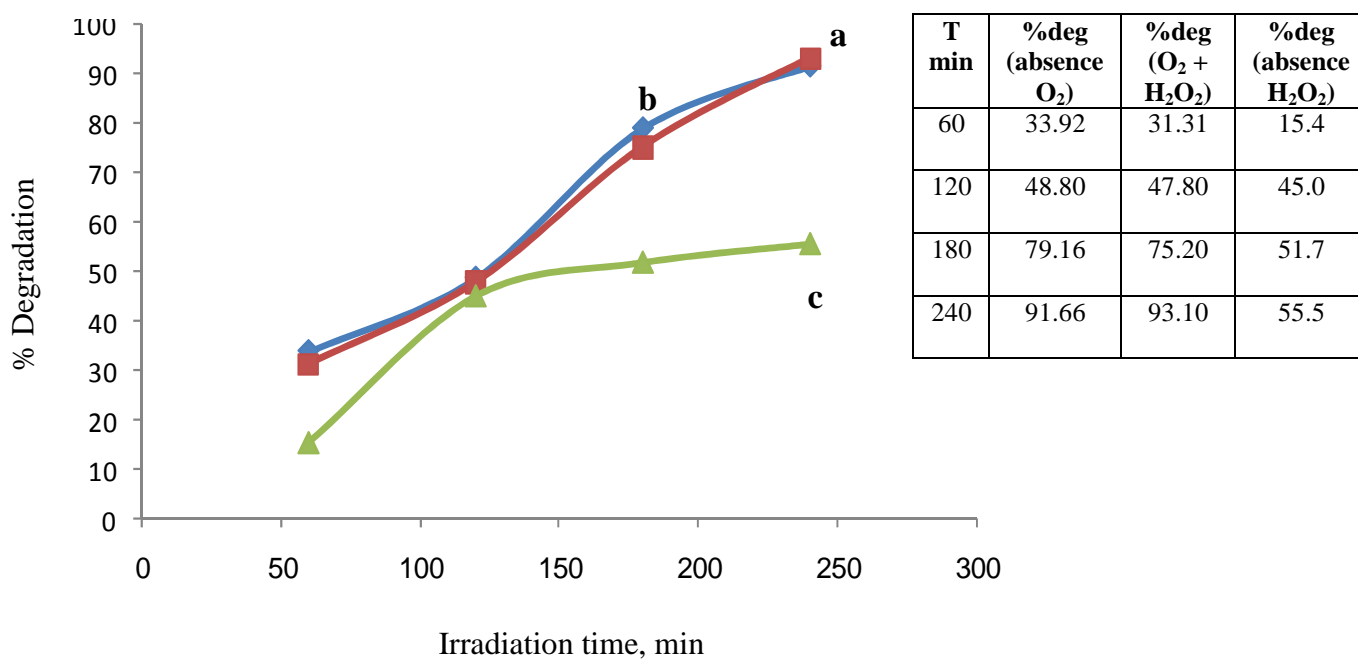


Figure (3-28): Photodegradation of phenol red at (a) presence of both O<sub>2</sub> and H<sub>2</sub>O<sub>2</sub> (b) presence of H<sub>2</sub>O<sub>2</sub> (c) presence of O<sub>2</sub>

On the other hand, our experimental outcomes verified that better efficiency of photodegradation process could be achieved (>94% degradation) by application of both oxygen gas and hydrogen peroxide in combination with TiO<sub>2</sub> (Figure 3-28). The positive sign of H<sub>2</sub>O<sub>2</sub> addition indicated that there was a direct relationship between the initial H<sub>2</sub>O<sub>2</sub> concentration and the yield of phenol red dye degradation, which increased for increasing H<sub>2</sub>O<sub>2</sub> concentration, i.e., the presence of H<sub>2</sub>O<sub>2</sub> in the reaction mixture plays a key role in the photocatalytic process which is in agreement with several authors [64, 66, 99].

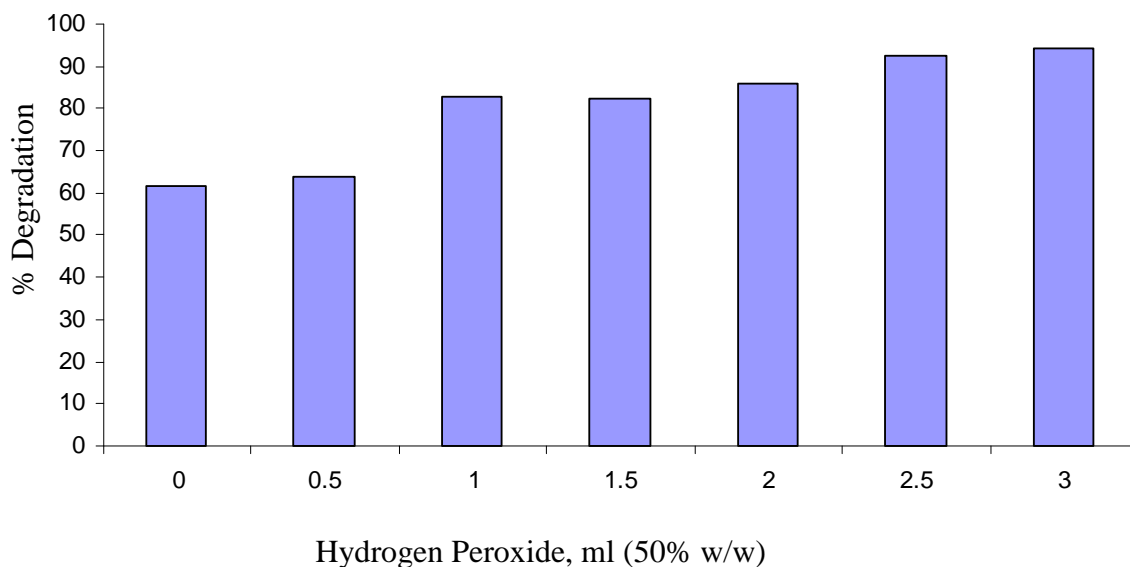
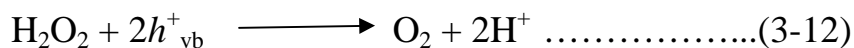


Figure (3-29): Influence of H<sub>2</sub>O<sub>2</sub> on the degradation yield of phenol red under optimum experimental conditions

We believe it is necessary to discuss in detail some aspects related to the effect of this electron acceptor. The addition of H<sub>2</sub>O<sub>2</sub> has been found to be beneficial, increasing the degradation yield, due to its electron acceptor nature. This beneficial effect can easily be explained in terms of (a) additional production of  $\cdot\text{OH}$ , which is a very strong oxidizing agent with standard redox potential of +2.8 V [10] through the following reactions under UV light radiation [69, 10]:



and (b) inhibition of  $e^- / h^+$  recombination which could be explained in terms of TiO<sub>2</sub> surface modification by H<sub>2</sub>O<sub>2</sub> adsorption and scavenging of photoproduced holes following the up coming reaction:



Hence, the described reactions above indicate that hydroxyl radicals are more likely to form in UV/TiO<sub>2</sub>/H<sub>2</sub>O<sub>2</sub> systems and other oxidizing species can also appear in the e<sup>-</sup>/h<sup>+</sup> generation process.

Figure (3-30) depicts a relatively low degradation yield for phenol red / H<sub>2</sub>O<sub>2</sub> / O<sub>2</sub> system is achieved when only TiO<sub>2</sub> is used in dark (26%) or when TiO<sub>2</sub> is absent (36%). However, phenol red could be degraded appreciably (94%) in this system by UV source illuminated TiO<sub>2</sub>. Accordingly, these experiments demonstrated that H<sub>2</sub>O<sub>2</sub>, O<sub>2</sub> gas, UV irradiation and the TiO<sub>2</sub> photocatalyst are needed for the effective photolysis of phenol red dye.

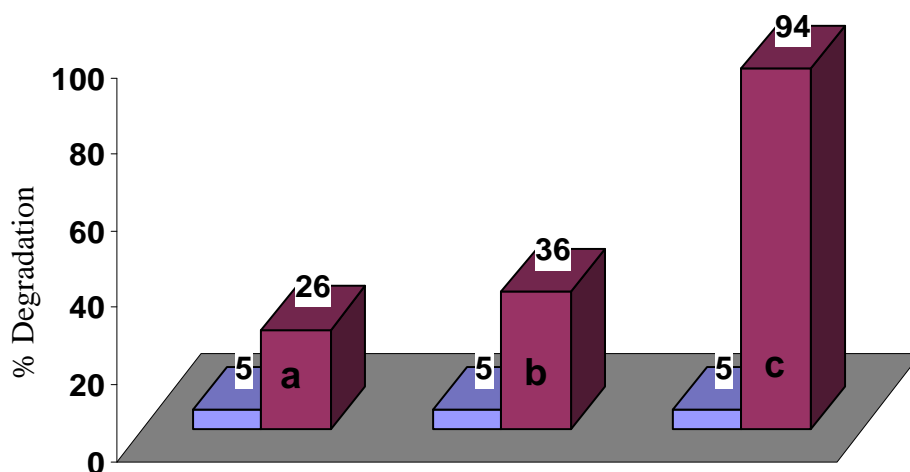


Figure (3-30): Degradation yields of phenol red after 5 hours UV photolysis under optimum experimental conditions for; (a) TiO<sub>2</sub> + H<sub>2</sub>O<sub>2</sub> + O<sub>2</sub> gas (without irradiation); (b) H<sub>2</sub>O<sub>2</sub> + O<sub>2</sub> gas + irradiation (without TiO<sub>2</sub>); (c) TiO<sub>2</sub> + H<sub>2</sub>O<sub>2</sub> + O<sub>2</sub> gas + irradiation; pH = 4.5, C<sub>0</sub> = 10 mg/l, H<sub>2</sub>O<sub>2</sub> = 3 ml (50% w/w), TiO<sub>2</sub> = 0.5 g/l

For further analysis of UV/TiO<sub>2</sub>/H<sub>2</sub>O<sub>2</sub> system which has been employed in this study, the plots of ln A<sub>t</sub> (as first order index) and 1/A<sub>t</sub> (as second order index) versus time were established in order to devote the R<sup>2</sup> values as one of the methodologies to assign the pseudo order of the photocatalytic degradation process of phenol red dye in the presence of hydrogen peroxide. This

mathematical technique has also been adopted by other researchers [100-101]. Figure (3-31) presents  $R^2$  values of 0.944 and 0.910 for  $\ln A_t$  vs. time, as pseudo first order evidence for the phenol red photodegradation process, using the UV/TiO<sub>2</sub>/H<sub>2</sub>O<sub>2</sub>, and UV/TiO<sub>2</sub>/O<sub>2</sub>/H<sub>2</sub>O<sub>2</sub> systems, respectively. Whereas, The poor  $R^2$  values of 0.764 and 0.681 for  $1/A_t$  vs. time, as pseudo second order indicator for the phenol red photodegradation process, reveals explicitly that the UV/TiO<sub>2</sub>/H<sub>2</sub>O<sub>2</sub> and UV/TiO<sub>2</sub>/O<sub>2</sub>/H<sub>2</sub>O<sub>2</sub> systems don't follow pseudo second order mechanism since they did not exhibit a linear behavior during photolysis reaction of phenol red. This finding agrees well with Garcia et al.[101] who concluded that the degradation of the real textile organic effluents happens through pseudo-first-order reaction when UV/TiO<sub>2</sub>/H<sub>2</sub>O<sub>2</sub> system is employed, due to the complete consumption of the added peroxide and Furthermore, the UV/TiO<sub>2</sub>/H<sub>2</sub>O<sub>2</sub> treatment has the advantage of leads to a final nontoxic residue due to the absence of residual peroxide.

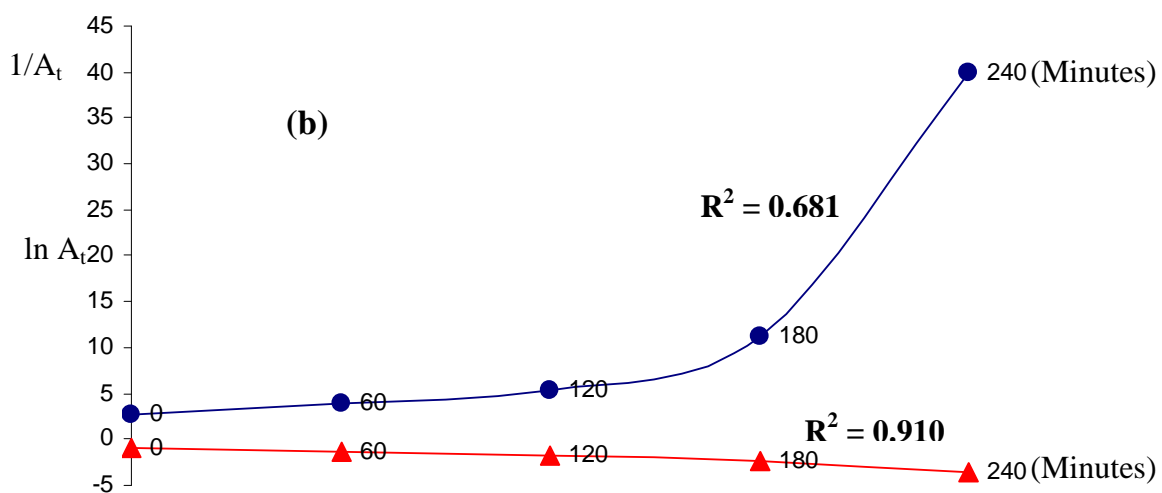
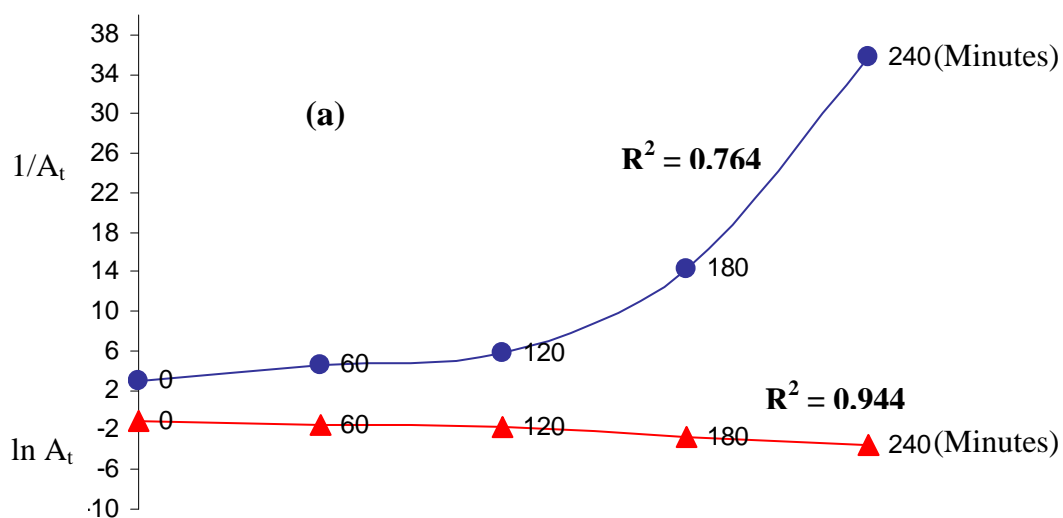
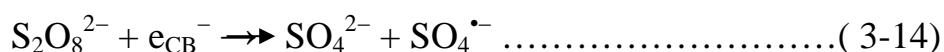
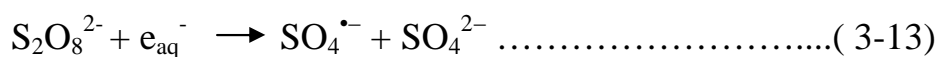


Figure (3- 31): Pseudo order of phenol red degradation with  $O_2$  gas and  $H_2O_2$  ( $A_t$ : Absorbance at time t and 432 nm); (a) Only  $H_2O_2$ ; (b)  $O_2$  gas and  $H_2O_2$

### 3.7.2 Influence of Na<sub>2</sub>S<sub>2</sub>O<sub>8</sub> on photocatalysis of phenol red

The use of persulfate has recently been the focus of attention for an alternative oxidant in the chemical oxidation of contaminants [102]. Persulfate is one of the strongest oxidants known in aqueous solution and has a higher potential ( $E^0 = 2.01$  V) than H<sub>2</sub>O<sub>2</sub> ( $E^0 = 1.76$  V) [103]. Furthermore, It has great capability for degrading numerous organic contaminants through free radicals (SO<sub>4</sub><sup>•-</sup> and <sup>•</sup>OH) generated in the persulfate system [104]. Additionally, the UV-irradiation contributes remarkably to generate a sulfate radical, a stronger oxidant ( $E^0 = 2.5-3.10$  V) [105] than persulfate according to the following equations [106]:



From Figure (3-32), we observe the enhancement of photodegradation yield of phenol red upon addition of sodium persulfate. The existence of two mmole of S<sub>2</sub>O<sub>8</sub><sup>2-</sup> in electrolysis solution could acquire > 95% photobleaching for the phenol red dye. This is mainly ascribed to the high oxidizing strength of the reactive radical intermediate, SO<sub>4</sub><sup>•-</sup>, ions which can exert a dual function; as strong oxidant themselves and as electron scavengers, thus inhibiting the electron-hole recombination at semiconductor surface. For further elaboration, Anipsitakis and his colleagues [107] have found, in their oxidation power comparison study between H<sub>2</sub>O<sub>2</sub> and S<sub>2</sub>O<sub>8</sub><sup>2-</sup>, that the sulphate radicals are stronger oxidants than the hydroxyl, especially at neutral pH. They further, explained this difference in reactivity according to the energy of their O-O bond. This bond in persulphate has been estimated to be 33.5 kcal/mol whereas in hydrogen peroxide it is 51 kcal/mol. Also the distance of the O-O bonds of these

oxidants; 1.453 A° in solid H<sub>2</sub>O<sub>2</sub> and 1.497 A° in persulphate. This suggests that persulphate is cleaved more easily than hydrogen peroxide, and thus the resulting sulphate radicals might be formed more readily than hydroxyl radicals.

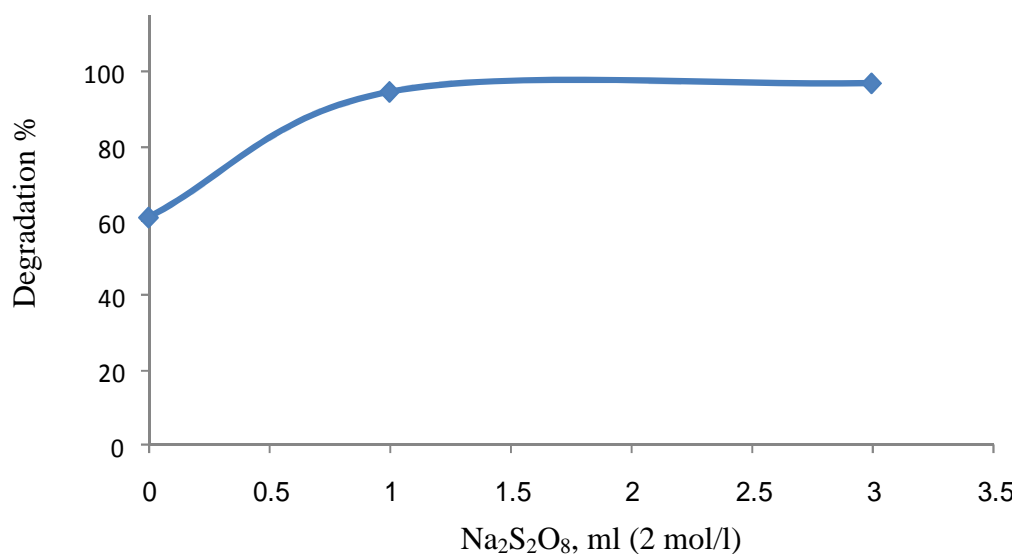


Figure (3-32): Effect of Na<sub>2</sub>S<sub>2</sub>O<sub>8</sub> on degradation percent of phenol red; C<sub>0</sub> = 10 mg/l, pH= 4.5, TiO<sub>2</sub> dosage = 40 mg, photolysis time 5 hrs

## 3.8 UV-VIS-FTIR spectral study

### 3.8.1 UV-VIS absorption profile

To examine the response of photocatalytic activities of nano TiO<sub>2</sub>, the absorption spectra of exposed samples at various time intervals were recorded and the rate of decolorization was observed in terms of change in the main intensity at  $\lambda$  max (432 nm) of the dye.

Figure (3-33) presents typical UV-VIS spectra of three absorption bands for phenol red (10 mg/L) located at 263, 432 and 590 nm. The main two visible region bands which are located at 432 and 590 nm, attributed to the chromophoric structure, are impacted by the pH of the media (Figure 3-3) where the solution is acidic and improve the absorption of phenol red on TiO<sub>2</sub> surface [59]. Whereas, the band located at 263 nm is assigned to benzoic ring [108]. The

counter-intuitive appearance of the band located at 590 nm in acidic medium (pH = 4.5) supports the high stability of the keto form, which is usual in basic medium as a keto-enol tautomerism product, due to the conjugation of the molecule.

The percentage of decolorization efficiency of samples has been calculated for the most intense absorption peak at 432 nm as follows [17]:

$$\text{Efficiency \%} = 100 \{ (A_o - A_t) / A_o \}$$

where  $A_o$  and  $A_t$  are initial absorbance and absorbance after irradiation at various time intervals, respectively. Also from Figure (3-33), which represents the time-dependent UV–Vis absorption spectra of phenol red during irradiation with nano  $\text{TiO}_2$  under UV light, it was found that  $\text{TiO}_2$  decolorizes phenol red evidently after 300 minutes of irradiation.

Under optimum operational conditions namely, pH = 4.5, nano powder loading = 0.5 g/l, UV light intensity =  $485 \times 10^{-10}$  Ein / sec. L and pollutant concentration = 10 ppm, we have observed a gradual photo decolorization of the polluted solution over 5 hours of irradiation vanishing > 90% of the pollutant. Also from Figure (3-33), increasing in the illumination time allows the absorption spectra to be shifted exponentially and vertically toward the low absorbance values for the main absorption band , 432 nm, suggesting that the chromophore responsible for the characteristic color of the compound, is destructed and subsequently degraded down. Furthermore, no new absorption bands appeared in either the visible or the UV spectra regions. This is also accompanied by simultaneous decrease of the intensities of other bands, 263 and 590 nm.

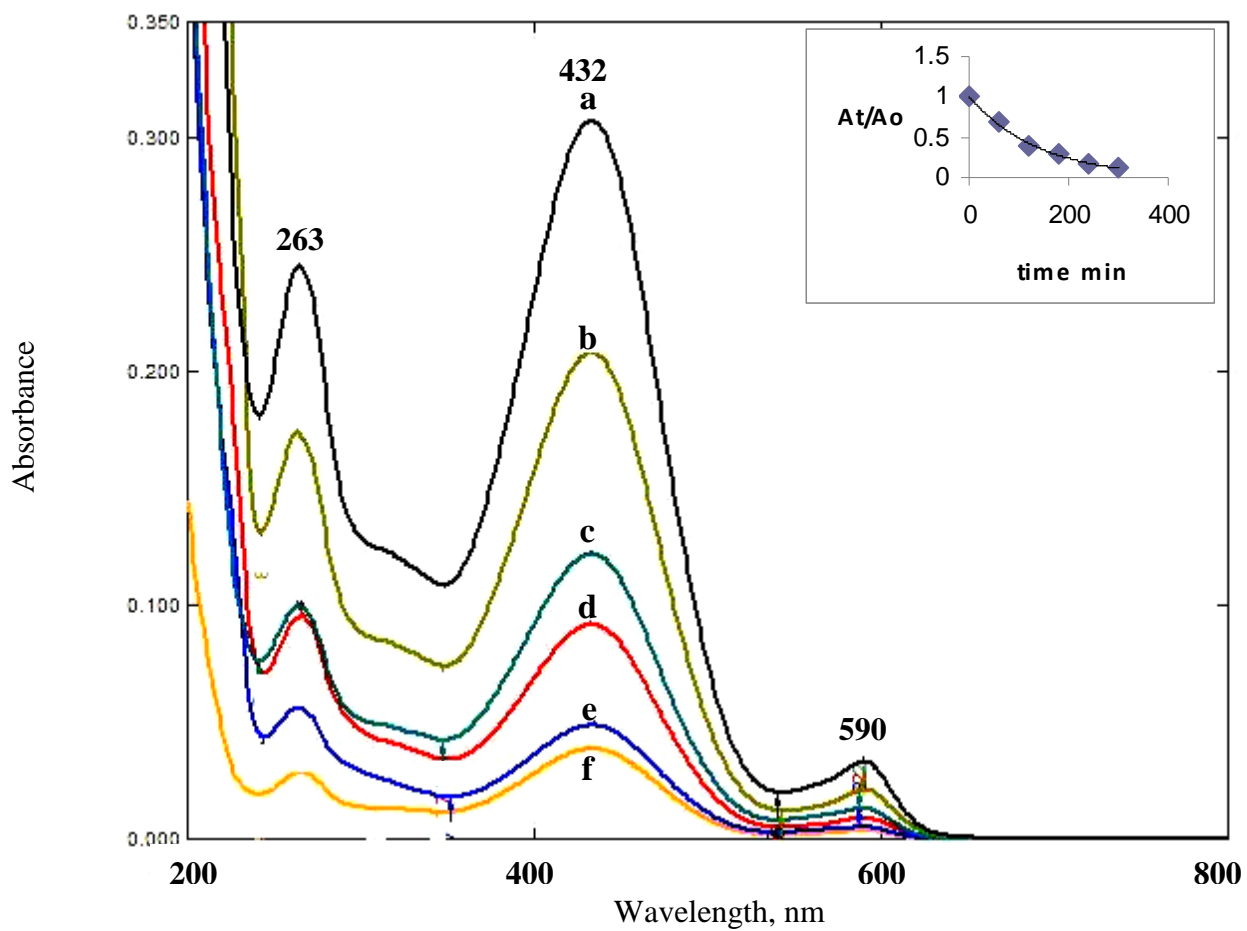


Figure (3-33): UV-VIS spectra changes of phenol red (10 mg/L) in aqueous nano TiO<sub>2</sub> dispersion (0.5 g/L) irradiated under UV light at varying times:(a) 0, (b) 1, (c) 2, (d) 3, (e) 4 and (f) 5 hours. Inset shows the normalized absorbance at 432 nm.

### 3.8.2 FTIR characterization of phenol red-TiO<sub>2</sub> system

For the description of the interaction between phenol red dye and TiO<sub>2</sub> catalyst, the Fourier transform infra-red (FTIR) technique has been exploited. Figure (3-34) shows the FTIR spectra of phenol red and phenol red bound to TiO<sub>2</sub>. The spectrum of pure phenol red showed the sulphonato group stretching at 1462 cm<sup>-1</sup>. Similar band (1480 cm<sup>-1</sup>) has also been assigned by Asiri et al. [65]. This band is completely disappeared in the spectrum of phenol red bound TiO<sub>2</sub>. Furthermore, the sharp stretching band at 3398 cm<sup>-1</sup> is attributed to the OH group in the pure phenol red [109]. This band disappeared as well and a new broad band appeared at 3275 cm<sup>-1</sup>. This confirms the adsorption of phenol red on TiO<sub>2</sub> surface as other anchoring groups [110]. Moreover, the appearance of a band at ~1096 cm<sup>-1</sup> for phenol red / TiO<sub>2</sub> spectrum is verification for the adsorption of phenol red onto TiO<sub>2</sub> and subsequent degradation. On the other hand, the shifts in the stretching frequencies of OH and C-O groups have also been reported previously by some computational authors [111-112] are ascribed to the adsorption onto TiO<sub>2</sub> powder particles.

On the basis of above findings, we report here that the interaction of phenol red with TiO<sub>2</sub> surface occurs through its sulphonato and phenolic collaging groups.

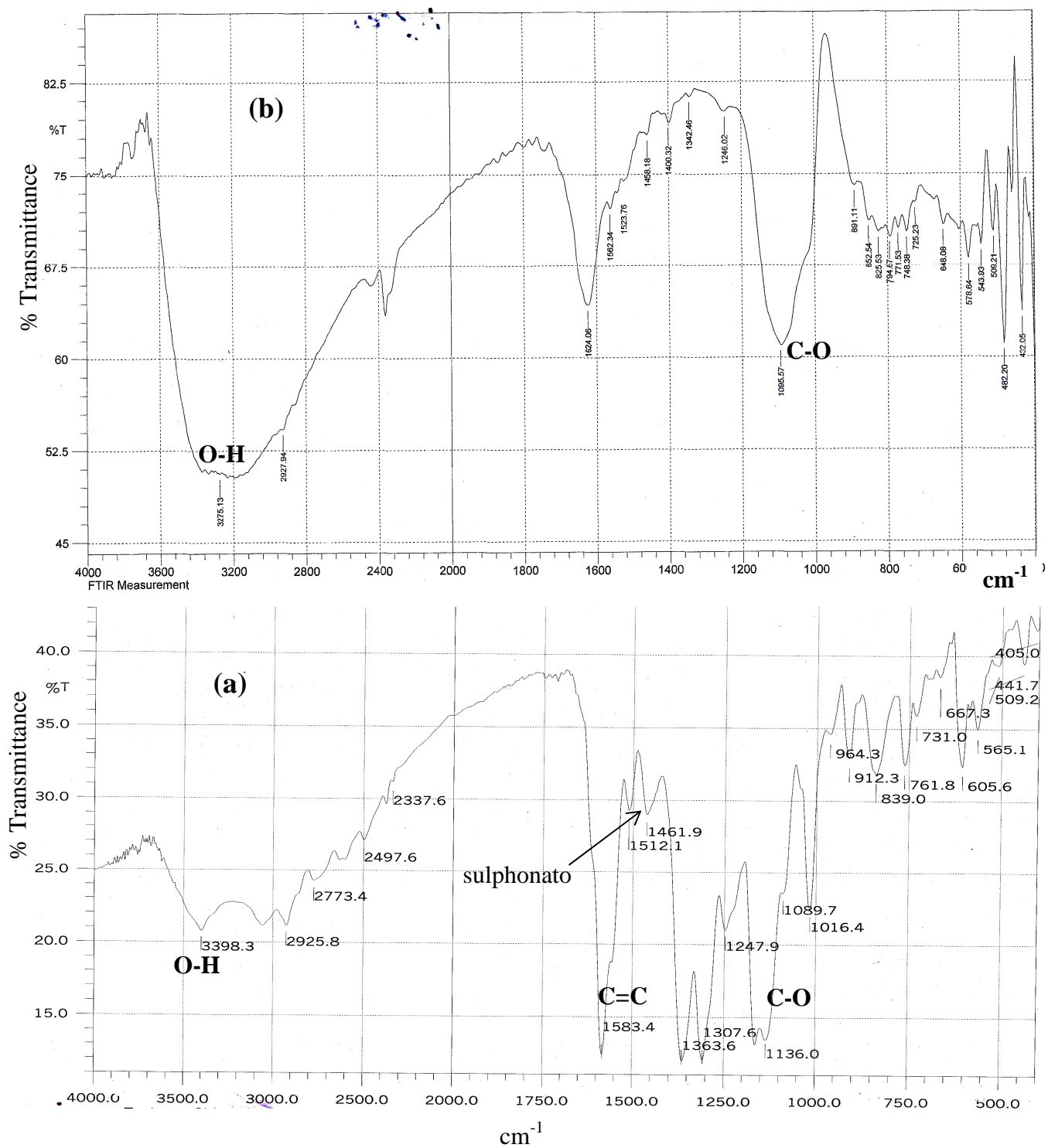


Figure (3-34): FTIR spectra of pure phenol red (a) and phenol red adsorbed onto  $\text{TiO}_2$  (b)

### 3.9 Computation of the thermodynamic functions

The photocatalytic degradation rate of different organic compounds depends on various operational parameters including temperature and corresponding thermodynamic functions [86]. Hence, since the reaction temperature could affect the degradation rate, the effect of temperature on photodegradation process of phenol red dye in aqueous TiO<sub>2</sub> suspension was studied at various temperatures in the range from 293 to 318 K. The apparent rate constant ( $k_{app}$ ) was evaluated at each temperature. An increase of degradation was observed with increasing temperature. The apparent rate constant and temperature can be expressed by Arrhenius relation as follows [56]:

$$k_{app} = Ae^{-E_a/RT} \dots\dots\dots(3-17)$$

where  $k_{app}$  is the apparent rate constant, A is the frequency factor or pre-exponential factor,  $E_a$  is the activation energy of the reaction, R is general gas constant ( 8.314 J mol<sup>-1</sup> K<sup>-1</sup> ) and T is the absolute temperature.

Translation of Eq. (3-17) resulted in the following equation;

$$\ln k_{app} = \ln A - E_a/RT \dots\dots\dots(3-18)$$

A linear plot of  $\ln k_{app}$  versus  $1/T$  yielded a straight line (Figure 3-35) from which the activation energy can be obtained and is given in Table (3-2). Chen and Ray [63] reported that the increase in rate constant is most likely due to the increasing collision frequency of molecules in the solution that increases with increasing temperature.

The other thermodynamic parameters for instance free energy of activation ( $\Delta G^\#$  ), enthalpy of activation( $\Delta H^\#$ ) and entropy of activation ( $\Delta S^\#$ ) were

calculated (Table 3-2) using activation energy and apparent rate constant and employing Eyring's equation as follows [113-114]:

$$k_{app} = k_B T/h \exp(-\Delta G^\ddagger/RT) \dots\dots\dots(3-19)$$

$$\Delta G^\ddagger = RT \times [\ln (k_B T/h) - \ln k_{app}] \dots\dots\dots(3-20)$$

$$\Delta G^\ddagger = RT \times [\ln (k_B/h) + \ln T - \ln k_{app}] \dots\dots\dots(3-21)$$

$$\Delta G^\ddagger = RT \times (23.76 + \ln T - \ln k_{app}) \dots\dots\dots(3-22)$$

Equation (3-18) can be rewritten as [115] :

$$d(\ln k_{app}) / dT = E_a / RT^2 \dots\dots\dots(3-23)$$

Likewise, Eq. (3-19) is rewritten as:

$$\ln k_{app} = \ln (k_B T/h) - \Delta H^\ddagger / RT + \Delta S^\ddagger / R \dots\dots\dots(3-24)$$

$$d(\ln k_{app}) / dT = 1 / T + \Delta H^\ddagger / RT^2 = (\Delta H^\ddagger + RT) / RT^2 \dots\dots(3-25)$$

Solving Eqs. (3-23) and (3-25) for the activation enthalpy gives,

$$\Delta H^\ddagger = E_a - RT \dots\dots\dots(3-26)$$

finally giving access to the entropy of activation,

$$\Delta S^\ddagger = (\Delta H^\ddagger - \Delta G^\ddagger) / T \dots\dots\dots(3-27)$$

where  $k_B$  is Boltzmann constant ( $1.3805 \times 10^{-23} \text{ J K}^{-1}$ ),  $h$  is Planck constant ( $6.6256 \times 10^{-34} \text{ J s}$ ).

From Table (3-2), it can be concluded that TiO<sub>2</sub> mediated photocatalytic degradation of phenol red is slightly affected by temperature change. Similar conclusion was drawn by other researchers [83, 116]. Nevertheless, an increase in temperature facilitates the reaction to compete more efficiently with electron–hole pair recombination. From Figure (3-35), we observed a decrease in the degradation rates at temperatures of 313 and 318. This could be most likely ascribed to desorption of phenol red dye at these temperatures, as long as the adsorption- desorption equilibrium plays a key role in the photocatalytic process, which is also verified through the estimated adsorption coefficient of phenol red in this thesis (paragraph 3.6.2). Several authors reported experimental evidence for the dependence of photocatalytic activity on temperature [116-117]. Furthermore, Soares et al. [117] stated that at a relatively high temperature (40 to 60°C), the limiting stage becomes the adsorption of the dye on the TiO<sub>2</sub>. Nevertheless, Gogate and Pandit [70] concluded that a photocatalytic reaction has a point or an optimum range of operation between 20 and 80°C. Whereas, Gaya and Abdullah [8] reported that the increase in temperature enhances recombination of charge carriers and desorption process of adsorbed reactant species, resulting in decrease of photocatalytic activity. Based on the above argument, it can be concluded that the temperature dependent steps in photocatalytic reaction are adsorption and desorption of reactants and products on the surface of photocatalyst.

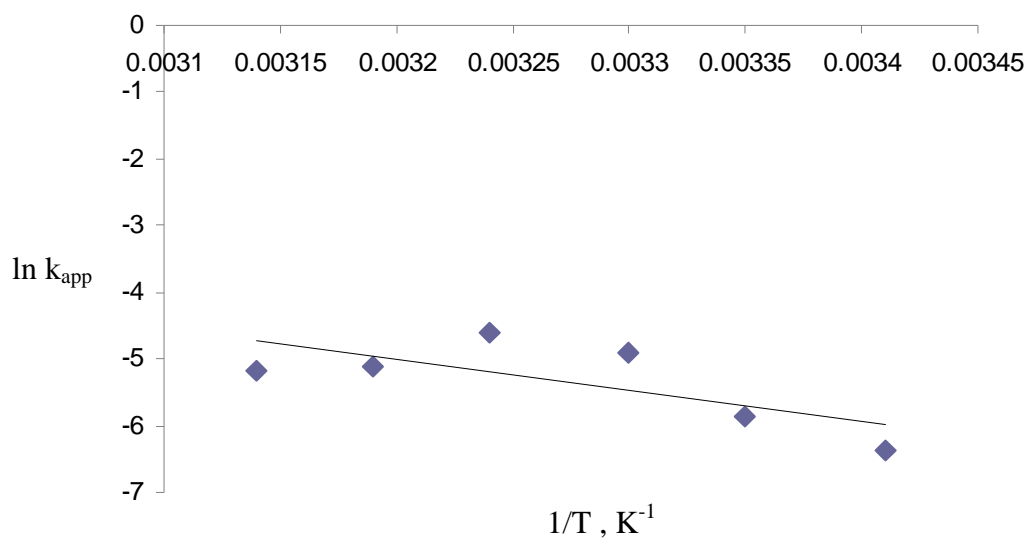


Figure (3-35) : Variation in apparent reaction rate with operational temperature (pH = 4.5; catalyst dosage = 0.5 g /l; C<sub>o</sub>= 10 mg/l)

Table (3-2): Thermodynamic parameters for the photocatalytic degradation of phenol red

T (K)	E <sub>a</sub> (kJ mol <sup>-1</sup> )	ΔG <sup>#</sup> (kJ mol <sup>-1</sup> )	ΔH <sup>#</sup> (kJ mol <sup>-1</sup> )	ΔS <sup>#</sup> (JK <sup>-1</sup> mol <sup>-1</sup> )
<b>293</b>	<b>38.227</b>	<b>87.25</b>	<b>35.79</b>	<b>-176</b>
<b>298</b>		<b>87.55</b>	<b>35.75</b>	<b>-174</b>
<b>303</b>		<b>86.57</b>	<b>35.71</b>	<b>-168</b>
<b>308</b>		<b>87.31</b>	<b>35.66</b>	<b>-168</b>
<b>313</b>		<b>90.10</b>	<b>35.62</b>	<b>-174</b>
<b>318</b>		<b>91.76</b>	<b>35.58</b>	<b>-177</b>

### 3-10 Reusability of the synthesized nano anatase TiO<sub>2</sub>

In order to examine the stability and reusability efficiency of the prepared nano anatase TiO<sub>2</sub> particles, the reusability of the photocatalyst was explored. The recovered TiO<sub>2</sub> nanopowder was reused for four consecutive runs without calcination, whereas the fifth run was carried out after calcination of the recovered TiO<sub>2</sub> nanopowder at 400C° for 4 hours. Figure (3-36) demonstrates a steady decrease in the activity of TiO<sub>2</sub> photocatalyst over four consecutive uses and an increase in the activity during the fifth run upon calcination. This strongly indicates on one hand, that the nature of the catalyst did not change during photocatalysis and on the other hand there is a quantitative adsorption of the phenol red on the surface of the catalyst.

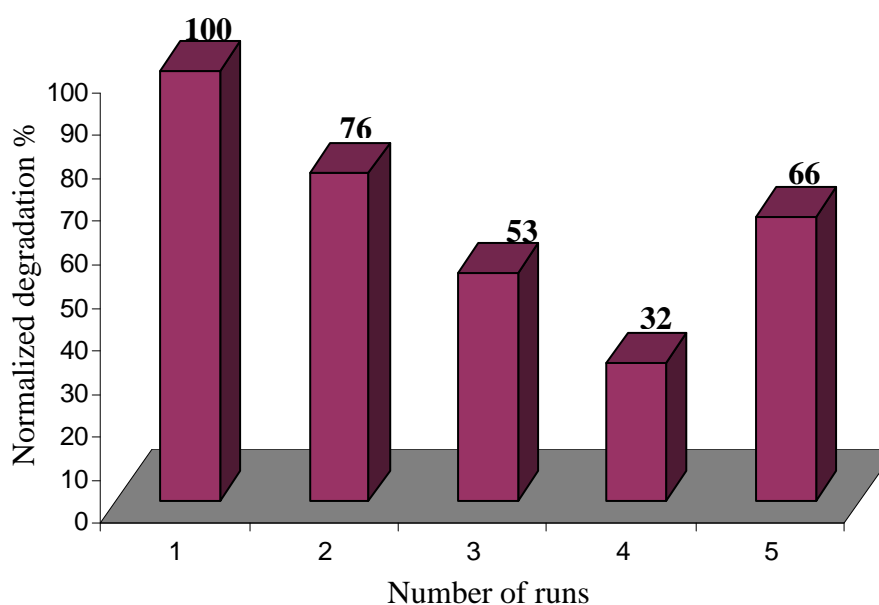


Figure (3-36): Effect of nano TiO<sub>2</sub> reuse on photodecolorization of phenol red.

Run 5 refers to calcined TiO<sub>2</sub> after four irradiation cycles.

## 3.11 Conclusions and Suggestions

### 3.11.1 Concluding remarks

The photocatalytic decolorization and degradation of the phenol red dye as a phenolic model moiety in aqueous solution was studied using synthesized nano anatase TiO<sub>2</sub> as a semiconductor catalyst under UV- light irradiation.

XRD pattern of the prepared nanometric anatase TiO<sub>2</sub> powder confirmed the neat anatase allotrope without rutile diffraction peaks stemming from high calcination temperatures. SEM and TEM images revealed smooth and highly dispersive surfaces with average size of 9-11 nm. The composition resulted has been consistent with that of the reference anatase specimen of TiO<sub>2</sub> as corroborated by EDXS measurements. The bandgap energy as determined from the diffused reflectance spectrum amounted to 3.4 eV, which was identical to that recorded for reference TiO<sub>2</sub> sample. BET measurements confirmed the mesoporosity with average surface area of 48 m<sup>2</sup>/g.

The influences of several operational parameters namely; phenol red initial concentration, TiO<sub>2</sub> dosage and particle size, UV light intensity and varying of photolysis solution pH, have been evaluated: the photocatalytic reaction is favored by a low particle size nano catalyst and relatively a high light intensity, whereas the best efficiency is obtained for 0.5 g/l TiO<sub>2</sub> dosage, photolysis solution pH of 4.5 and 10.3 ppm of initial dye concentration. Furthermore, the apparent quantum yield was also explicitly influenced by photolysis solution pH, TiO<sub>2</sub> dosage and initial dye concentration.

The kinetics and thermodynamics of the photocatalytic bleaching of phenol red by TiO<sub>2</sub> nanocatalyst has also been investigated. The kinetics of the photocatalytic oxidation follows a Langmuir–Hinshelwood model which demonstrates the pseudo first order with respect to the dye initial concentration

within the experimental concentration range. The rate of the photocatalytic degradation was enhanced by the addition of  $\text{H}_2\text{O}_2$ . Hydroxyl radicals contributed appreciably, other than  $\text{O}_2$  gas, in the photobleaching process indicating the remarkable role of hydroxyl type chemistry mechanism in the process. The participation of  $\bullet\text{OH}$  as active oxidising species was confirmed by using hydroxyl radical scavengers, where the rate of photodegradation was drastically reduced. On the other hand, an increase of the temperature has kind effect on kinetics and facilitates the degradation process to good extent. The effect of temperature from 293 to 318 K showed that the apparent rate constants follow the Arrhenius relation. The activation energy of the degradation of phenol red was found to be  $38 \text{ kJ mol}^{-1}$ .

The rate of photo decolorization of phenol red dye was monitored spectrophotometrically and it was recorded with respect to the change in intensity of absorption peak at 432 nm. It was observed that  $\text{TiO}_2$  decolorizes phenol red dramatically after 300 minutes of UV light irradiation.

### 3.11.2 Suggestions

In the light of the present research work, several suggestions can be reported:

1- The phenolic dyes are classified as high priority ecotoxicants due to their toxicity, persistence, i.e., low biodegradability, and carcinogenicity.

The initial step ( $e^- - h^+$  pair formation), in the photooxidative degradation of organic dyes on  $\text{TiO}_2$  is no longer questioned, but the subsequent details of the degradation pathway remain rather controversial. Accordingly, the recent work could be extended further to study detailed degradation mechanism employing various instrumental tools like HPLC, GC-MS...etc.

2- Since the immobilized TiO<sub>2</sub> system is highly effective for photocatalysis, because TiO<sub>2</sub> fine crystals are immobilized at high density at the surface of the particles, we would suggest adopting immobilized nano TiO<sub>2</sub> units, for the phodetoxification of organic dyes.

3- The study of the photocatalysis of the persisting pollutants, together with computational authentication, in aqueous effluents could be an interesting extension of this work.

4- The metal and non metal doping methodology of TiO<sub>2</sub> photocatalyst has attracted the attention of green chemistry researchers due to the exploitation of solar energy. Accordingly, we consolidate such line of research work to be adopted for the decontamination of persisting organic dyes like phenolic and azo pollutants.

**Republic of Iraq  
Ministry of Higher Education  
and Scientific Research  
Al-Nahrain University  
College of Science  
Department of Chemistry**



# **Photocatalytic Oxidation of Phenol Red on Nanocrystalline TiO<sub>2</sub> Particles**

**A Thesis Submitted to the College of Science Al-Nahrain  
University in partial fulfillment of the requirements for the  
Degree of Master of Science in Chemistry**

**By**

**Ahmed Abdullah Hussain**

**B.Sc. Chemistry–Al-Nahrain University-2011**

**Supervised by**

**Prof. Dr. Hilal S. Wahab**

## Supervisor Certification

I certify that this thesis entitled " Photocatalytic Oxidation of Phenolic Compounds on Nanocrystalline TiO<sub>2</sub> Particles" was prepared by " **Ahmed Abdullah Hussain**" under my supervision at the College of Science/Al-Nahrain University as a partial fulfillment of the requirements for the Degree of Master of Science in Chemistry.

Signature:

Name: **Dr. Hilal S. Wahab**

Scientific Degree: Prof.

Date:

In view of the available recommendation, I forward this thesis for debate by the Examining Committee.

Signature:

**Dr. Nasreen R. Jber**

Title: Head of Chemistry Department

Date:

Al-Nahrain University

## Table of Contents

No.	Subject	Page
<b>Chapter One</b>		
1	<b>Introduction</b>	
1-1	Advanced Oxidation Process (AOP)	1
1-2	Dyes and phenolic compounds as water ecotoxicants	6
1-2-1	Dyes	6
1-2-2	Phenolic compounds	8
1-3	Size effect of semiconductor particles	9
1-4	The nature of heterogeneous photocatalysis	13
1-5	Characteristic aspects of the photo induced TiO <sub>2</sub>	14
1-6	Photocatalytic degradation of phenols in aqueous TiO <sub>2</sub> suspension	19
1-7	Mechanism of exciton formation on TiO <sub>2</sub> surface	23
1-8	Literature survey	24
1-9	Scope of the present work	25
<b>Chapter Two</b>		
2	<b>Experimental part</b>	
2-1	Chemicals	26
2-1-1	Solid chemicals	26
2-1-2	Liquid chemicals	27
2-2	Procedures	27
2-2-1	Measurement of light intensity using actinometric method	27
2-2-2	TiO <sub>2</sub> nanoparticles catalyst synthesis	30

2-2-3	Preparation of phenol red and calibration curve	30
2-2-4	Determination of the light intensities for UV source at different distances using the actinometer solution	31
2-2-5	Testing of degradation of phenol red in the dark	32
2-2-6	Testing of Degradation of phenol red in the absence of TiO <sub>2</sub>	32
2-2-7	Multi results experiments by air equilibration	33
2-2-8	Effect of light intensity on the degradation of phenol red	33
2-2-9	Multi parameters measurement for O <sub>2</sub> equilibration	33
2-2-10	Effect of pH on the degradation of phenol red	34
2-2-11	Effect of irradiation time on the degradation of phenol red	34
2-2-12	Effect of H <sub>2</sub> O <sub>2</sub> on the degradation of phenol red	35
2-2-13	Effect of initial phenol red concentration on the rate of reaction	35
2-2-14	Effect of TiO <sub>2</sub> loading on the degradation of phenol red	36
2-2-15	Effect of particle size of TiO <sub>2</sub> on the degradation of phenol red	36
2-2-16	Effect of H <sub>2</sub> O <sub>2</sub> in the dark on the degradation of phenol red	37
2-2-17	Effect of H <sub>2</sub> O <sub>2</sub> in the absence of TiO <sub>2</sub> on the degradation of phenol red	37
2-2-18	Effect of temperature on the degradation of phenol red	37
2-2-19	Effect of Na <sub>2</sub> S <sub>2</sub> O <sub>8</sub> as oxidant	38
2-2-20	Effect of isopropanol as hydroxyl radical scavenger	38

2-2-21	General photolysis procedure	39
2-3	Instruments	40
2-3-1	Photolysis unit	40
2-3-2	Scanning Electron Microscopy (SEM)	42
2-3-3	Transmission Electron Microscopy (TEM)	43
2-3-4	Energy Dispersive X-ray Spectroscopy (EDXS)	44
2-3-5	X-ray diffraction Spectrometer (XRD)	45
2-3-6	Raman Spectrometer	46
2-3-7	Brunauer Emmett Teller (BET)	46
2-3-8	Diffused Reflectance UV-VIS Spectrometer	46
2-3-9	Ultra Violet-Visible spectrophotometer (UV-VIS)	46
2-3-10	Single beam VIS spectrophotometer	47
2-3-11	pH Meter	47
2-3-12	Muffle furnace	47
2-3-13	Drying cabinet	47
2-3-14	Centrifuge	47
2-3-15	Hot Plate	47
2-3-16	Fourier Transform Infrared Spectroscopy (FTIR)	48
<b>Chapter Three</b>		
3	<b>Results and Discussion</b>	49
3-1	UV-VIS spectroscopic feature of phenol red	49
3-2	Characterization of the synthesized nano anatase TiO <sub>2</sub> particles	52
3-2-1	Surface morphology	52
3-2-2	Energy and composition perspectives	54
3-2-3	Surface area , pore size and particle size aspects	58
3-3	Control experiments	61
3-4	Experimental optimization of photocatalysis parameters	62

3-4-1	Effect of varying the pH on the rate of photocatalysis	62
3-4-2	Influence of nano anatase TiO <sub>2</sub> loading	66
3-4-3	Impact of initial phenol red concentration	68
3-4-4	Influence of nano anatase TiO <sub>2</sub> particle size	73
3-5	Impacts of the photochemical parameters	76
3-5-1	The role of UV light source intensity	76
3-5-2	Rationalization of apparent quantum yield with some experimental variables	78
3-6	Kinetic Study	82
3-6-1	Effect of irradiation time on the rate of photocatalysis	82
3-6-2	Initial concentration and Langmuir-Hinshelwood model	84
3-7	Contribution of the added oxidants	89
3-7-1	Effect of H <sub>2</sub> O <sub>2</sub> on photocatalysis of phenol red	89
3-7-2	Influence of Na <sub>2</sub> S <sub>2</sub> O <sub>8</sub> on photocatalysis of phenol red	95
3-8	UV-VIS , FTIR spectral study	96
3-8-1	UV-VIS absorption profile	96
3-8-2	FTIR characterization of phenol red-TiO <sub>2</sub> system	99
3-9	Computation of the thermodynamic functions	101
3-10	Reusability of the synthesized nano anatase TiO <sub>2</sub>	105
3-11	Conclusions and Suggestions	106
3-11-1	Concluding remarks	106
3-11-2	Suggestions	107
<b>References</b>		109
Appendix	Published article	

## List of Abbreviations

<b>SEM</b>	Scanning electron microscopy
<b>EDXS</b>	Energy dispersive X-ray spectroscopy
<b>XRD</b>	X-ray diffraction
<b>DUR-UV-VIS</b>	Diffused reflectance UV-VIS spectrometry
<b>TEM</b>	Transmission electron microscopy
<b>BET</b>	Brunauer-Emmett-Teller
<b>UV-VIS</b>	Ultra violet-Visible spectrophotometer
<b>FTIR</b>	Fourier transform infrared spectroscopy
<b>k<sub>app</sub></b>	Apparent rate constant
<b>AOP</b>	Advanced oxidation process
<b>COD</b>	Chemical oxygen demand
<b>TOC</b>	Total organic carbon
<b>E<sub>g</sub></b>	Band gap energy
<b>HOMO</b>	Highest occupied molecular orbital
<b>LUMO</b>	Lowest unoccupied molecular orbital
<b>Mie resonance</b>	Gustav Mie (1868-1957)
<b>LMCT</b>	Ligand to metal charge transfer
<b>4-CP</b>	4-chlorophenol
<b>pzc</b>	Point of zero charge
<b>K<sub>ad</sub></b>	Adsorption equilibrium coefficient
<b>NFDW</b>	Nano filtered deionized water
<b>MPML</b>	Medium pressure mercury lamp

## List of Figures

Figure No.	Figure title	Page No.
1-1	Formation of electron-hole pairs on TiO <sub>2</sub> surface	6
1-2	model for particle growth	10
1-3	Quantum size effect on semiconductor bandgap	11
1-4	Effect of temperature on TiO <sub>2</sub> allotrops	16
1-5	Initial charge transfer pathways for TiO <sub>2</sub> photoelectrochemical mechanism	18
1-6	Surface complex mediated photodegradation of 4-CP on pure TiO <sub>2</sub> under visible light	21
1-7	Single electron transfer mechanism for ring opening of chlorocatechol	22
2-1	Calibration curve of Ferrous ion (Fe <sup>+2</sup> )	29
2-2	Calibration curve for phenol red	31
2-3	Schematic diagram for ; (a) emission spectra of the Medium Pressure Mercury Lamp (MPML); (b) photocatalysis cell; (c) absorption spectra of glass	42
3-1	Chemical structure of phenol red	49
3-2	UV-VIS spectrum of phenol red	50
3-3	Standard scan of phenol red at different pH values	50
3-4	Calibration curve for phenol red	51
3-5	Diffused reflectance UV-VIS absorption threshold for (a) standard nanopowder anatase TiO <sub>2</sub> reference specimen; (b) synthesized nanopowder anatase TiO <sub>2</sub>	55

3-6	X-ray Diffraction Spectroscopy (XRD) patterns of (a) standard nanopowder anatase TiO <sub>2</sub> reference specimen; (b) synthesized nanopowder anatase TiO <sub>2</sub>	56
3-7	Raman spectra for (a) standard nanopowder anatase TiO <sub>2</sub> reference specimen; (b) synthesized nanopowder anatase TiO <sub>2</sub>	56
3-8	BET measurements for nano anatase TiO <sub>2</sub> ; (a) Isotherm plot ; (b) pore size plot	59
3-9	The relative decrease in absorption intensity of phenol red as a function of irradiation time: (a) TiO <sub>2</sub> in dark; (b) UV irradiation in absence of TiO <sub>2</sub> ; (c) UV illumination in presence of TiO <sub>2</sub>	62
3-10	Variation of phenol red molecular structure at different pH values; (a) low pH; (b) moderate pH ; (c) high pH	64
3-11	effects of pH variation on the rate of photocatalysis of phenol red	65
3-12	Effects of pH variation on the degradation yield of phenol red	65
3-13	Degradation of phenol red at different TiO <sub>2</sub> loadings	67
3-14	Effect of TiO <sub>2</sub> catalyst loading on the degradation yield of phenol red; blue columns represent % degradation and red columns represent TiO <sub>2</sub> dosage	68
3-15	Effect of initial concentration of phenol red on the (a) remaining concentration and (b) degradation rate	71
3-16	(a) Variation of rate constant with phenol red initial concentration and (b) Variation of degradation percent of phenol red with its initial concentration	72

3-17	Influence of TiO <sub>2</sub> particle size on the rate of photolysis	74
3-18	rate of photoreactivity of TiO <sub>2</sub> with the average particle size	75
3-19	Degradation of phenol red at different size on nano TiO <sub>2</sub> particles	75
3-20	Variations of the initial rate and degradation yield as a function of light source intensity	77
3-21	Effect of loading of TiO <sub>2</sub> on quantum yield	80
3-22	Impacts of (a) phenol red initial concentration and (b) pH of photolysis media, on the quantum yield of the process.	81
3-23	Rate of degradation of phenol red at optimum condition	83
3-24	Degradation of phenol red at optimum conditions	84
3-25	Plot of ln(Ct/Co) vs. reaction time at different initial concentrations of phenol red	86
3-26	Langmuir-Hinshelwood model outcomes for the disappearance of phenol red at different initial concentrations	88
3-27	Virtual adsorption geometry of phenol red onto TiO <sub>2</sub> particle	88
3-28	Photodegradation of phenol red at (a) presence of both O <sub>2</sub> and H <sub>2</sub> O <sub>2</sub> (b) presence of H <sub>2</sub> O <sub>2</sub> (c) presence of O <sub>2</sub>	90
3-29	Influence of H <sub>2</sub> O <sub>2</sub> on the degradation yield of phenol red under optimum experimental conditions	91

3-30	Degradation yields of phenol red after 5 hours UV photolysis under optimum experimental conditions for; (a) $\text{TiO}_2 + \text{H}_2\text{O}_2 + \text{O}_2$ gas (without irradiation); (b) $\text{H}_2\text{O}_2 + \text{O}_2$ gas + irradiation (without $\text{TiO}_2$ ); (c) $\text{TiO}_2 + \text{H}_2\text{O}_2 + \text{O}_2$ gas + irradiation; pH = 4.5, $C_0 = 10$ mg/l, $\text{H}_2\text{O}_2 = 3$ ml (50% w/w), $\text{TiO}_2 = 0.5$ g/l	92
3-31	Pseudo order of phenol red degradation with $\text{O}_2$ gas and $\text{H}_2\text{O}_2$ (At: Absorbance at time t and 432 nm); (a) Only $\text{H}_2\text{O}_2$ : (b) $\text{O}_2$ gas and $\text{H}_2\text{O}_2$	94
3-32	Effect of $\text{Na}_2\text{S}_2\text{O}_8$ on degradation percent of phenol red	96
3-33	UV-VIS spectra changes of phenol red (10 mg/L) in aqueous nano $\text{TiO}_2$ dispersion irradiated under UV light at varying times. Inset shows the normalized absorbance at 432 nm.	98
3-34	FTIR spectra of pure phenol red (a) and phenol red adsorbed onto $\text{TiO}_2$ (b)	100
3-35	Variation in apparent reaction rate with operational temperature	104
3-36	Effect of nano $\text{TiO}_2$ reuse on photodecolorization of phenol red	105

## List of Images

Image No.	Image title	Page No.
2-1	Photolysis unit	41
2-2	Hitachi S-4700 FE-SEM	43
2-3	Hitachi HT7700 STEM	44
2-4	Hitachi S-3700N VP-SEM	45
2-5	Panalytical Philips diffractometer	45
2-6	Shimadzu UV-1650PC	46
2-7	Apel PD-303 single beam visible spectrophotometer	47
2-8	IR Prestige-21 Shimadzu	48
3-1	Scanning Electron Microscope (SEM) micrographs anatase TiO <sub>2</sub> with different magnifications; (a)200μm (b) 30 nm	53
3-2	Transmission Electron Microscope (TEM) micrograph of nano anatase TiO <sub>2</sub> particles	54
3-3	Energy Dispersive X-ray Spectroscopy (EDXS) image of (a) standard nanopowder anatase TiO <sub>2</sub> reference specimen; (b) synthesized nanopowder anatase TiO <sub>2</sub>	57
3-4	Scanning Electron Microscope (SEM) micrographs anatase TiO <sub>2</sub>	60
3-5	Transmission Electron Microscope (TEM) image of nano anatase TiO <sub>2</sub> particles	60

## List of Tables

<b>Table No.</b>	<b>Title of Table</b>	<b>Page No.</b>
3-1	Quantum yields of photodegradation of phenol red obtained at different intensities	78
3-2	Thermodynamic parameters for the photocatalytic degradation of phenol red	104

## List of Schemes

<b>Scheme No.</b>	<b>Title of Scheme</b>	<b>Page No.</b>
1-1	The mechanism of $\bullet\text{OH}$ radical formation on $\text{TiO}_2$ surface	20

## Abstract

In the current research study, the photocatalytic (photodecolorization) degradation of the phenolic model ecotoxicant, phenol red dye has been investigated using laboratory synthesized anatase TiO<sub>2</sub> nanoparticles in aqueous solution.

The prepared nano TiO<sub>2</sub> powder has been characterized using several advanced instruments including, Scanning Electron Microscopy (SEM), Energy Dispersive X-Ray Spectroscopy (EDXS), X-Ray Diffraction (XRD), Diffused Reflectance UV-VIS spectrometry (DUR-UV-VIS), Transmission Electron Microscopy (TEM), Brunauer–Emmett–Teller (BET) theory and Raman Spectrometry. Average particle size of 9, 9.95 and 11 nm was found using TEM, XRD and SEM, respectively. The surface area and pore size were also measured employing BET nitrogen adsorption apparatus which resulted in surface area of 48 m<sup>2</sup>/g and a pore size of 3.7 nm, which indicates the mesoporosity of the prepared nano anatase TiO<sub>2</sub> particles.

The impacts of several operational parameters for the photodegradation process were explored encompassing, TiO<sub>2</sub> loading, solution pH, initial phenol red concentration, UV light source intensity, photocatalyst particle size and added oxidants.

Under optimum experimental conditions, 4.5 solution pH, 500 mg/l TiO<sub>2</sub> loading and  $2.9 \times 10^{-5}$  mol /l (10.3 mg/l) phenol red, the value of the apparent rate constant,  $k_{app}$ , obtained has been 0.01052 min<sup>-1</sup> ( $17.53 \times 10^{-5}$  sec<sup>-1</sup>) and the half life of the process, accordingly is equal to 1.098 hours. The kinetic of phenol red photobleaching has also been studied and it was found that it follows the pseudo first order pattern regardless of reaction conditions.

Furthermore, the apparent quantum yield for the photodecolorization process was also determined and found to be approximately 0.1.

Results reveal that the photooxidation process of phenol red follows hydroxyl type chemistry in which the addition of hydrogen peroxide has contributed massively in the promotion of the process rate and yield, and further, suppressed to a great extent by addition of isopropanol as  $\cdot\text{OH}$  radical scavenger.

The main process activation thermodynamic parameters namely, Gibbs energy, enthalpy and entropy were also deduced following the computation of photolysis activation energy employing the well known Arrhenius relation.

### Committee Certification

We, the examining committee, certify that we have read this thesis entitled "**Photocatalytic Oxidation of Phenol Red on Nanocrystalline TiO<sub>2</sub> Particles**" and examined the student "**Ahmed Abdullah Hussain**" in its contents and that in our opinion; it is accepted for the Degree of Master of Science in/ chemistry.

Signature:

Name: **Dr. Ahlam M. Farhan**

Scientific Degree: Professor

Date:

(Chairman)

Signature:

Name: **Dr. Hussein I. Abdullah**

Scientific Degree: Assistant Professor

Date:

(Member)

Signature:

Name: **Dr. Taghreed A. Salman**

Scientific Degree: Assistant Professor

Date:

(Member)

Signature:

Name: **Dr. Hilal S. Wahab**

Scientific Degree: Professor

Date:

(Supervisor)

---

I, hereby certify upon the decision of the examining committee.

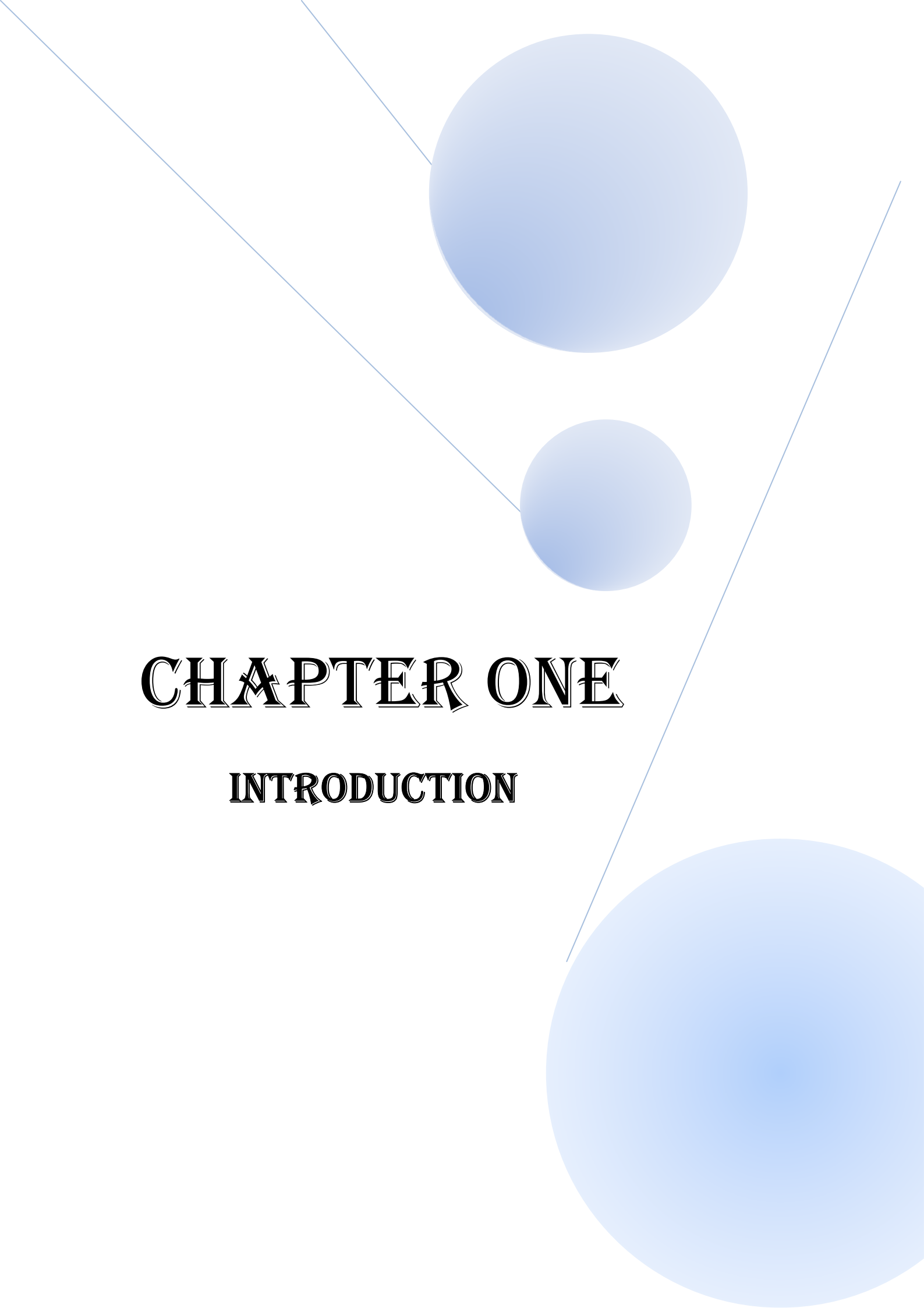
Signature:

Name: **Dr. Hadi M. A. Abood**

Scientific Degree: Assistant Professor

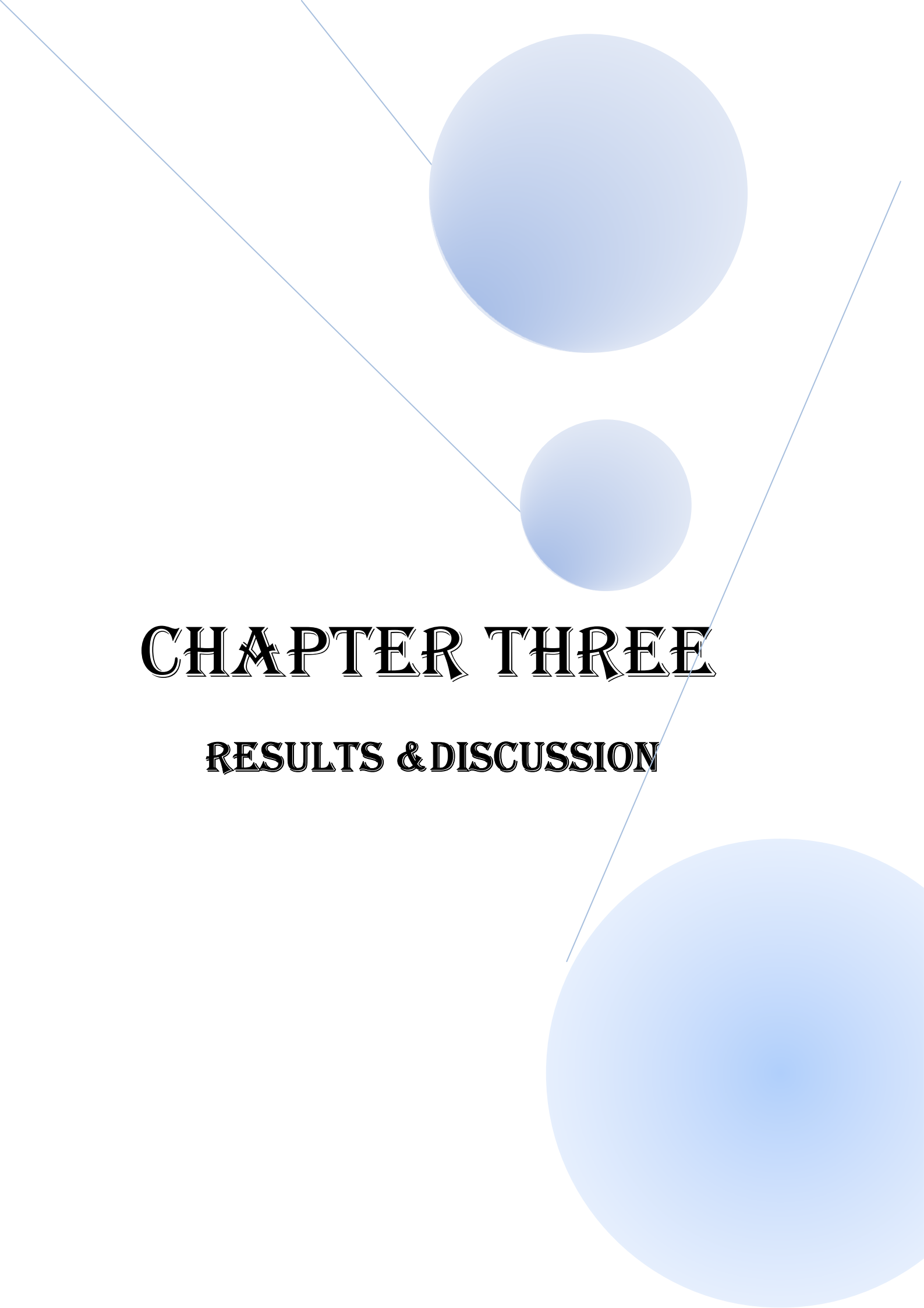
Title: Dean of the College of Science

Date:

The background features three light blue circles of varying sizes. A large circle is at the top center, a medium one is below it to the right, and a very large one is at the bottom right. Thin blue lines intersect the circles and extend across the page.

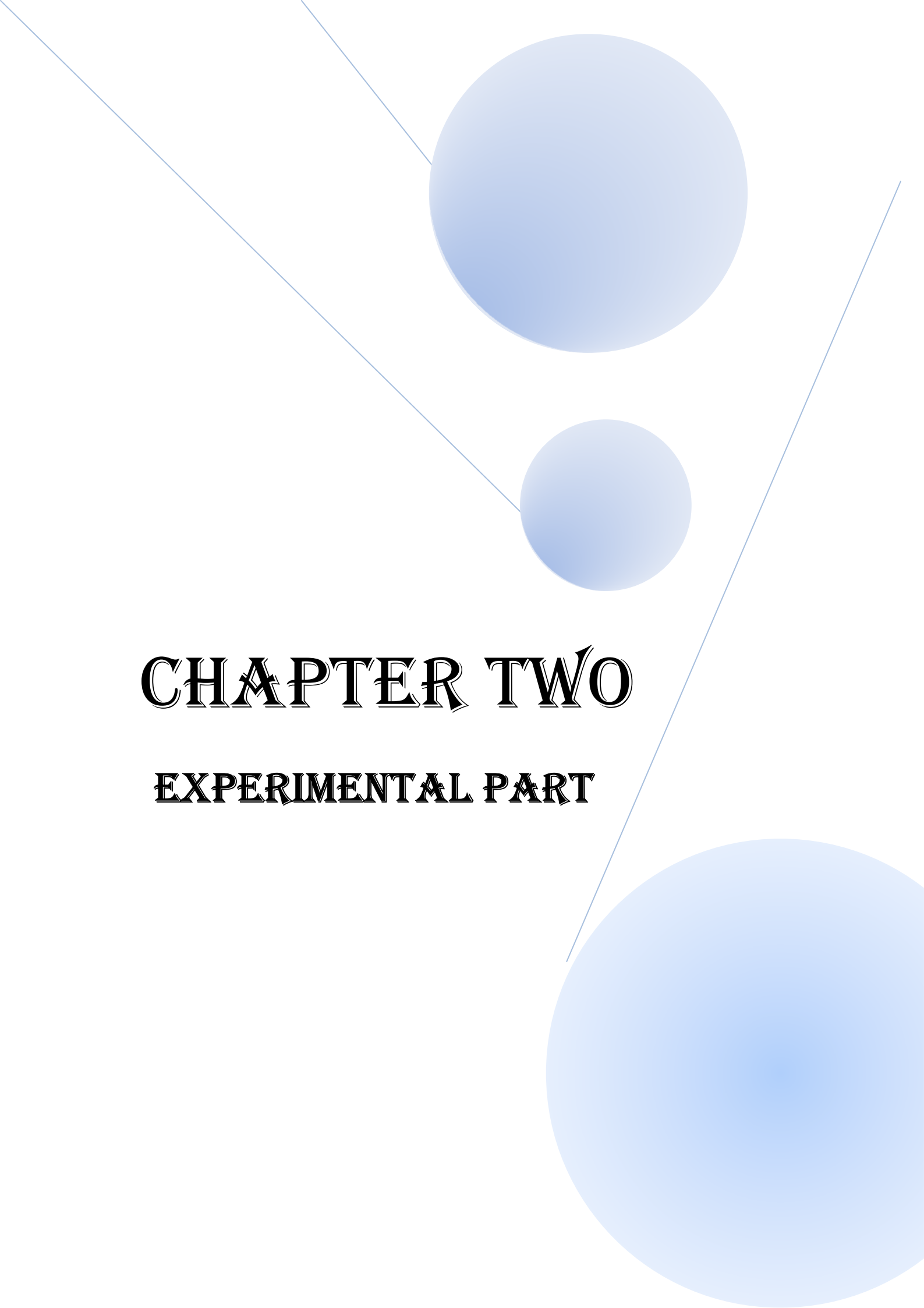
# CHAPTER ONE

## INTRODUCTION

The background features three light blue circles of varying sizes and two thin blue lines. One line starts from the top left and extends towards the center, while the other starts from the top right and extends towards the center. The circles are positioned at the top, middle, and bottom right of the page.

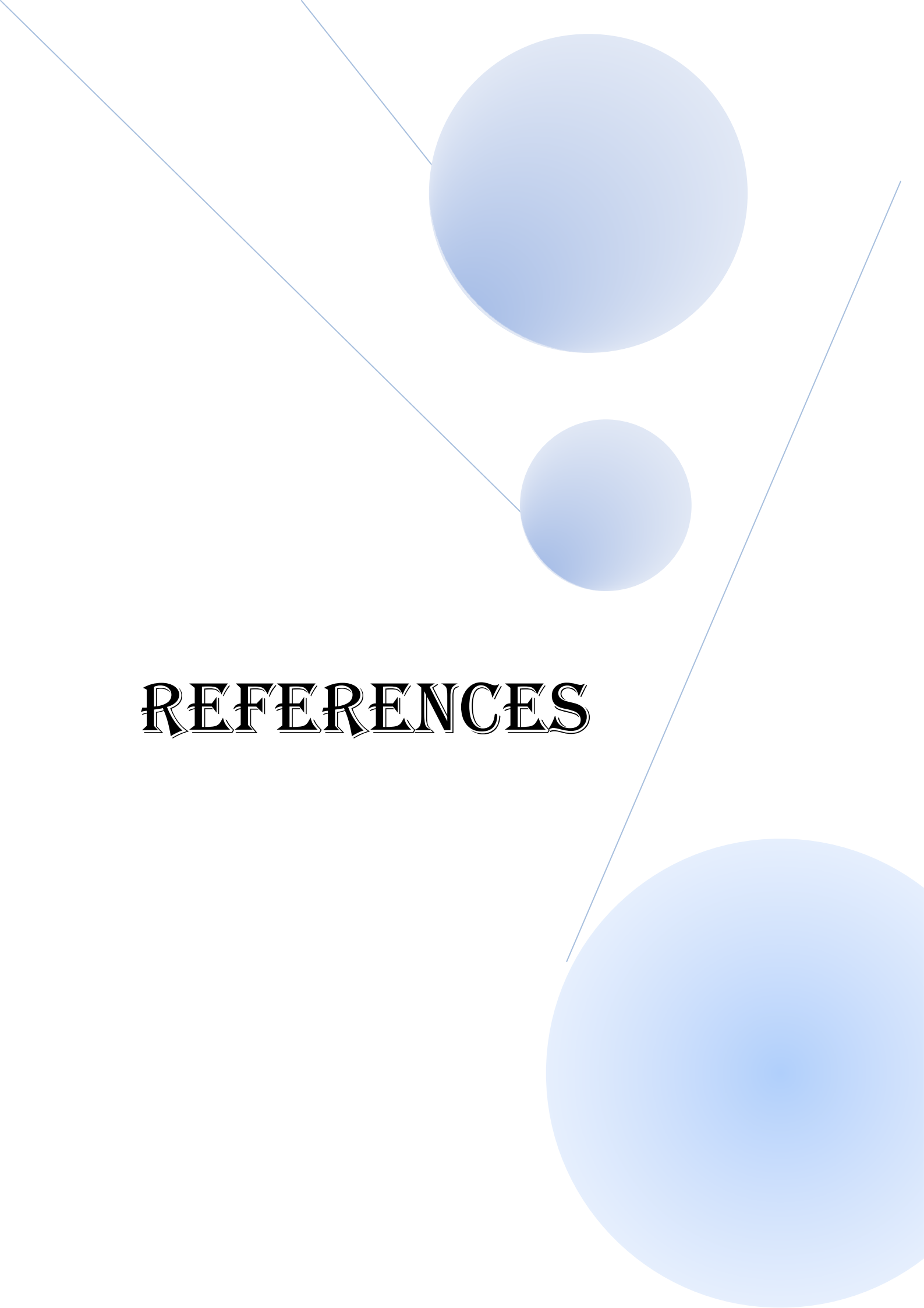
# CHAPTER THREE

## RESULTS & DISCUSSION

The background features three light blue circles of varying sizes and two thin blue lines. One line starts from the top left and extends towards the center, while the other starts from the top right and extends towards the center. The circles are positioned in the upper and lower right areas of the page.

# CHAPTER TWO

## EXPERIMENTAL PART

The background features a minimalist design with three blue circles of varying sizes and two thin blue lines. One large circle is at the top center, a smaller one is below it to the right, and another large circle is at the bottom right. Two lines intersect: one runs from the top left towards the bottom right, and another runs from the top center towards the bottom right.

# REFERENCES



جمهورية العراق  
وزارة التعليم العالي والبحث العلمي  
كلية العلوم | جامعة النهرين  
قسم الكيمياء

## الأكسدة الضوئية التحفيزية للفينول الاحمر على دقائق ثنائي أوكسيد التيتانيوم النانوبلوري

رسالة مقدمة الى كلية العلوم / جامعة النهرين  
كجزء من متطلبات نيل شهادة الماجستير  
في علوم الكيمياء

من قبل

احمد عبدالله حسين

بكالوريوس كيمياء / جامعة النهرين / ٢٠١١

باشرف

الاستاذ الدكتور هلال شهاب وهاب

# الإهداء

إلى من جرع الكأس فارغاً ليسقيني قطرة حب... إلى من كَلَّت أنامله ليقدّم لنا لحظة سعادة...  
إلى من حصد الأشواك عن دربي ليمهد لي طريق العلم... إلى القلب الكبير

(والدي العزيز)

إلى من أرضعتني الحب والحنان... إلى رمز الحب وبلسم الشفاء... إلى القلب الناصع بالبياض

(والدتي الحبيبة)

إلى القلوب الطاهرة الرقيقة والنفوس البرينة إلى رياحين حياتي

(إخوتي)

إلى من بوجودها أكتسب قوة ومحبة لا حدود لها

إلى من عرفت معها معنى الحياة

(حبيبتي)

الآن تفتح الأشرعة وترفع المرساة لتنتقل السفينة في عرض بحر واسع مظلم هو بحر الحياة

وفي هذه الظلمة لا يضيء إلا قنديل الذكريات

ذكريات الأخوة البعيدة

إلى الذين أحببتهم وأحبوني

(أصدقائي)

قَالُوا سُبْحَانَكَ لَا عِلْمَ لَنَا إِلَّا مَا عَلَّمْتَنَا إِنَّكَ  
أَنْتَ الْعَلِيمُ الْحَكِيمُ ﴿٣٢﴾

صدق الله العلي العظيم

سورة البقرة

الناسُ من جهة التمثيل أكفاء  
فإن يكن لهم من بعدٍ ذا نسبٍ  
ما الفضلُ إلا لأهل العلم إنهم  
وقيمة المرء ما قد كان يُحسِنه  
وقدر كلُّ امرئٍ ما كان يجهره  
فعيش بعلمٍ ولا تبغ به بدلاً

أبوهم آدمُ والأم حواءُ  
يُفأخرون به فالطينُ والماءُ  
على الهدى لمن استهدى أدلاءُ  
وللرجال على الأفعال أسماءُ  
والجاهلون لأهل العلم أعداءُ  
فالناسُ موتى وأهل العلم أحياءُ

علي ابن أبي طالب (ع)

## ***Acknowledgement***

*Above all else, I want to express my great thanks to Allah for his uncountable gifts and for helping me to present this thesis.*

*I wish to express my sincere gratitude and great appreciation to my supervisor **Dr. Hilal S. Wahab** for his supervision, continuous encouragement, advice, discussion and suggestions throughout my study.*

*I am very grateful to **staff** of department of chemistry, Al-Nahrain University, college of science for supporting and helping in this study.*

*I would like to thank all of my friends especially (Hussain Mohamad, Ali Najah, Atheer Fathel, Hanan H. Ali, Raghad Ali, Zahraa Abdulazeez, Ayah Jamal, and Yosra Haleem) and all friends that I hope will forgive me for not mentioning their names.*

***Ahmed A. Hussain***

## الخلاصة

انجزت هذه الدراسة البحثية للتفكك الضوئي للصبغة العضوية الفينول الاحمر كنموذج للملوثات الفينولية وذلك باستخدام ثنائي اوكسيد التيتانيوم النانوي المحضر مختبريا وفي وسط مائي.

استخدمت تقنيات تشخيصية عديدة مثل المجهر الالكتروني الماسح وحيود الاشعة السينية ومطياف الانتشار الانعكاسي والمجهر الالكتروني التناظري وطيف رامان لدراسة شكل السطح والحجم الحبيبي والمساحة السطحية وطاقة الفجوة لثنائي اوكسيد التيتانيوم النانوي المحضر. وجد ان متوسط حجم الحبيبة هو 9، 9.95، 11 نانو باستخدام مجهر الالكتروني الماسح، مطياف الانتشار الانعكاسي وحيود الاشعة السينية على التوالي.

وتم كذلك احتساب المساحة السطحية وحجم المسامات باستخدام منظومة BET حيث كانت النتائج للمساحة السطحية 48 م<sup>2</sup>/غم وحجم المسامات 3.7 نانو مما يؤكد كون ثنائي اوكسيد التيتانيوم النانوي ذات مسامات صغيرة. (mesoporos).

تمت دراسة تأثير العديد من المتغيرات التجريبية على عملية التفكك الضوئي مثل كمية ثنائي اوكسيد التيتانيوم النانوي، حامضية المحلول، التركيز الابتدائي للفينول الاحمر، شدة مصدر التشعيع، الحجم الحبيبي لثنائي اوكسيد التيتانيوم النانوي و اضافة المؤكسدات.

ثبتت الظروف التجريبية المثلى لعملية التفكك الضوئي لصبغة الفينول الاحمر عند الدالة الحامضية 4.5 والتركيز الابتدائي للفينول الاحمر مساويا الى 10.3 ملغم/لتر وكمية المحفز ثنائي اوكسيد التيتانيوم مساويا الى 500 ملغم/لتر، حيث تم الحصول على ثابت سرعة التفاعل بقيمة 0.01052 لكل دقيقة وعمر نصف العملية 1.098 ساعة عند الظروف المثلى.

اوضحت دراسة حركية التفكك الضوئي للفينول الاحمر بان العملية من الدرجة الاولى. اضافة على ذلك تم احتساب الناتج الكمي لعملية التفكك الضوئي حيث تساوي 0.1.

اظهرت النتائج بان عملية الاكسدة الضوئية للفينول الاحمر بواسطة ثنائي اوكسيد التيتانيوم النانوي تفضل كيمياء الهيدروكسيل لانه عند اضافة بيروكسيد الهايدروجين حفزت عملية التفكك وتحسنت وتاكيدا على هذا الكلام عند اضافة ايزو بروبانول ثبتت عملية تفكك الفينول الاحمر لانه يعتبر من اهم المثبطات لجذر الهيدروكسيل. وتم كذلك احتساب الدوال الترموديناميكية الاساسية لعملية التفكك الضوئي للفينول الاحمر مثل طاقة التنشيط وطاقة جيبس و الانتالبي و الانتروبي.